# Fermilab

## Constraints on anomalous Higgs boson couplings from its production and decay using the WW channel in proton–proton collisions at √(s) = 13 TeV

FERMILAB-PUB-24-0764-CMS

arXiv:2403.00657

EUROPEAN ORGANIZATION FOR NUCLEAR RESEARCH (CERN)

CERN-EP-2024-035
2024/08/20

CMS-HIG-22-008

# Constraints on anomalous Higgs boson couplings from its production and decay using the WW channel in proton-proton collisions at $\sqrt{s} = 13\,\text{TeV}$

The CMS Collaboration*



## Abstract

A study of the anomalous couplings of the Higgs boson to vector bosons, including *CP*-violation effects, has been conducted using its production and decay in the WW channel. This analysis is performed on proton-proton collision data collected with the CMS detector at the CERN LHC during 2016–2018 at a center-of-mass energy of 13 TeV, and corresponds to an integrated luminosity of $138\,\text{fb}^{-1}$. The different-flavor dilepton ($e\mu$) final state is analyzed, with dedicated categories targeting gluon fusion, electroweak vector boson fusion, and associated production with a W or Z boson. Kinematic information from associated jets is combined using matrix element techniques to increase the sensitivity to anomalous effects at the production vertex. A simultaneous measurement of four Higgs boson couplings to electroweak vector bosons is performed in the framework of a standard model effective field theory. All measurements are consistent with the expectations for the standard model Higgs boson and constraints are set on the fractional contribution of the anomalous couplings to the Higgs boson production cross section.

*Published in the European Physical Journal C as* doi:10.1140/epjc/s10052-024-12925-0.



*See Appendix A for the list of collaboration members

# 1 Introduction

After the discovery of the Higgs boson (H) by the ATLAS and CMS Collaborations in 2012 [1–3], the CMS [4–11] and ATLAS [12–18] experiments set constraints on the spin-parity properties of the Higgs boson and its couplings with gluons and electroweak (EW) gauge bosons, denoted here as Hgg and HVV, respectively. The Higgs boson quantum numbers are consistent with the standard model (SM) expectation $J^{PC} = 0^{++}$, but the possibility of small, anomalous couplings is not yet ruled out. In beyond-the-SM (BSM) theories, interactions with the Higgs boson may occur through several anomalous couplings, which lead to new tensor structures in the interaction terms that can be both $CP$-even or $CP$-odd. The $CP$-odd anomalous couplings between the Higgs boson and BSM particles may generate $CP$ violation in the interactions of the Higgs boson.

In this paper, we study the tensor structure of the Hgg and HVV couplings, and we search for several anomalous effects, including $CP$ violation, using the different-flavor dilepton ($e\mu$) final state from $H \to WW$ decays. The Higgs boson production processes include gluon fusion (ggH), EW vector boson fusion (VBF), and associated production with a W or Z boson (VH). Higgs boson production and decay processes are sensitive to certain anomalous contributions, which can be described by higher-dimensional operators in an effective field theory (EFT) [19] that can modify the kinematic distributions of the Higgs boson decay products and the particles from associated production.

Each production process of the Higgs boson is identified using its kinematic features, and events are assigned to corresponding production categories. The matrix element likelihood approach (MELA) [20–24] is employed to construct observables that are optimal for the measurement of anomalous couplings, or EFT operators, at the production vertex. These and other decay-based variables are used to explore all kinematic features of the events, giving the analysis sensitivity to simultaneous anomalous effects at the Higgs boson production and decay vertices. Fully simulated signal samples that include anomalous couplings incorporate the detector response into the analysis.

The analysis is based on the proton-proton (pp) collision data collected at the CERN LHC from 2016 to 2018, at a center-of-mass energy of 13 TeV, corresponding to an integrated luminosity of $138\,\text{fb}^{-1}$. This paper builds on a previous analysis conducted by the CMS Collaboration in the $H \to WW$ channel [25], which focused on measuring the Higgs boson production cross sections and coupling parameters in the so-called $\kappa$ framework [26]. We follow a formalism used in previous CMS analyses of anomalous couplings in Run 1 and Run 2 [4–11, 27, 28], focusing on the case where the Higgs boson is produced on-shell. The coupling parameters are extracted using the signal strength and the fractional contributions of the couplings to the cross section. A general study of the HVV interaction is performed with four anomalous couplings analyzed individually. Through SU(2) x U(1) symmetry considerations, the anomalous HVV couplings are reduced in number to three and analyzed simultaneously. The primary HVV coupling measurements are performed in terms of cross section fractions with additional interpretations in terms of EFT couplings included. A study of the Hgg interaction is also performed in terms of a $CP$-odd anomalous coupling cross section fraction.

This paper is organized as follows. The phenomenology of anomalous couplings is discussed in Section 2. Section 3 gives a brief overview of the CMS apparatus. Data sets and Monte Carlo (MC) simulation samples are discussed in Section 4. The event reconstruction and selection are outlined in Sections 5 and 6, respectively. Methods to estimate backgrounds are given in Section 7. In Section 8, we discuss the kinematic variables associated with Higgs boson production and decay. Sources of systematic uncertainties are presented in Section 9. The

results are presented and discussed in Section 10. Finally, a summary is given in Section 11. Tabulated results are provided in the HEPData record for this analysis [29].

## 2 Phenomenology

In this analysis, we investigate anomalous coupling effects in gluon fusion or electroweak Higgs boson production, as well as in its decay to WW pairs. A detailed discussion of the theoretical considerations can be found in Refs. [22, 24, 28]. The interaction of the spin-zero Higgs boson with two spin-one gauge bosons $V_1V_2$, such as WW, ZZ, Z$\gamma$, $\gamma\gamma$, or gg, can be parametrized by the scattering amplitude

$$\begin{aligned} A(\mathrm{HV_1V_2}) \sim & \left[ a_1^{\mathrm{VV}} + \frac{\kappa_1^{\mathrm{VV}} q_{\mathrm{V1}}^2 + \kappa_2^{\mathrm{VV}} q_{\mathrm{V2}}^2}{\left(\Lambda_1^{\mathrm{VV}}\right)^2} \right] m_{\mathrm{V1}}^2 \epsilon_{\mathrm{V1}}^* \epsilon_{\mathrm{V2}}^* \\ & + \frac{1}{v} a_2^{\mathrm{VV}} f_{\mu\nu}^{*(1)} f^{*(2),\mu\nu} + \frac{1}{v} a_3^{\mathrm{VV}} f_{\mu\nu}^{*(1)} \tilde{f}^{*(2),\mu\nu}, \end{aligned} \tag{1}$$

where $q_{\mathrm{V}i}$ and $\epsilon_{\mathrm{V}i}$ are the spin-one gauge boson four-momentum and polarization vectors, $m_{\mathrm{V1}}$ is the pole mass of the boson, $f^{(i),\mu\nu} = \epsilon_{\mathrm{V}i}^{\mu} q_{\mathrm{V}i}^{\nu} - \epsilon_{\mathrm{V}i}^{\nu} q_{\mathrm{V}i}^{\mu}$ and $\tilde{f}_{\mu\nu}^{(i)} = \frac{1}{2}\epsilon_{\mu\nu\rho\sigma} f^{(i),\rho\sigma}$ (with $\epsilon_{\mu\nu\rho\sigma}$ the Levi-Civita symbol), $\Lambda_1^{\mathrm{VV}}$ is the scale of BSM physics, and $v$ is the Higgs field vacuum expectation value.

The only leading tree-level contributions in the scattering amplitude are $a_1^{\mathrm{ZZ}} \neq 0$ and $a_1^{\mathrm{WW}} \neq 0$; other $a_1$ coupling parameters (Z$\gamma$, $\gamma\gamma$, gg) do not contribute because the pole mass vanishes. Additional ZZ and WW couplings are considered anomalous contributions. Anomalous terms arising in the SM via loop effects are typically small and are not yet accessible experimentally. The BSM contributions, however, could yield larger coupling parameters. Among the anomalous contributions, considerations of symmetry and gauge invariance require $\kappa_1^{\mathrm{ZZ}} = \kappa_2^{\mathrm{ZZ}}$, $\kappa_1^{\gamma\gamma} = \kappa_2^{\gamma\gamma} = 0$, $\kappa_1^{\mathrm{gg}} = \kappa_2^{\mathrm{gg}} = 0$, and $\kappa_1^{\mathrm{Z}\gamma} = 0$ [24]. The presence of $CP$-odd $a_3^{\mathrm{VV}}$ couplings together with any of the other couplings (all of them $CP$-even), will result in $CP$ violation. We reduce the number of independent parameters by assuming that $a_2^{\gamma\gamma}$, $a_3^{\gamma\gamma}$, $a_2^{\mathrm{Z}\gamma}$ and $a_3^{\mathrm{Z}\gamma}$ are constrained in direct decays of $\mathrm{H} \to \gamma\gamma$ and Z$\gamma$, therefore fixing them to be zero. The $a_2^{\mathrm{gg}}$ term results from loop effects in the SM.

The relationship between the ZZ and WW couplings is mostly relevant for VBF production. There are no kinematic differences between the ZZ and WW fusion processes; therefore, it is not possible to disentangle the couplings. One possibility is to set the ZZ and WW couplings to be equal, $a_i = a_i^{\mathrm{ZZ}} = a_i^{\mathrm{WW}}$, leaving four HVV anomalous couplings to be measured: $a_2$, $a_3$, $\kappa_1/(\Lambda_1)^2$, and $\kappa_2^{\mathrm{Z}\gamma}/(\Lambda_1^{\mathrm{Z}\gamma})^2$. The $a_1^{\mathrm{ZZ}} = a_1^{\mathrm{WW}}$ relationship also appears under custodial symmetry. This approach provides a general test of the Higgs boson Lagrangian tensor structure and a search for $CP$ violation in HVV interactions. In an alternative approach, the SU(2) $\times$ U(1) symmetry reduces the number of independent HVV anomalous couplings to three ($a_2$, $a_3$, and

$\kappa_1/(\Lambda_1)^2$) through the introduction of the following coupling parameter relationships [19] :

$$a_1^{WW} = a_1^{ZZ}, \tag{2}$$

$$a_2^{WW} = c_w^2 a_2^{ZZ}, \tag{3}$$

$$a_3^{WW} = c_w^2 a_3^{ZZ}, \tag{4}$$

$$\frac{\kappa_1^{WW}}{(\Lambda_1^{WW})^2} = \frac{1}{c_w^2 - s_w^2}\left(\frac{\kappa_1^{ZZ}}{(\Lambda_1^{ZZ})^2} - 2s_w^2\frac{a_2^{ZZ}}{m_Z^2}\right), \tag{5}$$

$$\frac{\kappa_2^{Z\gamma}}{(\Lambda_1^{Z\gamma})^2} = \frac{2s_w c_w}{c_w^2 - s_w^2}\left(\frac{\kappa_1^{ZZ}}{(\Lambda_1^{ZZ})^2} - \frac{a_2^{ZZ}}{m_Z^2}\right), \tag{6}$$

where $c_w$ and $s_w$ are the cosine and sine of the weak mixing angle, respectively, and $m_Z$ is the Z boson mass. With this approach, there is a linear relationship between the scattering amplitude couplings and the SM EFT (SMEFT) couplings in the Higgs basis [19] :

$$\delta c_z = \frac{1}{2}a_1^{ZZ} - 1, \tag{7}$$

$$c_{zz} = -\frac{2s_w^2 c_w^2}{e^2}a_2^{ZZ}, \tag{8}$$

$$\tilde{c}_{zz} = -\frac{2s_w^2 c_w^2}{e^2}a_3^{ZZ}, \tag{9}$$

$$c_{z\Box} = \frac{m_Z^2 s_w^2}{e^2}\frac{\kappa_1^{ZZ}}{(\Lambda_1^{ZZ})^2}, \tag{10}$$

where $e$ is the electron charge. The amplitude couplings may also be related to the SMEFT Warsaw basis [19, 30] couplings through the following translation [28, 31] :

$$\delta a_1^{ZZ} = \frac{v^2}{\Lambda^2}\left(2c_{H\Box} + \frac{6e^2}{s_w^2}c_{HWB} + (\frac{3c_w^2}{2s_w^2} - \frac{1}{2})c_{HD}\right), \tag{11}$$

$$\kappa_1^{ZZ} = \frac{v^2}{\Lambda^2}\left(-\frac{2e^2}{s_w^2}c_{HWB} + (1 - \frac{1}{2s_w^2})c_{HD}\right), \tag{12}$$

$$a_2^{ZZ} = -2\frac{v^2}{\Lambda^2}\left(s_w^2 c_{HB} + c_w^2 c_{HW} + s_w c_w c_{HWB}\right), \tag{13}$$

$$a_3^{ZZ} = -2\frac{v^2}{\Lambda^2}\left(s_w^2 c_{H\tilde{B}} + c_w^2 c_{H\tilde{W}} + s_w c_w c_{H\tilde{W}B}\right), \tag{14}$$

where $\Lambda$ is the UV cutoff of the theory (set to 1 TeV), and $\delta a_1^{ZZ}$ is a correction to the SM value of $a_1^{ZZ}$. Further discussion on the EFT operators corresponding to the couplings considered here may be found in Chapter 2.2 of Ref. [19]. The assumed constraints on $a_2^{\gamma\gamma}$, $a_3^{\gamma\gamma}$, $a_2^{Z\gamma}$ and $a_3^{Z\gamma}$ imply that only one of the three coupling parameters $c_{HW}$ , $c_{HWB}$, and $c_{HB}$ is independent; the same is also true for their $CP$-odd counterparts $c_{H\tilde{W}}$, $c_{H\tilde{W}B}$, and $c_{H\tilde{B}}$. Therefore, we have four independent HVV couplings in both the Higgs and Warsaw basis. All the EFT couplings are expected to be zero in the SM.

We thus adopt two approaches to the HVV coupling study. In Approach 1, we use the $a_i^{ZZ} = a_i^{WW}$ relationship and individually analyze each of the four anomalous couplings. In Approach 2, we enforce the SU(2) x U(1) relationships from Eqs. (2–6) and analyze the three independent anomalous couplings both individually and simultaneously. Approach 1 may be considered to follow the relationships from Eqs. (2–5) in the limiting case $c_w = 1$.

Table 1: The cross sections ($\sigma_i$) of the anomalous contributions ($a_i$) relative to the SM value ($\sigma_1$) used to define the fractional cross sections $f_{ai}$ for the Approach 1 and 2 coupling relationships. For the $\kappa_1$ and $\kappa_2^{Z\gamma}$ couplings, the numerical values $\Lambda_1 = \Lambda_1^{Z\gamma} = 100\,\text{GeV}$ are chosen to keep all coefficients of similar order of magnitude.

| $f_{ai}$ | $a_i$ | Approach 1 $\sigma_i/\sigma_1$ | Approach 2 $\sigma_i/\sigma_1$ |
|---|---|---|---|
| $f_{a2}$ | $a_2$ | 0.361 | 6.376 |
| $f_{a3}$ | $a_3$ | 0.153 | 0.153 |
| $f_{\Lambda 1}$ | $\kappa_1$ | 0.682 | 5.241 |
| $f_{\Lambda 1}^{Z\gamma}$ | $\kappa_2^{Z\gamma}$ | 1.746 | — |

It is convenient to measure the fractional contribution of the anomalous couplings to the Higgs boson cross section rather than the anomalous couplings themselves. For the anomalous HVV couplings, the effective fractional cross sections $f_{ai}$ are defined as

$$f_{ai} = \frac{|a_i|^2\sigma_i}{\sum_j |a_j|^2\sigma_j}\,\text{sign}\left(\frac{a_i}{a_1}\right), \tag{15}$$

where $\sum_j$ sums over all the coupling parameters considered, including $a_1$, and $\sigma_i$ is the cross section for the process corresponding to $a_i = 1$ and $a_{j\neq i} = 0$. Many systematic uncertainties cancel out in the ratio, and the physical range is conveniently bounded between $-1$ and $+1$. Our primary measurements are performed in terms of cross section fractions, with additional interpretations in terms of the SMEFT Higgs and Warsaw basis couplings also included. For consistency with previous CMS measurements, the $\sigma_i$ coefficients used to define the fractional cross sections correspond to the $\text{gg} \to \text{H} \to \text{VV} \to 2\text{e}2\mu$ process [28]. The numerical values are given in Table 1 as calculated using the JHUGEN simulation [20–23]. Two sets of values are shown corresponding to the different coupling relationships adopted in Approach 1 and 2.

It has been shown that the angular correlations of the associated jets in the ggH + 2 jets process are sensitive to anomalous Hgg coupling effects at the production vertex [32]. The quark-quark initiated process, $\text{qq} \to \text{qqH}$, corresponds to the gluon scattering topology sensitive to anomalous effects. For the anomalous Hgg coupling, the effective fractional cross section can be defined as

$$f_{a3}^{\text{ggH}} = \frac{|a_3^{\text{gg}}|^2\sigma_3^{\text{gg}}}{|a_2^{\text{gg}}|^2\sigma_2^{\text{gg}} + |a_3^{\text{gg}}|^2\sigma_3^{\text{gg}}}\,\text{sign}\left(\frac{a_3^{\text{gg}}}{a_2^{\text{gg}}}\right). \tag{16}$$

The $\sigma_3^{\text{gg}}$ and $\sigma_2^{\text{gg}}$ cross sections correspond to $a_3^{\text{gg}} = 1, a_2^{\text{gg}} = 0$ and $a_2^{\text{gg}} = 1, a_3^{\text{gg}} = 0$, respectively, and are equal. With this analysis it is not possible to distinguish the top quark, bottom quark, and heavy BSM particle contributions in the gluon fusion loop. As such, the Hgg coupling is treated as an effective coupling with heavy degrees of freedom integrated out.

## 3 The CMS detector

The CMS apparatus [33] is a multipurpose, nearly hermetic detector, designed to identify electrons, muons, photons, and (charged and neutral) hadrons [34–37]. A global reconstruction "particle-flow" (PF) algorithm [38] combines the information provided by the all-silicon inner tracker and by the crystal electromagnetic and brass-scintillator hadron calorimeters, operating inside a 3.8 T superconducting solenoid, with data from gas-ionization muon detectors interleaved with the solenoid return yoke, to build $\tau$ leptons, jets, missing transverse momentum, and other physics objects [39–41].

Events of interest are selected using a two-tiered trigger system [42, 43]. The first level (L1), composed of custom hardware processors, uses information from the calorimeters and muon detectors to select events at a rate of around 100 kHz within a fixed latency of about 4 $\mu$s [42]. The second level, known as the high-level trigger (HLT), consists of a farm of processors running a version of the full event reconstruction software optimized for fast processing, and reduces the event rate to around 1 kHz before data storage [43]. A more detailed description of the CMS detector, together with a definition of the coordinate system and kinematic variables, can be found in Ref. [33].

## 4 Data sets and simulation

The data sets included in this analysis were recorded with the CMS detector in 2016, 2017, and 2018, and correspond to integrated luminosities of 36.3, 41.5, and 59.7 fb$^{-1}$, respectively [44–46]. The collision events must fulfill HLT selection criteria that require the presence of one or two leptons satisfying isolation and identification requirements. For the 2016 data set, the single-electron trigger has a transverse momentum ($p_T$) threshold of 25 GeV for electrons with pseudorapidity $|\eta| < 2.1$ and 27 GeV for $2.1 < |\eta| < 2.5$, whereas the single-muon trigger has a $p_T$ threshold of 24 GeV for $|\eta| < 2.4$. For the 2017 (2018) data set, the $p_T$ threshold is 35 (32) GeV for the single-electron trigger (covering $|\eta| < 2.5$) and 27 (24) GeV for the single-muon trigger ($|\eta| < 2.4$). The dilepton e$\mu$ trigger has $p_T$ thresholds of 23 and 12 GeV for the leading and subleading leptons, respectively, with the same coverage in pseudorapidity for electrons and muons as above. During the first part of data taking in 2016, a lower $p_T$ threshold of 8 GeV for the subleading muon was used.

Monte Carlo event generators are used to model the signal and background processes. For each process, three independent sets of simulated events, corresponding to the three years of data taking, are used. This approach includes year-dependent effects in the CMS detector, data taking, and event reconstruction. All simulated events corresponding to a given data set share the same set of parton distribution functions (PDFs), underlying event (UE) tune, and parton shower (PS) configuration. The PDF sets used are NNPDF 3.0 [47, 48] for 2016 and NNPDF 3.1 [49] for 2017 and 2018. The CUETP8M1 [50] tune is used to describe the UE in 2016 simulations, whereas the CP5 [51] tune is adopted in 2017 and 2018 simulated events. The MC samples are interfaced with PYTHIA 8.226 [52] in 2016, and 8.230 in 2017 and 2018, for the modeling of UE, PS, and hadronization. Standard Model Higgs boson production through ggH, VBF, and VH is simulated at next-to-leading order (NLO) accuracy in quantum chromodynamics (QCD), including finite quark mass effects, using POWHEG v2 [53–59]. The MINLO HVJ [58] extension of POWHEG v2 is used for the simulation of WH and quark-induced ZH production, providing NLO accuracy for the VH + 0- and 1-jet processes. For ggH production, the simulated events are weighted to match the NNLOPS [60, 61] prediction in the hadronic jet multiplicity ($N_{jet}$) and Higgs boson $p_T$ distributions. The weighting is based on $p_T$ and $N_{jet}$ as computed in the simplified template cross section scheme 1.0 [62]. The MINLO HJJ [63] generator, which provides NLO accuracy for $N_{jet} \geq 2$, is also used for ggH production. The associated production processes with top quarks ($t\bar{t}H$) and bottom quarks ($b\bar{b}H$) are simulated with POWHEG v2 and MADGRAPH5_aMC@NLO v2.2.2 [64], respectively, and have a negligible contribution in the analysis phase space. All SM Higgs boson samples are normalized to the cross sections recommended in Ref. [19]. The Higgs boson mass in the event generation is assumed to be 125 GeV, while a value of 125.38 GeV [65] is used for the calculation of cross sections and branching fractions. The decay to a pair of W bosons and subsequently to leptons or hadrons is performed using the JHUGEN v5.2.5 generator in 2016, and v7.1.4 in 2017 and 2018, for ggH, VBF, and quark-

induced ZH samples. The Higgs boson and W boson decays are performed using PYTHIA 8.212 for the other signal simulations.

The ggH, VBF, and VH Higgs boson events with HVV anomalous couplings are generated with JHUGEN at LO accuracy. With respect to the $\kappa_2^{Z\gamma}/(\Lambda_1^{Z\gamma})^2$ coupling parameter discussed in Section 2, the sign convention of the photon field is determined by the sign in front of the gauge fields in the covariant derivative. In this analysis, we define the covariant derivative $D_\mu = \partial_\mu - ie\sigma^i W_\mu^i/(2s_w) + ieB_\mu/(2c_w)$ following the convention in JHUGEN [31]. The JHUGEN and POWHEG SM Higgs boson simulations were compared after parton showering and no significant differences in the distributions of kinematic observables were found. We adopt the JHUGEN simulation to describe the kinematic features in all production modes with HVV anomalous couplings. The expected yields are scaled to match the SM theoretical predictions [19] for inclusive cross sections and the POWHEG SM prediction of relative event yields in the event categorization based on associated particles. Simulation of the ggH + 2 jets process with Hgg anomalous couplings is done using MINLO X0JJ [66] at NLO in QCD. A large number of signal samples with various anomalous couplings were generated. The MELA package [20–24] contains a library of matrix elements from JHUGEN for different Higgs boson signal hypotheses. Matrix elements from different coupling signal hypotheses, but with the same production mechanism, are used to reweight the generated signal events. This procedure is used in the construction of the predictions for the different coupling components and their interference, allowing us to cover all points in the signal model phase space with sufficient statistical precision.

Background events are produced using several simulations. The quark-initiated nonresonant WW process is simulated with POWHEG v2 [67] at NLO accuracy for inclusive production. A reweighting is performed to match the diboson $p_T$ spectrum computed at NNLO+NNLL QCD accuracy [68, 69]. The MCFM v7.0 [70–72] generator is used to simulate gluon-induced WW production at LO accuracy, with the normalization chosen to match the NLO cross section [73]. Nonresonant EW production of WW pairs with two additional jets is simulated at LO accuracy with MADGRAPH5_aMC@NLO v2.4.2 using the MLM matching and merging scheme [74]. Top quark pair production ($t\bar{t}$) and single top quark processes, including tW, s- and t-channel contributions, are simulated with POWHEG v2 [75–77]. A reweighting of the top quark and antiquark $p_T$ spectrum at parton level is performed for the $t\bar{t}$ simulation in order to match the NNLO and next-to-next-to-leading logarithm (NNLL) QCD predictions, including also the NLO EW contribution [78].

The Drell–Yan (DY) production of a charged-lepton pair is simulated with MADGRAPH5_aMC@NLO v2.4.2 at NLO accuracy with up to two additional partons, using the FxFx matching and merging scheme [79]. Production of a W boson associated with an initial state radiation photon ($W\gamma$) is simulated with MADGRAPH5_aMC@NLO v2.4.2 at NLO accuracy with up to 1 additional parton, using the FxFx jet merging. Diboson processes containing at least one Z boson or a virtual photon ($\gamma^*$) with a mass as low as 100 MeV are generated with POWHEG v2 [67] at NLO accuracy. Production of a W boson in association with a $\gamma^*$ ($W\gamma^*$) for masses below 100 MeV is simulated by PYTHIA 8.212 in the parton showering of $W\gamma$ events. Triboson processes with inclusive decays are also simulated at NLO accuracy with MADGRAPH5_aMC@NLO v2.4.2.

For all processes, the detector response is simulated using a detailed description of the CMS detector, based on the GEANT4 toolkit [80]. The distribution of additional pp interactions within the same or nearby bunch crossings (pileup) in the simulation is reweighted to match that observed in data. The efficiency of the trigger system is evaluated in data on a per lepton

basis using dilepton events consistent with the Z boson decay. The overall efficiencies of the trigger selections used in the analysis are obtained as the average of the per-lepton efficiencies weighted by their probability. The resulting efficiencies are applied directly on simulated events.

## 5 Event reconstruction

The identification and measurement of the properties of individual particles (PF candidates) in an event is achieved in the PF algorithm by combining information from various subdetectors. Electrons are identified and their momenta are measured in the pseudorapidity interval $|\eta| < 2.5$ by combining tracks in the silicon tracker with spatially compatible energy deposits in the electromagnetic calorimeter. Muons are identified and their momenta are measured in the pseudorapidity range $|\eta| < 2.4$ by matching tracks in the muon system and the silicon tracker. For better rejection of nonprompt leptons, increasing the sensitivity of the analysis, leptons are required to be isolated and well reconstructed using a set of criteria based on the quality of the track reconstruction, shape of calorimetric deposits, and energy flux in the vicinity of the particle's trajectory [34, 35]. In addition, a selection based on a dedicated multivariate analysis (MVA) tagger developed for the CMS $\mathrm{t\bar{t}H}$ analysis [81] is added in all channels for muon candidates.

Multiple pp interaction vertices are identified from tracking information by use of the adaptive vertex fitting algorithm [82]. The primary pp interaction vertex is taken to be the vertex corresponding to the hardest scattering in the event, evaluated using tracking information alone, as described in Section 9.4.1 of Ref. [83]. Leptons are required to be associated to the primary vertex using transverse and longitudinal impact parameter criteria [34, 35].

Hadronic jets are clustered from PF candidates using the infrared- and collinear-safe anti-$k_{\mathrm{T}}$ algorithm with distance parameters of 0.4 (AK4) and 0.8 (AK8). The jet momentum is determined as the vectorial sum of all particle momenta in the jet. The AK8 jets considered are required to be reconstructed within the silicon tracker acceptance ($|\eta| < 2.4$), whereas AK4 jets are reconstructed in the range $|\eta| < 4.7$. For AK4 jets, contamination from pileup is suppressed using charged-hadron subtraction which removes charged PF candidates originating from vertices other than the primary interaction vertex. The residual contribution from neutral particles originating from pileup vertices is removed by means of an event-by-event jet-area-based correction to the jet four-momentum [84]. For AK8 jets, the pileup-per-particle identification algorithm (PUPPI) [85] is used to mitigate the effect of pileup at the reconstructed-particle level, making use of local shape information, event pileup properties, and tracking information. Additional selection criteria are applied to remove jets potentially dominated by instrumental effects or reconstruction failures [84].

The AK8 jets are used to reconstruct hadronic V boson decays in a single merged jet when the decay products are highly collimated. This approach targets boosted W or Z bosons originating from the VH production mode. Such Lorentz-boosted V decays are identified using the ratio of the 2- to 1-subjettiness [86], $\tau_2/\tau_1$, and the groomed jet mass $m_{\mathrm{J}}$. The groomed mass is calculated after applying a modified mass drop algorithm [87, 88], known as the soft-drop algorithm [89], with parameters $\beta = 0$, $z_{\mathrm{cut}} = 0.1$, and $R_0 = 0.8$. The algorithm also identifies two hard subjets within the AK8 jet.

We refer to the identification of jets likely originating from bottom quarks as b tagging [90, 91]. For each AK4 jet in the event, a score is calculated through a multivariate combination of different jet properties, making use of boosted decision trees and deep neural networks. A jet

is considered b-tagged if its associated score exceeds a threshold, tuned to achieve a certain tagging efficiency as measured in $\mathrm{t\bar{t}}$ events. The chosen working point corresponds to about 90% efficiency for bottom quark jets and to a mistagging rate of about 10% for light-flavor or gluon jets and of about 50% for charm quark jets.

The missing transverse momentum vector $\vec{p}_{\mathrm{T}}^{\,\mathrm{miss}}$ is computed as the negative vector sum of the transverse momenta of all the PF candidates in an event, and its magnitude is denoted as $p_{\mathrm{T}}^{\mathrm{miss}}$ [41]. The PUPPI algorithm is applied to reduce the pileup dependence of the $\vec{p}_{\mathrm{T}}^{\,\mathrm{miss}}$ observable by computing the $\vec{p}_{\mathrm{T}}^{\,\mathrm{miss}}$ from the PF candidates weighted by their probability to originate from the primary interaction vertex [41].

## 6 Event selection

The analysis is performed using $\mathrm{H} \to \mathrm{WW}$ candidate events in the $\mathrm{e}\mu$ final state. For an event to be selected, the transverse momenta of the leading lepton $p_{\mathrm{T}}^{\ell 1}$ and the subleading lepton $p_{\mathrm{T}}^{\ell 2}$ must be greater than 25 and 13 GeV, respectively. The $p_{\mathrm{T}}^{\ell 2}$ threshold in the case of a muon is lowered to 10 GeV for the 2016 data set because of the lower threshold in the corresponding HLT algorithm. Events containing additional leptons with $p_{\mathrm{T}} > 10$ GeV are discarded. The dilepton system is required to have an invariant mass $m_{\ell\ell}$ greater than 12 GeV and transverse momentum $p_{\mathrm{T}}^{\ell\ell}$ above 30 GeV. A requirement on the missing transverse momentum of $p_{\mathrm{T}}^{\mathrm{miss}} > 20$ GeV is implemented. We define transverse mass discriminating variables $m_{\mathrm{T}}^{\mathrm{H}}$ and $m_{\mathrm{T}}^{\ell 2}$ as

$$m_{\mathrm{T}}^{\mathrm{H}} = \sqrt{2 p_{\mathrm{T}}^{\ell\ell} p_{\mathrm{T}}^{\mathrm{miss}} [1 - \cos \Delta\Phi(\vec{p}_{\mathrm{T}}^{\,\ell\ell}, \vec{p}_{\mathrm{T}}^{\,\mathrm{miss}})]}, \tag{17}$$

$$m_{\mathrm{T}}^{\ell 2} = \sqrt{2 p_{\mathrm{T}}^{\ell 2} p_{\mathrm{T}}^{\mathrm{miss}} [1 - \cos \Delta\Phi(\vec{p}_{\mathrm{T}}^{\,\ell 2}, \vec{p}_{\mathrm{T}}^{\,\mathrm{miss}})]}, \tag{18}$$

and select events with $m_{\mathrm{T}}^{\mathrm{H}} > 60$ GeV and $m_{\mathrm{T}}^{\ell 2} > 30$ GeV. The $m_{\mathrm{T}}^{\mathrm{H}}$ requirement suppresses the $\mathrm{DY} \to \tau\tau$ background process and avoids overlap with the $\mathrm{H} \to \tau\tau$ analysis [11]. To ensure orthogonality with a future off-shell $\mathrm{H} \to \mathrm{WW}$ analysis we require $m_{\mathrm{T}}^{\mathrm{H}} < 125$ GeV. In addition, the region $76.2 < m_{\ell\ell} < 106.2$ GeV is excluded to avoid overlap with the off-shell $\mathrm{H} \to \mathrm{ZZ} \to 2\ell 2\nu$ analysis [10]. These requirements will simplify a future combination of Higgs boson decay final states. Finally, events with any b-tagged jets with $p_{\mathrm{T}} > 20$ GeV are vetoed. These base selection criteria are summarized in Table 2.

Table 2: Summary of the base selection criteria.

| Variable | Selection |
|---|---|
| Number of leptons | 2 ($\mathrm{e}\mu$ of opposite charge) |
| $p_{\mathrm{T}}^{\ell 1}$ | >25 GeV |
| $p_{\mathrm{T}}^{\ell 2}$ | >13 GeV (10 GeV for 2016 data) |
| $m_{\ell\ell}$ | 12–76.2 GeV or >106.2 GeV |
| $p_{\mathrm{T}}^{\ell\ell}$ | >30 GeV |
| $p_{\mathrm{T}}^{\mathrm{miss}}$ | >20 GeV |
| $m_{\mathrm{T}}^{\ell 2}$ | >30 GeV |
| $m_{\mathrm{T}}^{\mathrm{H}}$ | 60–125 GeV |
| $N_{\mathrm{jet}}$ (b jets) | 0 |

For the HVV coupling analysis, exclusive selection criteria, which are based on the associated jet activity in the event, are applied that target the ggH, VBF, and VH production processes.

The AK4 (AK8) jets considered are required to have $p_T > 30\ (200)$ GeV. In the ggH channel, zero or one AK4 jet is required in the event. For the VBF and Resolved VH channels, we require two AK4 jets with dijet masses of $m_{jj} > 120$ GeV and $60 < m_{jj} < 120$ GeV, respectively. The Boosted VH channel requires the presence of a V-tagged AK8 jet (V jet); such jets have a groomed mass in the region $65 < m_J < 105$ GeV and satisfy the requirement $\tau_2/\tau_1 < 0.4$. In the other channels, a V jet veto is implemented to ensure orthogonality. These production channels for the HVV coupling study are summarized in Table 3.

Table 3: Summary of the ggH, VBF, and VH production channels used for the HVV coupling study.

| Variable | ggH | VBF | Resolved VH | Boosted VH |
|---|---|---|---|---|
| $N_{jet}$ (V jets) | 0 | 0 | 0 | >0 |
| $N_{jet}$ (AK4 jets) | 0 & 1 | 2 | 2 | — |
| $m_{jj}$ | — | >120 GeV | 60–120 GeV | — |

As the production vertex of the ggH + 2 jets process is sensitive to anomalous Hgg coupling effects, we use a 2-jet ggH channel that follows the VBF selection described above for the Hgg coupling analysis. The HWW decay vertex is not sensitive to anomalous Hgg effects, and so decay-based variables are not studied in this channel. This permits a relatively tight selection of $m_{\ell\ell} < 55$ GeV which is beneficial for background suppression. The 0- and 1-jet ggH channels are also included to constrain the ggH signal strength. All channels included for the Hgg coupling study are summarized in Table 4.

Table 4: Summary of ggH channel selections used for the Hgg coupling study.

| Variable | ggH | 2-jet ggH |
|---|---|---|
| $N_{jet}$ (AK4 jets) | 0 & 1 | 2 |
| $m_{jj}$ | — | >120 GeV |
| $m_{\ell\ell}$ | — | <55 GeV |

Control regions (CRs) are defined using the base selection criteria together with a set of alternative requirements summarized in Table 5. They are used to validate the background description and to estimate the number of background events in the signal region (SR). A dedicated $\tau\tau$ CR targets events from the DY process $Z \to \tau\tau$ with $\tau$ leptons decaying leptonically to produce the e$\mu$ final state. Also a top quark CR is defined to enhance events with one or more top quarks decaying to a W boson and bottom quark. Splitting events according to the number of associated jets, separate $\tau\tau$ and top quark CRs are defined for the 0-, 1- and 2-jet SRs. An additional CR with an enhanced contribution from the nonresonant WW background is used in the 2-jet SR. All CRs are used in the final data fit to constrain the DY, top quark, and WW background normalizations.

Table 5: Summary of the $\tau\tau$, top quark, and WW control region requirements.

| Variable | $\tau\tau$ | top quark | WW |
|---|---|---|---|
| $m_{\ell\ell}$ | 40–80 GeV | >50 GeV | >106.2 GeV |
| $m_T^H$ | <60 GeV | — | 60–125 GeV |
| $m_T^{\ell 2}$ | — | >30 GeV | >30 GeV |
| $N_{jet}$ (b jets) | 0 | >0 | 0 |

Additional $\tau\tau$, top quark, and WW CRs are defined requiring a V jet. These CRs are used to validate the background description in the Boosted VH channel. However, they generally do

not have a sufficient number of events to significantly constrain the background normalizations in the final fit to the data. As such, we rely on the 2-jet CRs to determine the normalizations to be used in the Boosted VH channel. Agreement between data and the background prediction in the V jet CRs is observed when using normalizations determined in the 2-jet CRs.

# 7 Background estimation

The nonprompt-lepton backgrounds originating from leptonic decays of heavy quarks, hadrons misidentified as leptons, and electrons from photon conversions are suppressed by identification and isolation requirements imposed on electrons and muons. In this analysis, the nonprompt-lepton background primarily originates from W+jets events and is estimated from data, as described in detail in Ref. [92]. The procedure involves measuring the rate at which a nonprompt lepton passing a loose selection further passes a tight selection (misidentification rate) and the corresponding rate for a prompt lepton to pass this selection (prompt rate). The misidentification rate is measured in a data sample enriched in multijet events, whereas the prompt rate is measured using a tag-and-probe method [93] in a data sample enriched in DY events. The nonprompt-lepton background estimation is validated with data in a CR enriched with W+jets events, in which a pair of same-sign leptons is required.

The backgrounds from top quark processes and nonresonant WW production are estimated using a combination of MC simulations and the dedicated CRs described in the previous section. The normalisations of these backgrounds are left as free parameters in the fit, keeping different parameters for each jet multiplicity region. The top quark background normalization is measured from the observed data in the top quark enriched CRs. A separate normalization parameter is included for the quark-induced and gluon-induced WW backgrounds. For the 2-jet regions, the WW enriched CR is used to constrain the WW background normalisation parameters. In the 0- and 1-jet channels, these parameters are constrained directly in the signal regions, which span the high $m_{\ell\ell}$ phase space enriched in WW events.

The DY $\to \tau\tau$ background process is estimated with a data-embedding technique [94]. As for the top quark and WW backgrounds, the DY normalization is left unconstrained in the data fit. The DY $\to \tau\tau$ enriched CR described in Section 6 is used to constrain the free normalization parameters in the 0-, 1-, 2-jet regions. The data-embedded samples cover the events that pass the e$\mu$ triggers, which represent the vast majority of the selected events. The remaining DY $\to \tau\tau$ events, which enter the analysis through the single-lepton triggers ($\approx$5% of the total), are estimated using MC simulation.

The WZ and W$\gamma^*$ background contributions are simulated as described in Section 4, and a data-to-simulation scale factor is derived in a three-lepton CR, as described in Ref. [92]. The contribution of the W$\gamma$ process may also be a background because of photon conversions in the detector material. This process is estimated using MC simulation and validated using data in a CR requiring events with a leading $\mu$ and a trailing e with same sign and a separation in $\Delta R = \sqrt{\Delta\phi^2 + \Delta\eta^2}$ (where $\phi$ is the azimuthal angle in radians) smaller than 0.5. Triple vector boson production is a minor background in all channels and is estimated using MC simulation.

# 8 Observables and kinematic discriminants

In this paper, we search for anomalous HVV and Hgg coupling effects by studying:

1. the two quark jets from VBF and VH production (HVV coupling);

2. the H → WW decay products (HVV coupling); and
3. the two quark jets from ggH + 2 jets production (Hgg coupling).

The VBF, VH, and ggH production and decay topologies relevant for the HVV coupling are illustrated in Fig. 1.

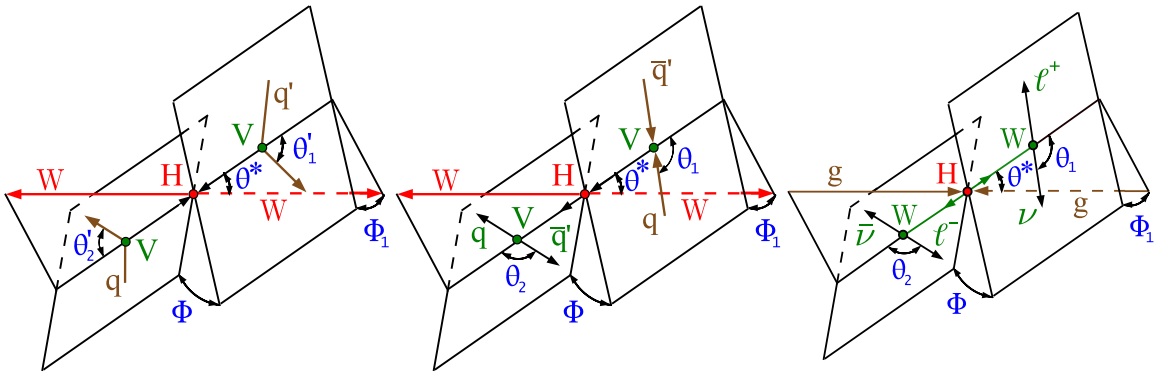


Figure 1: Topologies of the Higgs boson production and decay for vector boson fusion $qq' \to qq'H$ (left), $q\bar{q}' \to VH$ (center), and gluon fusion with decay $gg \to H \to 2\ell 2\nu$ (right). For the electroweak production topologies, the intermediate vector bosons and their decays are shown in green and the $H \to WW$ decay is marked in red. For the $gg \to H \to 2\ell 2\nu$ topology, the W boson leptonic decays are shown in green. In all cases, the incoming particles are depicted in brown and the angles characterizing kinematic distributions are marked in blue. Five angles fully characterize the orientation of the production and decay chain and are defined in the suitable rest frames.

When combined with the momentum transfer of the vector bosons, the five angles illustrated for VBF/VH production provide complete kinematic information for production and decay of the Higgs boson. The illustration for Higgs boson production via ggH in association with two jets is identical to the VBF diagram, except for replacing the intermediate vector bosons by gluons. Full production kinematic information is extracted for VBF, VH, and ggH + 2 jets candidate events using discriminants built from the matrix element calculations of the MELA package. The MELA approach is designed to reduce the number of observables to a minimum, while retaining all essential information. To form the production-based MELA kinematic discriminants, we use jets to reconstruct the four-momentum of the associated production particles. The presence of two neutrinos in the final state means it is not possible to reconstruct the four-momentum of all the Higgs boson decay products. Therefore, decay-based kinematic discriminants built from matrix elements are not used in this analysis. Instead, we rely on kinematic variables related to the measured final state of the Higgs boson decay. The strategies used for each of the topologies listed above are now discussed in more detail.

## 8.1 Kinematic features of two quark jets in VBF and VH channels

Kinematic distributions of associated particles in VBF and VH production are sensitive to the anomalous HVV couplings of the Higgs boson. As illustrated in Fig. 1, a set of seven observables can be defined for the VBF and VH production topologies : $\Omega = \{\theta_1^{(\prime)}, \theta_2^{(\prime)}, \theta^*, \Phi, \Phi_1, q_1^2, q_2^2\}$, with $q_1^2$ and $q_2^2$ the squared four-momenta of the vector bosons [22]. Three types of discriminants are defined using the full kinematic description characterized by $\Omega$. The first type of discriminant is designed to separate signal and background Higgs boson production processes:

$$\mathcal{D}_{\text{sig}} = \frac{\mathcal{P}_{\text{sig}}(\Omega)}{\mathcal{P}_{\text{sig}}(\Omega) + \mathcal{P}_{\text{bkg}}(\Omega)}, \tag{19}$$

where the probability density $\mathcal{P}$ for a specific process is calculated from the matrix elements provided by the MELA package. The second type of discriminant separates the anomalous coupling BSM process from that of the SM:

$$\mathcal{D}_{\text{BSM}} = \frac{\mathcal{P}_{\text{BSM}}(\Omega)}{\mathcal{P}_{\text{BSM}}(\Omega) + \mathcal{P}_{\text{SM}}(\Omega)}. \tag{20}$$

Throughout this document the generic BSM label is generally replaced by the specific anomalous coupling state targeted. For the $a_3$ $CP$-odd and $a_2$ $CP$-even coupling parameters, we use, respectively, $\mathcal{D}_{0-}$ and $\mathcal{D}_{0+}$, whereas for the $\Lambda_1$ coupling parameters we use $\mathcal{D}_{\Lambda_1}$ and $\mathcal{D}^{Z\gamma}_{\Lambda_1}$. The third type of discriminant isolates the interference contribution:

$$\mathcal{D}_{\text{int}} = \frac{\mathcal{P}^{\text{int}}_{\text{SM-BSM}}(\Omega)}{\mathcal{P}_{\text{SM}}(\Omega) + \mathcal{P}_{\text{BSM}}(\Omega)}, \tag{21}$$

where $\mathcal{P}^{\text{int}}_{\text{SM-BSM}}$ is the interference part of the probability distribution for a process with a mixture of the SM and BSM contributions. The $CP$ label is generally used for the $a_3$ coupling parameter, as the BSM signal in this case is a pseudoscalar and the interference discriminant is a $CP$-sensitive observable. The $\mathcal{P}$ values are normalized to give the same integrated cross sections in the relevant phase space of each process. Such normalization leads to a balanced distribution of events in the range between 0 and 1 for $\mathcal{D}_{\text{sig}}$ and $\mathcal{D}_{\text{BSM}}$, and between $-1$ and $+1$ for $\mathcal{D}_{\text{int}}$.

The selected events are split into three main production channels: VBF, Resolved VH, and Boosted VH. In the first two channels, the four-momenta of the two AK4 jets assigned as the associated particles are used in the MELA probability calculation. For the Boosted VH category, we use the four-momentum of the two subjets of the V-tagged AK8 jet. An estimate of the Higgs boson four-momentum is also required for the probability calculation. This can not be measured directly since the final state contains two neutrinos. As such, we construct a proxy Higgs boson four-momentum in the following manner. The $p_{\text{x}}$ and $p_{\text{y}}$ of the dineutrino system are estimated from the $\vec{p}_{\text{T}}^{\text{miss}}$ in a given event. The corresponding $p_{\text{z}}$ is then set to equal that of the dilepton system, which is based on the observed correlation between these variables at the generator level for simulated signals. Finally, the mass of the dineutrino system is set equal to the mean value of the generator-level dineutrino mass. The resulting four-momentum can then be combined with that of the measured dilepton system to create a proxy Higgs boson four-momentum. We note that the MELA probability calculation for the production vertices is largely based on the kinematic features of the associated particles, so the reconstruction of the proxy Higgs boson has a relatively small effect on the final discriminants. As an illustrative example of the MELA based discriminants used in this analysis, Fig. 2 shows the $\mathcal{D}_{0-}$ discriminant in the VBF and Resolved VH production channels for a number of different signal hypotheses. The discriminants are designed to target the dominant signal production process in a given channel.

In the VBF channel, a $\mathcal{D}_{\text{VBF}}$ discriminant is constructed, following Eq. (19), where $\mathcal{P}_{\text{sig}}$ corresponds to the probability for the VBF production hypothesis, and $\mathcal{P}_{\text{bkg}}$ corresponds to that of gluon fusion production in association with two jets. The discriminant is also suitable for separating SM backgrounds from the VBF signal process. In the Resolved and Boosted VH channels, the corresponding discriminants do not give a significant level of separation with

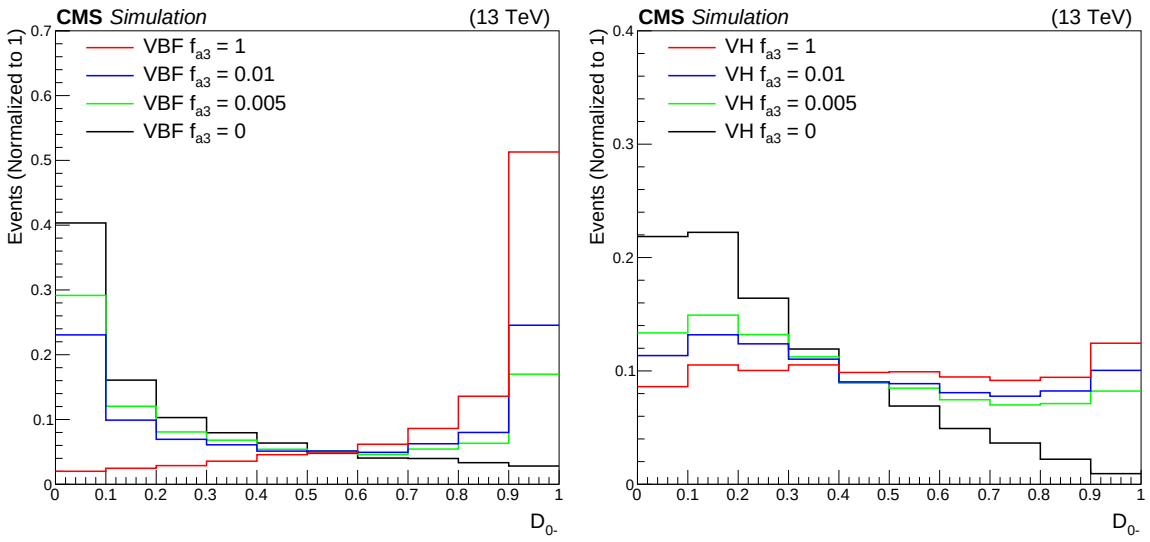


Figure 2: The $\mathcal{D}_{0-}$ discriminant in the VBF (left) and Resolved VH (right) production channels for a number of VBF (left) and VH (right) signal hypotheses. Pure $a_1$ ($f_{a3} = 0$) and $a_3$ ($f_{a3} = 1$) HVV signal hypotheses are shown along with two mixed coupling hypotheses ($f_{a3} = 0.005$ and $f_{a3} = 0.01$). All distributions are normalized to unity.

respect to ggH production or SM backgrounds. This is due to the relatively tight selection criteria, which limit the phase space to VH-like events. Hence, these discriminants are not included in the VH channels.

The $\mathcal{D}_{CP}$ discriminant is sensitive to the sign of the interference between the $CP$-even SM and $CP$-odd BSM states. An asymmetry between the number of events detected with positive and negative $\mathcal{D}_{CP}$ values is expected for mixed $CP$ states. Therefore, a forward-backward categorization (forward defined as $\mathcal{D}_{CP} > 0$ and backward as $\mathcal{D}_{CP} < 0$) is used to analyze the $CP$-odd couplings. Similarly, $\mathcal{D}_{\text{int}}$ gives sensitivity to the sign of the interference between the SM and $a_2$ HVV BSM states. A forward-backward $\mathcal{D}_{\text{int}}$ categorization is also included. The value of $\mathcal{D}_{\text{int}}$ used to define the categories is chosen to symmetrize the SM Higgs boson expectation. In the case of the $\Lambda_1$ measurements, the interference discriminants were shown to be highly correlated with the $\mathcal{D}_{\text{BSM}}$ discriminants and so are not considered.

We now discuss the categorization and construction of the final multidimensional discriminants used for the two HVV coupling approaches defined in Section 2. The binning of the final discriminants was optimized to ensure sufficient statistical precision in the predictions of all bins, while retaining the kinematic information required to discriminate between the SM and anomalous coupling signal hypotheses.

### 8.1.1 VBF/VH analysis strategy for Approach 1

In Approach 1, each of the four anomalous HVV coupling parameters ($a_2$, $a_3$, $\kappa_1/(\Lambda_1)^2$, and $\kappa_2^{Z\gamma}/(\Lambda_1^{Z\gamma})^2$) are analyzed separately. For this purpose, we construct a multidimensional discriminant for each of the four anomalous couplings in the VBF, Resolved VH, and Boosted VH channels.

In the VBF channel, we use two bins of the production discriminant $\mathcal{D}_{\text{VBF}}$, corresponding to low and high purity, using a bin boundary of 0.75. The $m_{\ell\ell}$ variable, which is sensitive to anomalous effects at the H $\to$ WW decay vertex, is included with two bins in the range 12–76.2 GeV. A bin boundary of 45 GeV is chosen based on the expected signal shape changes

induced by anomalous effects. Finally, one of the $\mathcal{D}_{\text{BSM}}$ discriminants is included with ten equally sized bins. Depending on the anomalous coupling under study this discriminant may be $\mathcal{D}_{0+}$, $\mathcal{D}_{0-}$, $\mathcal{D}_{\Lambda_1}$ or $\mathcal{D}_{\Lambda_1}^{Z\gamma}$.

For the VH channels, the $m_{\ell\ell}$ and $\mathcal{D}_{\text{BSM}}$ observables are used to build 2D kinematic discriminants. The $m_{\ell\ell}$ bins are the same as for the VBF channel. In the Resolved VH channel, we use four $\mathcal{D}_{\text{BSM}}$ bins of equal size. For the Boosted VH case, three variable bins with boundaries of 0.6 and 0.8 are used, a large first bin is chosen because relatively little signal is expected at low values of $\mathcal{D}_{\text{BSM}}$. A distinct multidimensional discriminant is constructed for each anomalous coupling hypothesis in the VH channels.

For the $a_3$ coupling parameter, a forward-backward categorization of events based on $\mathcal{D}_{CP}$ is implemented. In the case of the $a_2$ coupling parameter, $\mathcal{D}_{\text{int}}$ is largely correlated with $\mathcal{D}_{0+}$ in the VH channels. Therefore, a forward-backward $\mathcal{D}_{\text{int}}$ categorization is implemented only in the VBF channel. Figures 3–5 show the discriminants used in the final fit to the data for the $a_2$, $a_3$, $\kappa_1/(\Lambda_1)^2$, and $\kappa_2^{Z\gamma}/(\Lambda_1^{Z\gamma})^2$ Approach 1 coupling studies in the VBF and VH channels. A summary of the observables used in the HVV Approach 1 analysis may be found in Table 6.

### 8.1.2 VBF/VH analysis strategy for Approach 2

In Approach 2, we use one categorization strategy and build one multidimensional discriminant in each channel to target all the HVV coupling parameters ($a_2$, $a_3$, $\kappa_1/(\Lambda_1)^2$) simultaneously. In the VBF channel, the $\mathcal{D}_{CP}$ and $\mathcal{D}_{\text{int}}$ discriminants are used to create four interference categories. Both $\mathcal{D}_{\text{VBF}}$ and $m_{\ell\ell}$ are used as for Approach 1. All three $\mathcal{D}_{\text{BSM}}$ discriminants that target the $a_2, a_3$ and $\kappa_1/(\Lambda_1)^2$ coupling parameters are included. However, the number of bins we implement is limited by the number of simulated events. Also the $\mathcal{D}_{\text{BSM}}$ discriminants are significantly correlated and so have similar performance for all couplings. Therefore, we use the $CP$-odd discriminant $\mathcal{D}_{0-}$ and just one of the $CP$-even discriminants, $\mathcal{D}_{0+}$, both with three bins and bin boundaries of 0.1 and 0.9. A dedicated rebinning strategy is applied to the $[\mathcal{D}_{0-}, \mathcal{D}_{0+}]$ distribution merging bins dominated by the SM Higgs boson prediction or with low precision in the background prediction. In the VH channels, just two categories using $\mathcal{D}_{CP}$ are defined and the discriminant is built using $m_{\ell\ell}$ as for Approach 1. Again, both $\mathcal{D}_{0-}$ and $\mathcal{D}_{0+}$ are chosen for the final discriminant. For the Resolved VH channel, we use three bins with boundaries of 0.25 and 0.75, whereas for the Boosted VH case we use two bins with a boundary of 0.8. The same rebinning strategy described for the VBF channel is applied to both Resolved and Boosted VH multidimensional discriminants. Table 6 includes a summary of the observables used in the HVV Approach 2 analysis.

## 8.2 Kinematic features of H $\rightarrow$ WW decay products in 0- and 1-jet ggH channels

Similar to the SM H $\rightarrow$ WW analysis [25], we use $m_{\ell\ell}$ and $m_{\text{T}}$ to build 2D discriminants in the 0- and 1-jet ggH channels. The distributions have nine bins for $m_{\ell\ell}$ in the range 12–200 GeV and six bins for $m_{\text{T}}$ in the range 60–125 GeV. The bin widths vary and are optimized to achieve good separation between the SM Higgs boson signal and backgrounds, as well as between the different anomalous coupling signal hypotheses. In particular, a finer binning with respect to the SM H $\rightarrow$ WW analysis is implemented in regions where anomalous effects are most significant. Figure 6 shows the $[m_{\text{T}}, m_{\ell\ell}]$ distributions in the 0- and 1-jet ggH channels. The same $[m_{\text{T}}, m_{\ell\ell}]$ discriminant is used to study all HVV anomalous couplings for both Approach 1 and 2.

### 8.3 Kinematic features of two quark jets in 2-jet ggH channel

For the Hgg coupling, we adopt a similar approach to the VBF $CP$ study, where the $CP$-odd $a_3$ HVV coupling parameter is included. In this case, the optimal observables are $\mathcal{D}_{0-}^{\text{ggH}}$ and $\mathcal{D}_{CP}^{\text{ggH}}$, targeting the $CP$-odd $a_3$ Hgg coupling parameter. A forward-backward categorization is implemented using $\mathcal{D}_{CP}^{\text{ggH}}$, and the $\mathcal{D}_{\text{VBF}}$ and $\mathcal{D}_{0-}^{\text{ggH}}$ observables are used to build 2D discriminants. The $m_{\ell\ell}$ variable is not considered in this case because it is not sensitive to anomalous Hgg effects. For $\mathcal{D}_{\text{VBF}}$, the bin boundary is relaxed to 0.5 to ensure sufficient ggH events are accepted in the more VBF-like bin. For $\mathcal{D}_{0-}$, eight (five) bins are used in the more (less) VBF-like bin with larger bin sizes at the extremes of the distribution to ensure sufficient precision in the background and signal predictions. The 0- and 1-jet channels discussed previously are also included in this study to constrain the ggH signal strength. The $[\mathcal{D}_{\text{VBF}}, \mathcal{D}_{0-}^{\text{ggH}}]$ distributions used to analyze the Hgg $a_3$ anomalous coupling in the 2-jet ggH channel are shown in Fig. 7. A summary of the observables used in the Hgg analysis is given in Table 6.

Table 6: The kinematic observables used for the interference based categorization and for the final discriminants used in the fits to data to study the HVV and Hgg couplings. For each of the anomalous HVV couplings in Approach 1, we have a dedicated analysis in the VBF and VH channels. In Approach 2, we use one analysis to target all anomalous HVV couplings simultaneously.

| Analysis | Channel | Categorization | Final discriminant |
|---|---|---|---|
| HVV Approach 1 | VBF ($a_2$) | $\mathcal{D}_{\text{int}}$ | $[\mathcal{D}_{\text{VBF}}, m_{\ell\ell}, \mathcal{D}_{0+}]$ |
| | VBF ($a_3$) | $\mathcal{D}_{CP}$ | $[\mathcal{D}_{\text{VBF}}, m_{\ell\ell}, \mathcal{D}_{0-}]$ |
| | VBF ($\kappa_1$) | — | $[\mathcal{D}_{\text{VBF}}, m_{\ell\ell}, \mathcal{D}_{\Lambda 1}]$ |
| | VBF ($\kappa_2^{Z\gamma}$) | — | $[\mathcal{D}_{\text{VBF}}, m_{\ell\ell}, \mathcal{D}_{\Lambda_1}^{Z\gamma}]$ |
| | VH ($a_2$) | — | $[m_{\ell\ell}, \mathcal{D}_{0+}]$ |
| | VH ($a_3$) | $\mathcal{D}_{CP}$ | $[m_{\ell\ell}, \mathcal{D}_{0-}]$ |
| | VH ($\kappa_1$) | — | $[m_{\ell\ell}, \mathcal{D}_{\Lambda 1}]$ |
| | VH ($\kappa_2^{Z\gamma}$) | — | $[m_{\ell\ell}, \mathcal{D}_{\Lambda_1}^{Z\gamma}]$ |
| | 0- & 1-jet ggH | — | $[m_{\text{T}}, m_{\ell\ell}]$ |
| HVV Approach 2 | VBF | $\mathcal{D}_{CP}$, $\mathcal{D}_{\text{int}}$ | $[\mathcal{D}_{\text{VBF}}, m_{\ell\ell}, \mathcal{D}_{0-}, \mathcal{D}_{0+}]$ |
| | VH | $\mathcal{D}_{CP}$ | $[m_{\ell\ell}, \mathcal{D}_{0-}, \mathcal{D}_{0+}]$ |
| | 0- & 1-jet ggH | — | $[m_{\text{T}}, m_{\ell\ell}]$ |
| Hgg | 2-jet ggH | $\mathcal{D}_{CP}^{\text{ggH}}$ | $[\mathcal{D}_{\text{VBF}}, \mathcal{D}_{0-}^{\text{ggH}}]$ |
| | 0- & 1-jet ggH | — | $[m_{\text{T}}, m_{\ell\ell}]$ |

## 9 Systematic uncertainties

The signal extraction is performed using binned templates to describe the various signal and background processes. Systematic uncertainties that change the normalization or shape of the templates are included. All the uncertainties are modeled as nuisance parameters that are profiled in the maximum likelihood fit described in Section 10. The systematic uncertainties arise from both experimental or theoretical sources.

### 9.1 Experimental uncertainties

The following experimental systematic uncertainties are included in the final fit to data:

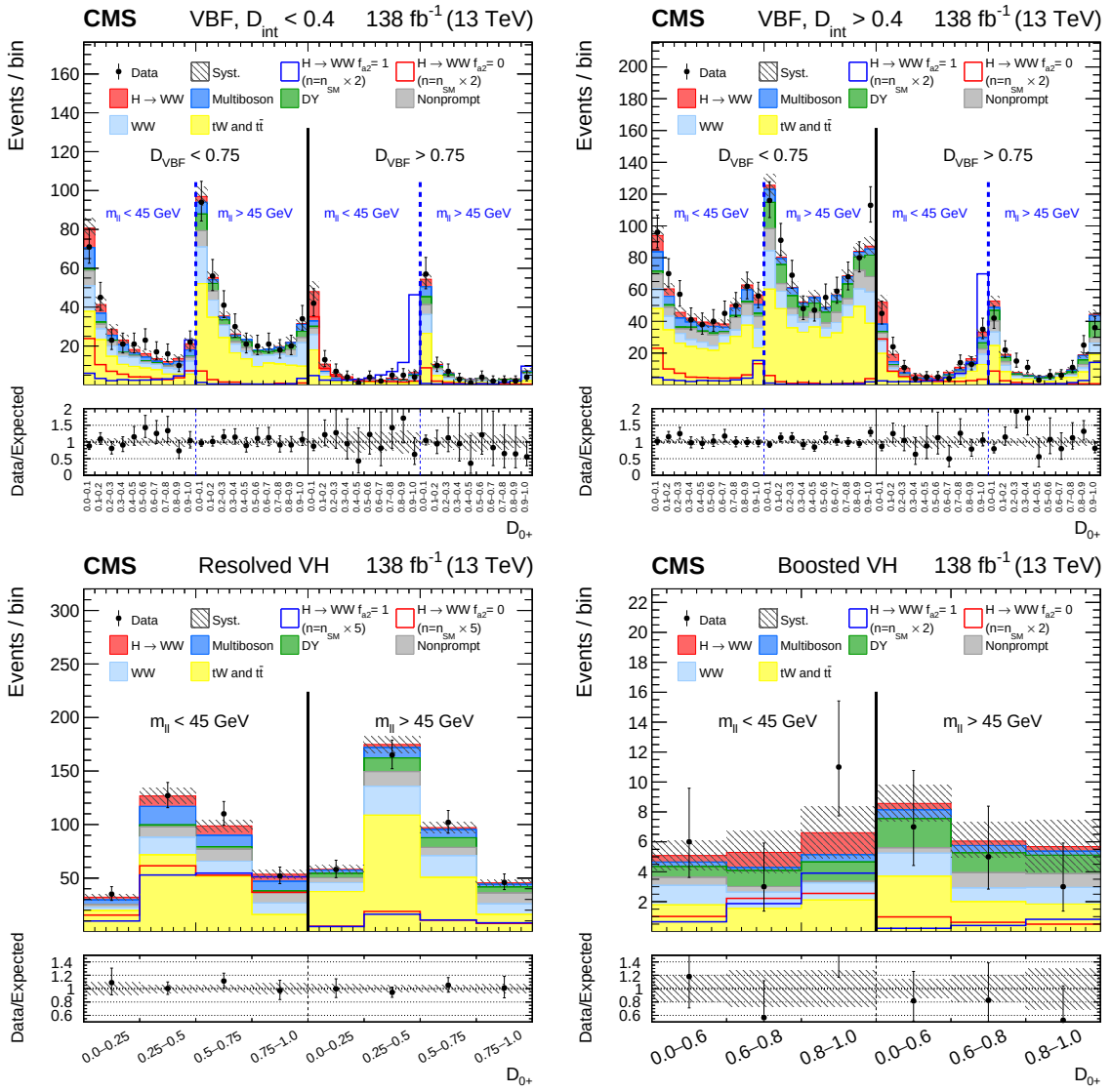


Figure 3: Observed and predicted distributions after fitting the data for $[\mathcal{D}_{\text{VBF}}, m_{\ell\ell}, \mathcal{D}_{0+}]$ in the VBF channel (upper), and for $[m_{\ell\ell}, \mathcal{D}_{0+}]$ in the Resolved VH (lower left) and Boosted VH (lower right) channels. For the VBF channel, the $\mathcal{D}_{\text{int}} < 0.4$ (left) and $\mathcal{D}_{\text{int}} > 0.4$ (right) categories are shown. The predicted Higgs boson signal is shown stacked on top of the background distributions. For the fit, the $a_1$ and $a_2$ HVV coupling contributions are included. The corresponding pure $a_1$ ($f_{a2} = 0$) and $a_2$ ($f_{a2} = 1$) signal hypotheses are also shown superimposed, their yields correspond to the predicted number of SM signal events scaled by an arbitrary factor to improve visibility. The uncertainty band corresponds to the total systematic uncertainty. The lower panel in each figure shows the ratio of the number of events observed to the total prediction.

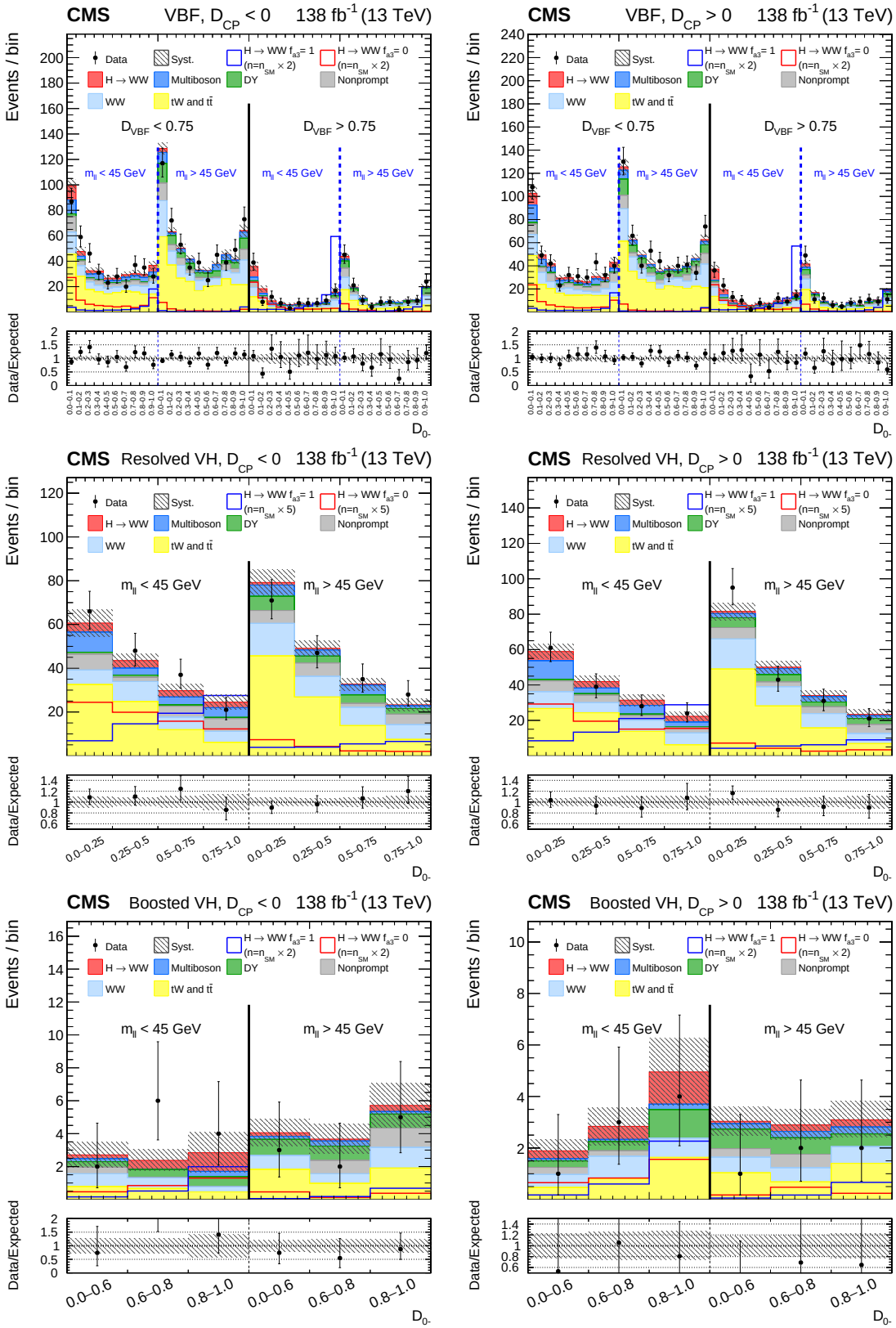


Figure 4: Observed and predicted distributions after fitting the data for $[\mathcal{D}_{\text{VBF}}, m_{\ell\ell}, \mathcal{D}_{0-}]$ in the VBF channel (upper), and for $[m_{\ell\ell}, \mathcal{D}_{0-}]$ in the Resolved VH (middle) and Boosted VH (lower) channels. For each channel, the $\mathcal{D}_{CP} < 0$ (left) and $\mathcal{D}_{CP} > 0$ (right) categories are shown. For the fit, the $a_1$ and $a_3$ HVV coupling contributions are included. More details are given in the caption of Fig. 3.

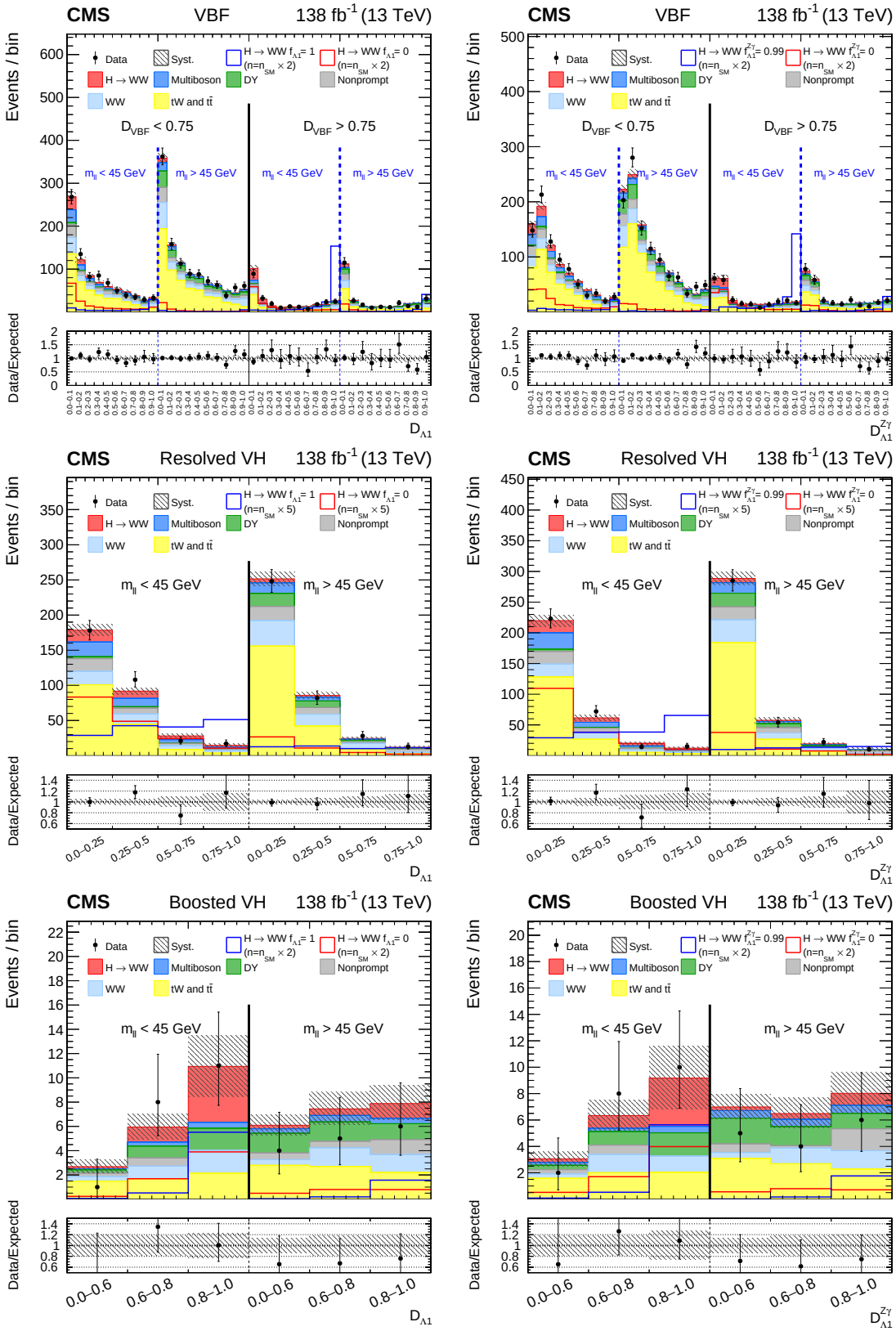


Figure 5: Observed and predicted distributions after fitting the data for $[\mathcal{D}_{\text{VBF}}, m_{\ell\ell}, \mathcal{D}_{\Lambda 1}]$ (upper left) and $[\mathcal{D}_{\text{VBF}}, m_{\ell\ell}, \mathcal{D}_{\Lambda 1}^{Z\gamma}]$ (upper right) in the VBF channel, and for $[m_{\ell\ell}, \mathcal{D}_{\Lambda 1}]$ (left) and $[m_{\ell\ell}, \mathcal{D}_{\Lambda 1}^{Z\gamma}]$ (right) in the Resolved VH (middle) and Boosted VH (lower) channels. For the fits, the $a_1$ and $\kappa_1/(\Lambda_1)^2$ (left) or $a_1$ and $\kappa_2^{Z\gamma}/(\Lambda_1^{Z\gamma})^2$ (right) HVV coupling contributions are included. More details are given in the caption of Fig. 3.

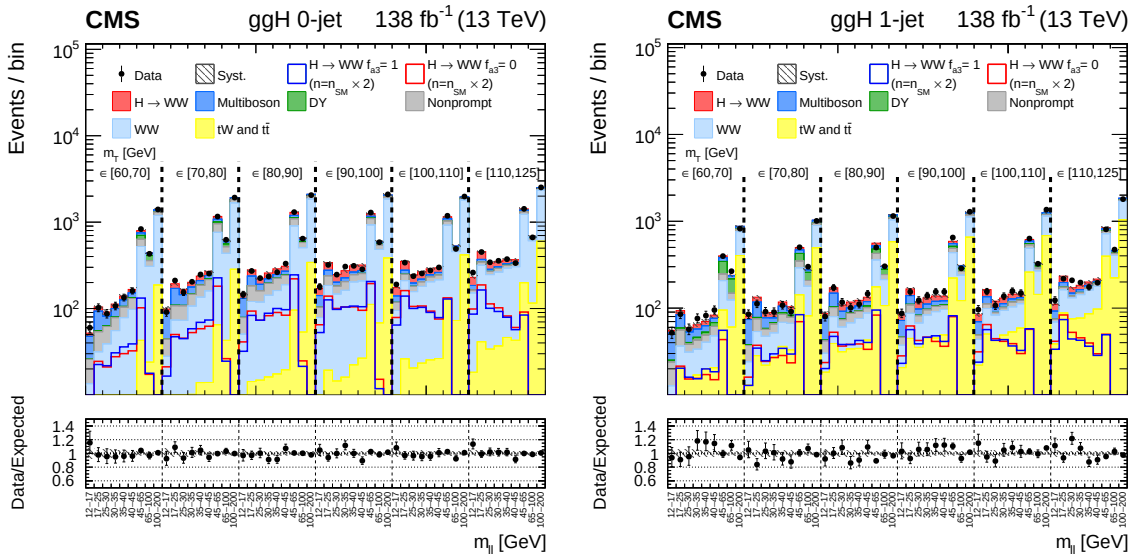


Figure 6: Observed and predicted distributions after fitting the data for $[m_{\mathrm{T}}, m_{\ell\ell}]$ in the 0- (left) and 1-jet (right) ggH channels. For the fit, the $a_1$ and $a_3$ HVV coupling contributions are included. More details are given in the caption of Fig. 3.

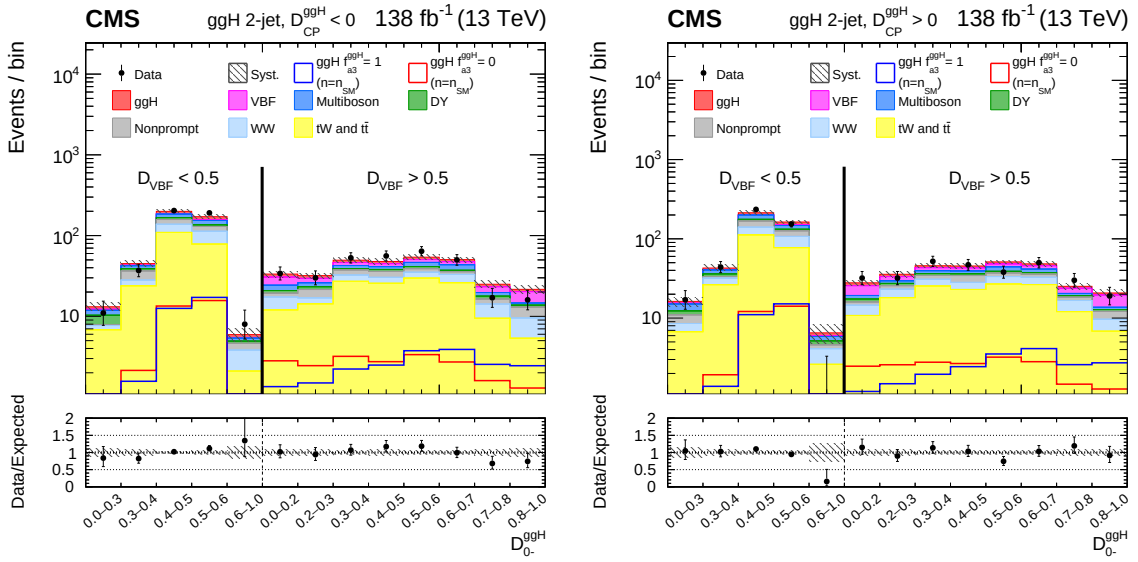


Figure 7: Observed and predicted distributions after fitting the data for $[\mathcal{D}_{\mathrm{VBF}}, \mathcal{D}_{0-}^{\mathrm{ggH}}]$ in the 2-jet ggH channel. Both the $\mathcal{D}_{\mathrm{CP}}^{\mathrm{ggH}} < 0$ (left) and $\mathcal{D}_{\mathrm{CP}}^{\mathrm{ggH}} > 0$ (right) categories are shown. In this case, the VBF and ggH signals are shown separately. For the fit, the $a_2^{\mathrm{gg}}$ and $a_3^{\mathrm{gg}}$ coupling contributions are included. The corresponding pure $a_2^{\mathrm{gg}}$ ($f_{a3}^{\mathrm{ggH}} = 0$) and $a_3^{\mathrm{gg}}$ ($f_{a3}^{\mathrm{ggH}} = 1$) signal hypotheses are also shown superimposed, their yields correspond to the predicted number of SM signal events. More details are given in the caption of Fig. 3.

- The total uncertainty associated with the measurement of the integrated luminosity for 2016, 2017, and 2018 is 1.2% [44], 2.3% [45], and 2.5% [46], respectively. This uncertainty is partially correlated among the three data sets, resulting in an overall uncertainty of 1.6%.
- The systematic uncertainty in the trigger efficiency is determined by varying the tag lepton selection criteria and the Z boson mass window used in the tag-and-probe

method. It affects both the normalization and the shape of the signal and background distributions, and is kept uncorrelated among data sets. The total normalization uncertainty is less than 1%.

- The tag-and-probe method is also used to determine the lepton identification and isolation efficiency. Corrections are applied to account for any discrepancy in the efficiencies measured in data and simulation. The corresponding systematic uncertainty is about 1% for electrons and 2% for muons.
- The uncertainties in the determination of the lepton momentum scale mainly arise from the limited data sample used for their estimation. The impact on the normalization of the signal and background templates ranges between 0.6–1.0% for the electron momentum scale and is about 0.2% for the muon momentum scale. They are treated as uncorrelated among the three data-taking years.
- The jet energy scale uncertainty is modeled by implementing eleven independent nuisance parameters corresponding to different jet energy correction sources, six of which are correlated among the three data sets. Their effects vary in the range of 1–10%, mainly depending on the jet multiplicity in the analysis phase space. Another source of uncertainty arises from the jet energy resolution smearing applied to simulated samples to match the $p_{\mathrm{T}}$ resolution measured in data. The effect varies in a range of 1–5%, depending on the jet multiplicity and is uncorrelated among the data sets. These uncertainties are included for both AK4 and AK8 jets. In addition, the $m_{\mathrm{J}}$ scale and resolution, and V tagging corrections with their corresponding uncertainties are included for V-tagged AK8 jets. These variables are calibrated in a top quark-antiquark sample enriched in hadronically decaying W bosons [95].
- The effects of the unclustered energy scale, jet energy scale, and lepton $p_{\mathrm{T}}$ scales are included for the calculation of the missing transverse momentum. The resulting normalization systematic uncertainty is 1–10% and is treated as uncorrelated among the years.
- Both the normalization and shape of the signal and background templates are affected by the jet pileup identification uncertainty. The effect is below 1%.
- The uncertainty associated with the b tagging efficiency is modeled by seventeen nuisance parameters out of which five are of a theoretical origin and are correlated among the three data sets. The remaining set of four parameters per data set are treated as uncorrelated as they arise from the statistical accuracy of the efficiency measurement [90].
- Estimation of the nonprompt-lepton background is affected by the limited size of the data sets used for the misidentification rate measurements. It is also affected by the difference in the flavor composition of jets misidentified as leptons between the misidentification rate measurement region (enriched in multijet events) and the signal phase space. The effects on the nonprompt-lepton background estimation range between a few percent to about 10% depending on the SR and are treated as nuisance parameters uncorrelated between electrons and muons and among the three data sets. A normalization uncertainty of 30% [92] is assigned to fully cover for any discrepancies with respect to data in a W+jets CR and is treated as uncorrelated among data sets.
- The statistical uncertainties due to the limited number of simulated events are also included for all bins of the background distributions used to extract the results [96].

### 9.2 Theoretical uncertainties

Multiple theoretical uncertainties are considered and are correlated among data sets, unless stated otherwise:

- The uncertainties related to the choice of PDF and $\alpha_S$ have a minor effect on the shape of the distributions. Therefore, only normalization effects related to the event acceptance and to the cross section are included. However, these uncertainties are not considered for the backgrounds that have their normalization constrained through data in dedicated CRs. For the Higgs boson signal processes, these uncertainties are calculated by the LHC Higgs cross section working group [19].
- The theoretical uncertainties arising from missing higher-order corrections in the cross section calculations are also included. Background simulations are reweighted to the alternative scenarios corresponding to renormalization $\mu_R$ and factorization $\mu_F$ scales varied by factors 0.5 or 2 and the envelopes of the varied templates are taken as the one standard deviations. For background processes that have their normalization constrained through data in dedicated CRs, we consider only the shape effect of the uncertainties coming from the missing higher-order corrections. The WW nonresonant background has the uncertainties derived by varying $\mu_R$, $\mu_F$, and the resummation scale. For the ggH and VBF signal processes, the effects of the missing higher-order corrections on the overall cross section are decoupled into multiple sources according to the recipes described in Ref. [19].
- The uncertainty due to the pileup modeling was included for the main simulated background processes (DY, WW, top quark) as well as the ggH and VBF signals. The effect is determined by varying the total inelastic pp cross section (69.2 mb [97, 98]) within the assigned 5% uncertainty.
- The PS modeling mainly affects the jet multiplicity, causing migration of events between categories that results in template shape changes. Associated uncertainties are evaluated by reweighting events with varied PS weights computed with PYTHIA 8.212. The effect on the signal strength is found to be below 1%.
- Uncertainties associated with UE modeling are evaluated by varying the UE tune parameters used in the MC sample generation. Systematic uncertainties are correlated between the 2017 and 2018 data sets since they share the same UE tunes, whereas for 2016 the uncertainty is considered uncorrelated. The UE uncertainty has a minimal effect on the template shapes and affects the normalization by about 1.5%.
- A 15% uncertainty is applied to the relative fraction of the gg-induced component in nonresonant WW production [99]. The relative fraction between single top quark and $t\bar{t}$ processes is assigned a systematic uncertainty of 8% [100]. Additional process-specific (DY, VZ, V$\gamma$, V$\gamma^*$) uncertainties, related to corrections to account for possible discrepancies between data and simulation, are assigned and are correlated among data sets.

## 10 Results

The optimization and validation of the analysis were performed using simulation and data in CRs. The data in the SRs were examined once all details of the analysis were finalized. For the final results, we perform a binned maximum likelihood fit to the data combining all channels and data-taking periods. The statistical approach was developed by the ATLAS and CMS Collaborations in the context of the LHC Higgs Combination Group [101]. The likelihood

function is defined for candidate events as:

$$\mathcal{L}(\text{data}|\mu_{\text{ggH}}, \mu_{\text{EW}}, f_{ai}, \theta) = \prod_{\text{j}} \text{Poisson}(n_{\text{j}}|s_{\text{j}}(\mu_{\text{ggH}}, \mu_{\text{EW}}, f_{ai}, \theta) + b_{\text{j}}(\theta))p(\tilde{\theta}|\theta), \quad (22)$$

where j runs over all bins and $n_{\text{j}}$ is the observed number of data events in each bin. Total signal and background expectations in each bin are represented by $s_{\text{j}}$ and $b_{\text{j}}$, respectively. The individual signal and background processes considered in each category are described using binned templates of multidimensional discriminants as described in Section 8. Each signal process is parametrized as a linear combination of terms originating from the SM, and anomalous couplings and their interference. The signal expectation depends on the parameters $\mu_{\text{ggH}}$, $\mu_{\text{EW}}$, and $f_{ai}$, and is constrained by the data fit. Both the signal and background expectations are functions of $\theta$, which represents the full set of nuisance parameters corresponding to the systematic uncertainties. The CRs described in Section 6 are included in the fit in the form of single bins, representing the number of events in each CR.

The $\mu_{\text{ggH}}$ and $\mu_{\text{EW}}$ parameters correspond to the Higgs boson signal strength modifiers for the ggH and VBF/VH signals, respectively. Signal yields for the VBF and VH processes are related to each other because the same HVV couplings enter both in production and decay of the Higgs boson. The ggH signal is initiated predominantly by the top fermion couplings and is unrelated to the VBF and VH production mechanisms. As the signal strength modifiers are free parameters in the fit, the overall signal event yield is not used to discriminate between alternative signal hypotheses. The $f_{ai}$ parameter corresponds to the anomalous coupling cross section fraction and determines the shape of the signal expectation. The cross section fraction for the SM coupling is simply taken as $1 - |f_{ai}|$. In Approach 1, the SM and just one anomalous HVV coupling are included, and each $f_{ai}$ is thus studied independently. Depending on the particular anomalous coupling under investigation, $f_{ai}$ may represent $f_{a2}$, $f_{a3}$, $f_{\Lambda 1}$, or $f_{\Lambda 1}^{\text{Z}\gamma}$. For Approach 2, the SM and three anomalous HVV couplings are included. In this case, $f_{ai}$ represents $f_{a2}$, $f_{a3}$ and $f_{\Lambda 1}$, which are studied simultaneously. It is explicitly required that $|f_{a2}| + |f_{a3}| + |f_{\Lambda 1}| \leq 1$ to avoid probing an unphysical parameter space. Finally, there is just one anomalous coupling corresponding to $f_{a3}^{\text{ggH}}$ to consider for the Hgg vertex. For this study, we also include the effect of the $CP$-odd HVV anomalous coupling on the VBF process. This is achieved by including $f_{a3}$ as a free parameter in the fit. The $p(\tilde{\theta}|\theta)$ are the probability density functions (PDFs) for the observed values of the nuisance parameters, $\tilde{\theta}$, obtained from calibration measurements. The systematic uncertainties that affect only the normalizations of the signal and background processes are treated as PDFs following a log-normal distribution, whereas shape-altering systematic uncertainties are treated as Gaussian PDFs [101].

Additional interpretations in terms of the SMEFT Higgs and Warsaw basis coupling parameters are also considered using Eqs. (7–10) and Eqs. (11–14), respectively. In each case, four independent couplings are studied simultaneously and the effect of the couplings on the total width of the Higgs boson is taken into account. For the $f_{ai}$ measurements, this effect is absorbed by the signal strength modifiers. A parameterization of the partial widths of the main Higgs boson decay modes as a function of the couplings is used to determine the effect on the Higgs boson width [24, 28].

The likelihood is maximized with respect to the signal modifier parameters and with respect to the nuisance parameters. Confidence level (CL) intervals are determined from profile likelihood scans of the respective parameters. The allowed 68% and 95% CL intervals are defined using the set of parameter values at which the profile likelihood function $-2\Delta \ln \mathcal{L} = 1.00$ and 3.84 [102], respectively, for which exact coverage is expected in the asymptotic limit [103]. The likelihood value at a given $f_{ai}$ is determined by the shape of the signal hypothesis and the rel-

ative signal event yields between categories. Expected results are obtained using the Asimov data set [104] constructed using the SM values of the signal modifier parameters.

For Approach 1, where we assume $a_i^{ZZ} = a_i^{WW}$, the expected and observed $f_{a2}$, $f_{a3}$, $f_{\Lambda 1}$, and $f_{\Lambda 1}^{Z\gamma}$ likelihood scans are shown in Fig. 8. Significant interference effects for negative values of $f_{a2}$, around $-0.25$, and positive values of $f_{\Lambda 1}$, around 0.5, are evident. Relatively large changes in the signal shape with respect to the SM are predicted at these values. Also evident are narrow minima around $f_{ai} = 0$. The anomalous coupling terms in Eq. (1) have a $q_i^2$ dependence, which can be larger at the VBF/VH production vertex than at the Higgs decay vertex. This causes the cross section and the shape of the VBF/VH signal hypothesis to change rapidly with $f_{ai}$. For $f_{\Lambda 1}^{Z\gamma}$, there are no anomalous effects at the Higgs decay vertex and so the only structure present is the narrow minimum related to the VBF/VH production vertex. The axis scales are varied to improve the visibility of important features for $f_{a2}$ and $f_{\Lambda 1}$. For Approach 2, where the SU(2) x U(1) coupling relationships from Eqs. (2–6) are adopted, the expected and observed $f_{a2}$, $f_{a3}$ and $f_{\Lambda 1}$ likelihood scans are shown in Fig. 9. The results are shown for each $f_{ai}$ separately with the other two $f_{ai}$ either fixed to zero or left floating in the fit. The measured values of the signal strength parameters correspond to $\mu_{EW} = 0.9^{+0.19}_{-0.24}$ and $\mu_{ggH} = 0.9^{+0.38}_{-0.20}$ when all parameters float simultaneously. It is notable that the observed $-2\Delta \ln \mathcal{L}$ profile values are generally lower than expected. This is consistent with a downward statistical fluctuation in the number of VBF and VH events. The lowest $\mu_{EW}$ value measured is 0.82 for the Approach 1 $f_{a3}$ fit which can be compared with the highest value of 0.97 for the corresponding $f_{\Lambda 1}$ fit. In each case, the uncertainty in $\mu_{EW}$ is about 20% and as such all fitted values are consistent with both the SM and each other. More generally, all anomalous HVV coupling parameter measurements are consistent with the expectations for the SM Higgs boson. The p-value compatibility of the full Approach 2 fit, where all signal parameters float simultaneously, with the SM is 91%. A summary of constraints on the anomalous HVV coupling parameters with the best fit values and allowed 68% and 95% CL intervals are shown in Table 7. The most stringent constraints on the HVV anomalous coupling cross section fractions are at the per mille level. Some constraints are less stringent than expected due to the fitted values of $\mu_{EW}$ being lower than the SM expectation. The observed correlation coefficients between HVV anomalous coupling cross section fractions and signal strength modifiers are displayed in Fig. 10.

For the SMEFT Higgs basis interpretation, the expected and observed constraints on the $\delta c_z$, $c_{z\Box}$, $c_{zz}$, and $\tilde{c}_{zz}$ coupling parameters are shown in Fig. 11. Table 8 presents a summary of the constraints on the couplings whereas Fig. 10 reports the observed correlation coefficients between them. For the Warsaw basis interpretation, the expected and observed constraints on the $c_{H\Box}$, $c_{HD}$, $c_{HW}$, $c_{HWB}$, $c_{HB}$, $c_{H\tilde{W}}$, $c_{H\tilde{W}B}$, and $c_{H\tilde{B}}$ coupling parameters are presented in Table 9. To cover all the Warsaw basis coupling parameters, three independent fits to the data were performed with a different choice of four independent couplings in each. A summary of the constraints on the SMEFT Higgs and Warsaw basis coupling parameters is presented in Fig. 12.

Finally, the expected and observed $f_{a3}^{ggH}$ likelihood scans are shown in Fig. 13. The result is consistent with the expectation for a SM Higgs boson. Excluding the effect of the *CP*-odd HVV anomalous coupling, by fixing $f_{a3}$ to zero, has a negligible effect. For $|f_{a3}^{ggH}|$ approaching unity, the observed $-2\Delta \ln \mathcal{L}$ profile values are larger than expected. This is consistent with downward statistical fluctuations in the data for a couple of bins where sensitivity to the $a_3$ Hgg coupling contribution is enhanced (Fig. 7 left). The constraint on the anomalous Hgg coupling parameter with the best fit value and allowed 68% CL interval is shown in Table 7.

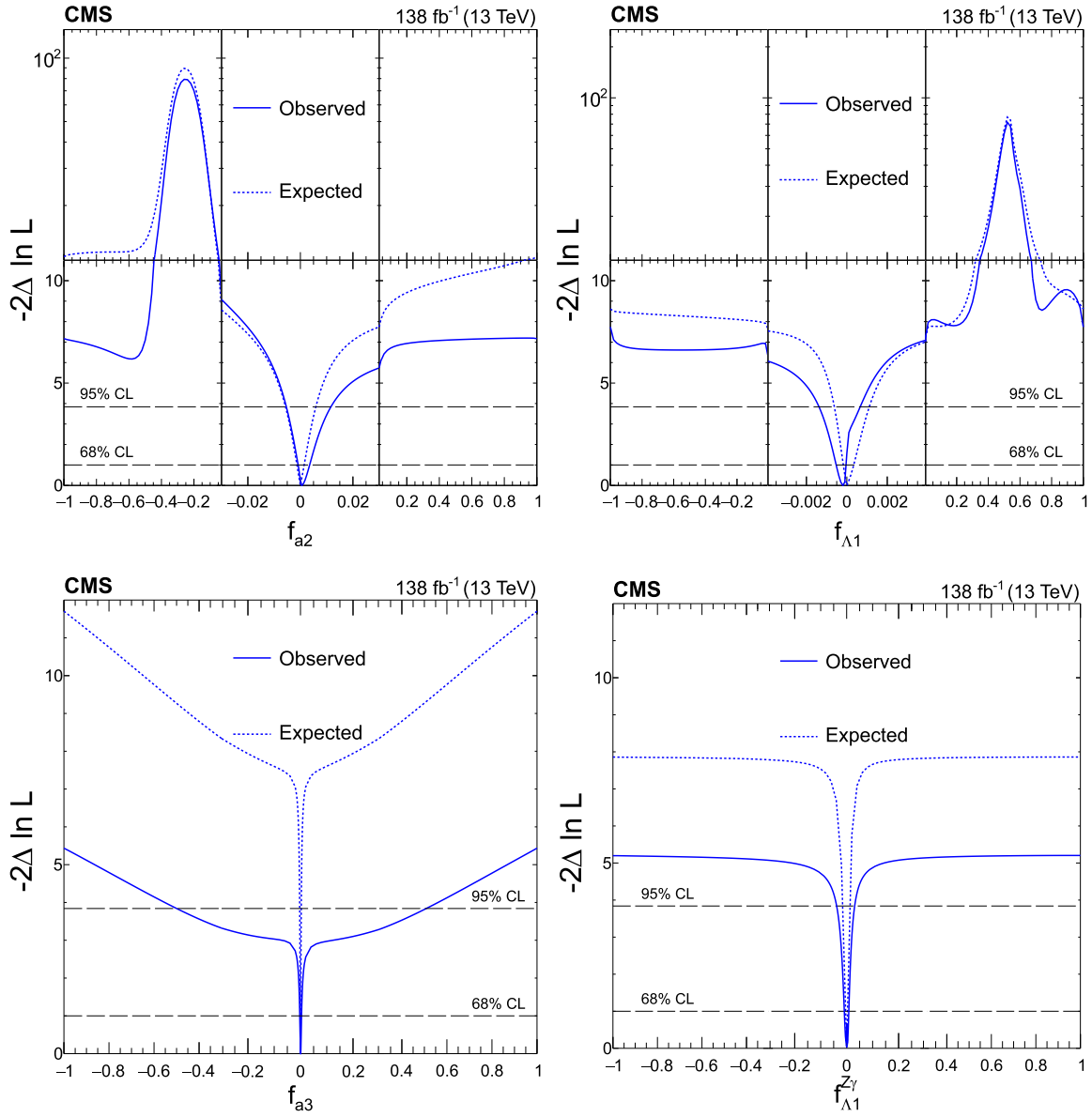


Figure 8: Expected (dashed) and observed (solid) profiled likelihood on $f_{a2}$ (upper left), $f_{\Lambda 1}$ (upper right), $f_{a3}$ (lower left), and $f_{\Lambda 1}^{Z\gamma}$ (lower right) using Approach 1. In each case, the signal strength modifiers are treated as free parameters. The dashed horizontal lines show the 68 and 95% CL regions. Axis scales are varied for $f_{a2}$ and $f_{\Lambda 1}$ to improve the visibility of important features.

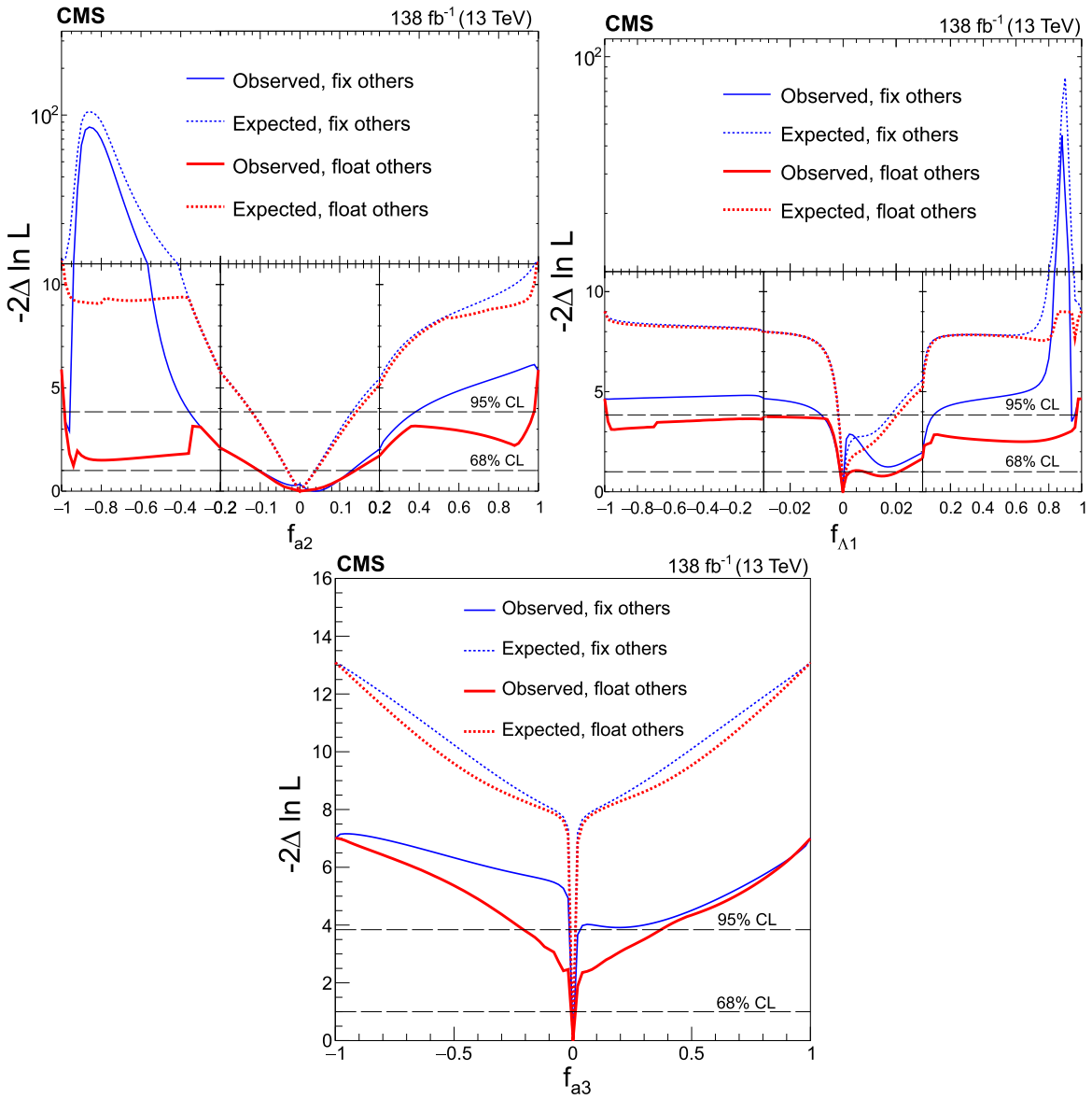


Figure 9: Expected (dashed) and observed (solid) profiled likelihood on $f_{a2}$ (upper left), $f_{\Lambda 1}$ (upper right) and $f_{a3}$ (bottom) using Approach 2. The other two anomalous coupling cross section fractions are either fixed to zero (blue) or left floating in the fit (red). In each case, the signal strength modifiers are treated as free parameters. The dashed horizontal lines show the 68 and 95% CL regions. Axis scales are varied for $f_{a2}$ and $f_{\Lambda 1}$ to improve the visibility of important features.

## 11 Summary

This paper presents a study of the anomalous couplings of the Higgs boson (H) with vector bosons, including $CP$ violating effects, using its associated production with hadronic jets in gluon fusion, electroweak vector boson fusion, and associated production with a W or Z boson, and its subsequent decay to a pair of W bosons. The results are based on the proton-proton collision data set collected by the CMS detector at the LHC during 2016–2018, corresponding to an integrated luminosity of 138 $\text{fb}^{-1}$ at a center-of-mass energy of 13 TeV. The analysis targets the different-flavor dilepton (e$\mu$) final state, with kinematic information from associated jets

Table 7: Summary of constraints on the anomalous HVV and Hgg coupling parameters with the best fit values and allowed 68 and 95% CL (in square brackets) intervals. For Approach 1, each $f_{ai}$ is studied independently. For Approach 2, each $f_{ai}$ is shown separately with the other two cross section fractions either fixed to zero or left floating in the fit. In each case, the signal strength modifiers are treated as free parameters.

| Analysis | $f_{ai}$ | | Observed ($\times 10^{-3}$) | Expected ($\times 10^{-3}$) |
|---|---|---|---|---|
| HVV Approach 1 | $f_{a2}$ | best fit | 0.5 | 0.0 |
| | | 68% CL | $[-0.8, 3.5]$ | $[-1.4, 1.3]$ |
| | | 95% CL | $[-5.7, 12.0]$ | $[-5.2, 6.1]$ |
| | $f_{a3}$ | best fit | 0.9 | 0.0 |
| | | 68% CL | $[-2.7, 4.1]$ | $[-0.7, 0.7]$ |
| | | 95% CL | $[-553.0, 561.0]$ | $[-2.8, 2.9]$ |
| | $f_{\Lambda 1}$ | best fit | $-0.2$ | 0.0 |
| | | 68% CL | $[-0.5, 0.0]$ | $[-0.2, 0.5]$ |
| | | 95% CL | $[-1.4, 0.7]$ | $[-0.6,1.4]$ |
| | $f_{\Lambda 1}^{Z\gamma}$ | best fit | 3.0 | 0.0 |
| | | 68% CL | $[-11.0, 9.1]$ | $[-5.0, 3.8]$ |
| | | 95% CL | $[-55.0, 42.0]$ | $[-14.0, 11.0]$ |
| HVV Approach 2 (Fix others) | $f_{a2}$ | best fit | 38.0 | 0.0 |
| | | 68% CL | $[-112.2, 129.3]$ | $[-30.9,37.5]$ |
| | | 95% CL | $[-376.6, 430.0] \cup [-989.2, -826.3]$ | $[-126.1,136.8]$ |
| | $f_{a3}$ | best fit | 0.8 | 0.0 |
| | | 68% CL | $[-0.8, 3.5]$ | $[-0.8,1.1]$ |
| | | 95% CL | $[-7.6, 58.8]$ | $[-3.4,4.3]$ |
| | $f_{\Lambda 1}$ | best fit | $-0.15$ | 0.0 |
| | | 68% CL | $[-1.21, 0.16]$ | $[-0.4,0.4]$ |
| | | 95% CL | $[-19.5, 118.5] \cup [909.9, 964.1]$ | $[-1.7,18.9]$ |
| HVV Approach 2 (Float others) | $f_{a2}$ | best fit | $-1.0$ | 0.0 |
| | | 68% CL | $[-104.1, 139.9]$ | $[-31.1,39.8]$ |
| | | 95% CL | $[-986.4, 981.2]$ | $[-127.5,148.7]$ |
| | $f_{a3}$ | best fit | 0.34 | 0.0 |
| | | 68% CL | $[-0.69, 3.4]$ | $[-1.0,1.2]$ |
| | | 95% CL | $[-201.3, 361.5]$ | $[-4.3,5.3]$ |
| | $f_{\Lambda 1}$ | best fit | $-0.1$ | 0.0 |
| | | 68% CL | $[-1.08, 3.78] \cup [7.2, 20.7]$ | $[-0.4,0.9]$ |
| | | 95% CL | $[-994.8, 993.9]$ | $[-1.9,21.4]$ |
| Hgg | $f_{a3}^{ggH}$ | best fit | $-34$ | 0 |
| | | 68% CL | $[-721, 383]$ | $[-1000, 1000]$ |
| | | 95% CL | $[-1000, 1000]$ | $[-1000, 1000]$ |

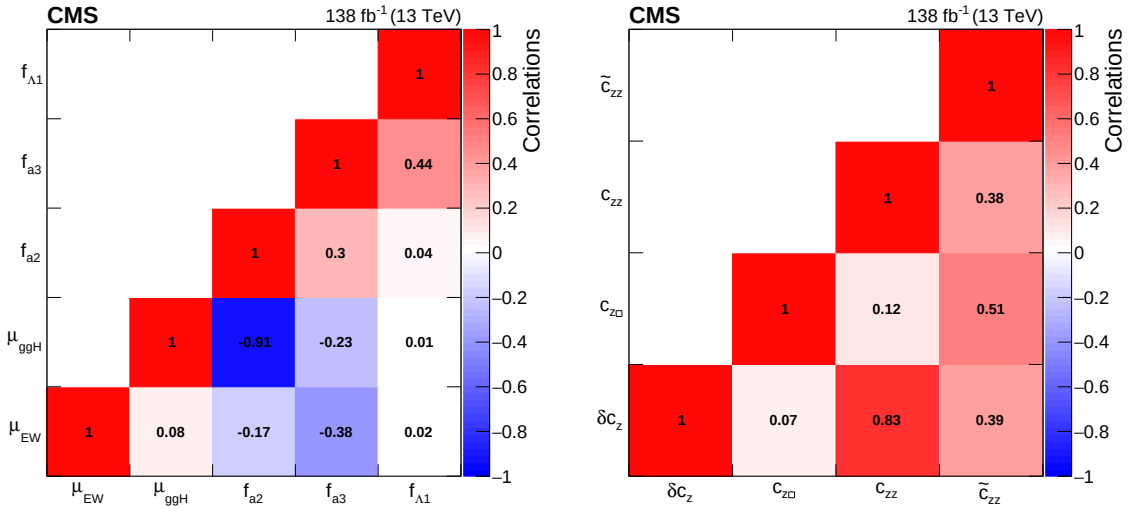


Figure 10: The observed correlation coefficients between HVV anomalous coupling cross section fractions and signal strength modifiers (left) and between SMEFT Higgs basis coupling parameters (right).

Table 8: Summary of constraints on the SMEFT Higgs basis coupling parameters with the best fit values and 68% CL uncertainties. All four couplings are studied simultaneously.

| Coupling | Observed | Expected |
|---|---|---|
| $\delta c_z$ | $-0.06^{+0.09}_{-0.16}$ | $0.00^{+0.08}_{-0.10}$ |
| $c_{z\Box}$ | $0.01^{+0.02}_{-0.06}$ | $0.00^{+0.02}_{-0.02}$ |
| $c_{zz}$ | $0.03^{+0.30}_{-0.52}$ | $0.00^{+0.23}_{-0.29}$ |
| $\tilde{c}_{zz}$ | $-0.17^{+0.42}_{-0.30}$ | $0.00^{+0.29}_{-0.32}$ |

Table 9: Summary of constraints on the SMEFT Warsaw basis coupling parameters with the best fit values and 68% CL uncertainties. Only one of $c_{HW}$ , $c_{HWB}$, and $c_{HB}$ is independent, the same is also true for $c_{H\tilde{W}}$, $c_{H\tilde{W}B}$, and $c_{H\tilde{B}}$. Three independent fits to the data were performed with a different choice of four independent couplings in each.

| Coupling | Observed | Expected |
|---|---|---|
| $c_{H\Box}$ | $-0.76^{+1.43}_{-3.43}$ | $0.00^{+1.37}_{-1.84}$ |
| $c_{HD}$ | $-0.12^{+0.93}_{-0.32}$ | $0.00^{+0.43}_{-0.30}$ |
| $c_{HW}$ | $0.08^{+0.43}_{-0.87}$ | $0.00^{+0.37}_{-0.48}$ |
| $c_{HWB}$ | $0.17^{+0.88}_{-1.79}$ | $0.00^{+0.77}_{-0.96}$ |
| $c_{HB}$ | $0.03^{+0.13}_{-0.26}$ | $0.00^{+0.11}_{-0.14}$ |
| $c_{H\tilde{W}}$ | $-0.26^{+0.67}_{-0.50}$ | $0.00^{+0.48}_{-0.52}$ |
| $c_{H\tilde{W}B}$ | $-0.54^{+1.37}_{-1.03}$ | $0.00^{+0.99}_{-1.07}$ |
| $c_{H\tilde{B}}$ | $-0.08^{+0.20}_{-0.15}$ | $0.00^{+0.15}_{-0.16}$ |

combined using matrix element techniques to increase sensitivity to anomalous effects at the production vertex. Dedicated Monte Carlo simulation and matrix element reweighting provide modeling of all kinematic features in the production and decay of the Higgs boson with

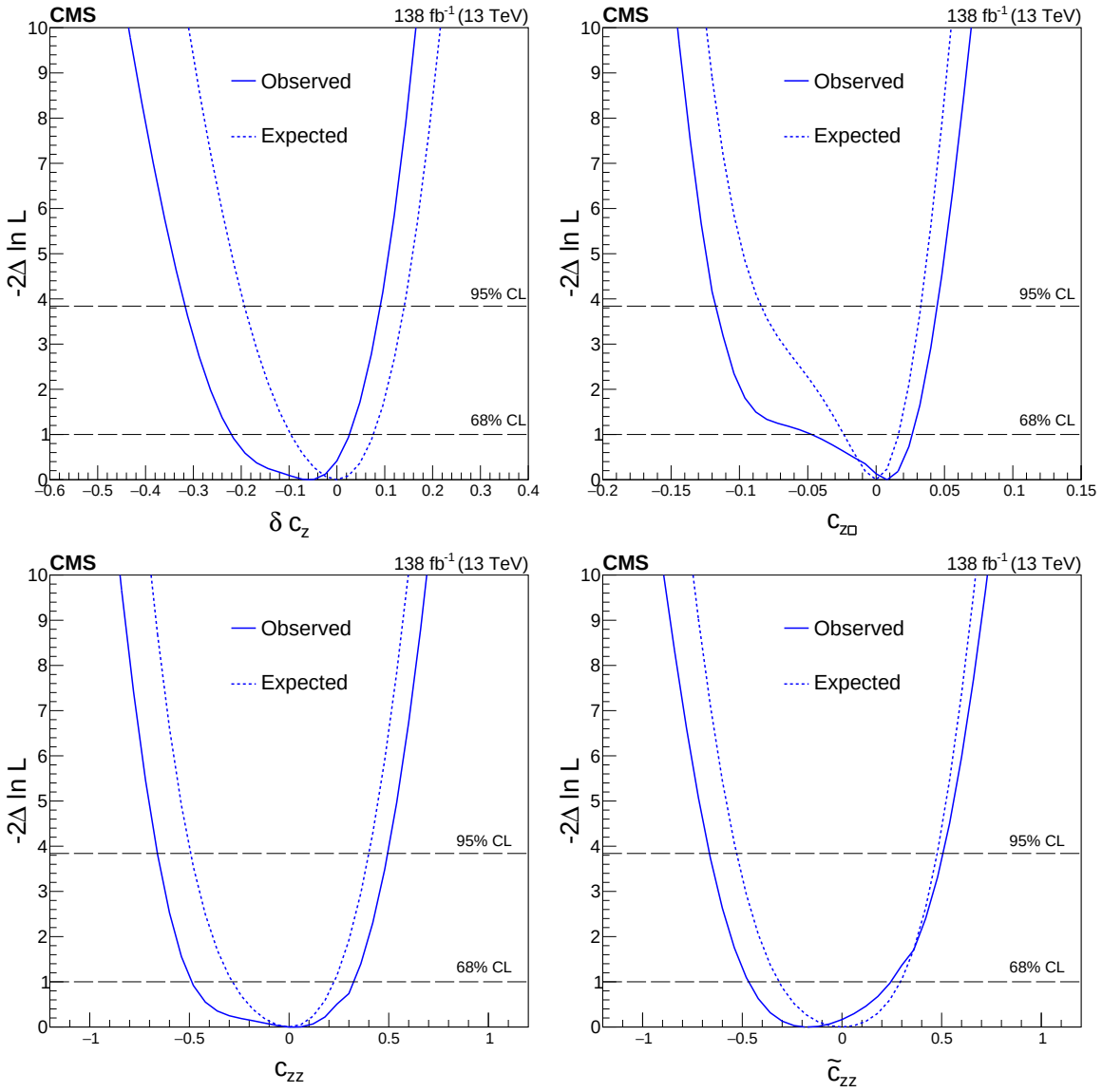


Figure 11: Expected (dashed) and observed (solid) profiled likelihood on the $\delta c_z$ (upper left), $c_{z\Box}$ (upper right), $c_{zz}$ (lower left), and $\tilde{c}_{zz}$ (lower right) couplings of the SMEFT Higgs basis. All four couplings are studied simultaneously. The dashed horizontal lines show the 68 and 95% CL regions.

full simulation of detector effects. A simultaneous measurement of four Higgs boson couplings to electroweak vector bosons has been performed in the framework of a standard model effective field theory. All measurements are consistent with the expectations for the standard model Higgs boson and constraints are set on the fractional contribution of the anomalous couplings to the Higgs boson cross section. The most stringent constraints on the HVV anomalous coupling cross section fractions are at the per mille level. These results are in agreement with those obtained in the $H \to ZZ$ and $H \to \tau\tau$ channels, and also significantly surpass those of the previous $H \to WW$ anomalous coupling analysis from the CMS experiment in both scope and precision.

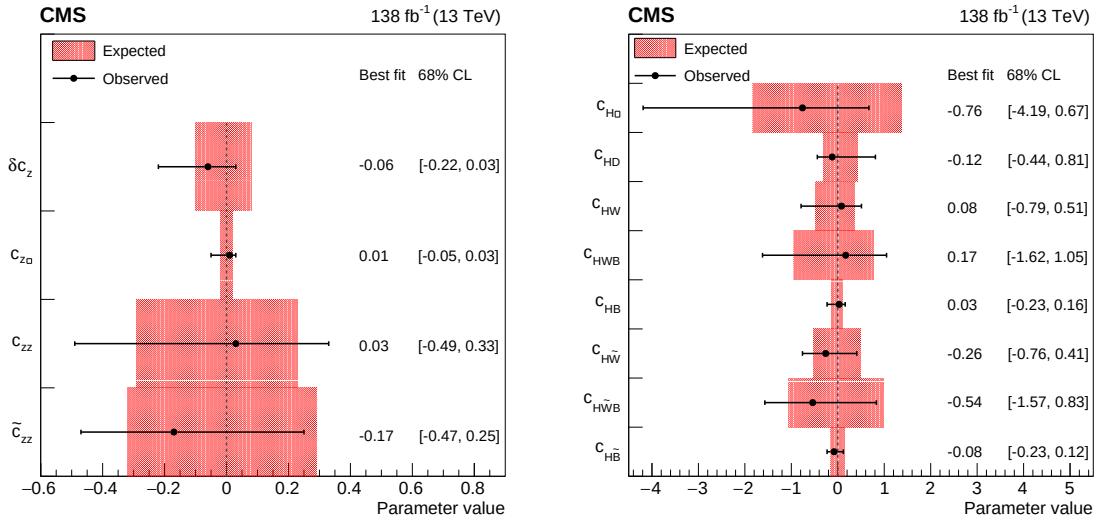


Figure 12: Summary of constraints on the SMEFT Higgs (left) and Warsaw (right) basis coupling parameters with the best fit values and 68% CL uncertainties. For the Warsaw basis, only one of $c_{\mathrm{HW}}$ , $c_{\mathrm{HWB}}$, and $c_{\mathrm{HB}}$ is independent, the same is also true for $c_{\mathrm{H\tilde{W}}}$, $c_{\mathrm{H\tilde{W}B}}$, and $c_{\mathrm{H\tilde{B}}}$.

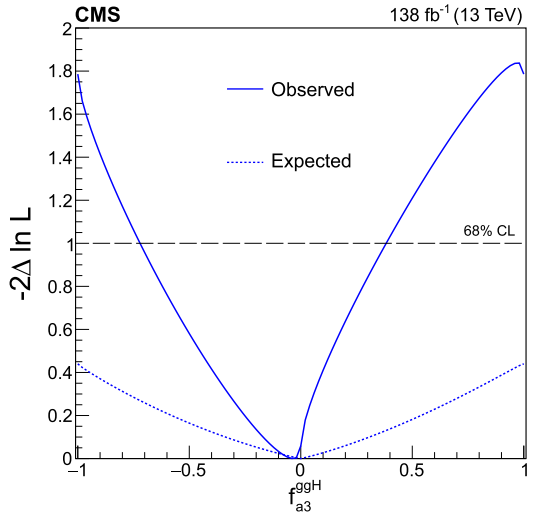


Figure 13: Expected (dashed) and observed (solid) profiled likelihood on $f_{a3}^{\mathrm{ggH}}$. The signal strength modifiers and the $CP$-odd HVV anomalous coupling cross section fraction are treated as free parameters. The crossing of the observed likelihood with the dashed horizontal line shows the observed 68% CL region.

## Acknowledgments

We congratulate our colleagues in the CERN accelerator departments for the excellent performance of the LHC and thank the technical and administrative staffs at CERN and at other CMS institutes for their contributions to the success of the CMS effort. In addition, we gratefully acknowledge the computing centers and personnel of the Worldwide LHC Computing Grid and other centers for delivering so effectively the computing infrastructure essential to our analyses. Finally, we acknowledge the enduring support for the construction and operation of the LHC, the CMS detector, and the supporting computing infrastructure provided by the following funding agencies: SC (Armenia), BMBWF and FWF (Austria); FNRS and

FWO (Belgium); CNPq, CAPES, FAPERJ, FAPERGS, and FAPESP (Brazil); MES and BNSF (Bulgaria); CERN; CAS, MoST, and NSFC (China); MINCIENCIAS (Colombia); MSES and CSF (Croatia); RIF (Cyprus); SENESCYT (Ecuador); ERC PRG, RVTT3 and MoER TK202 (Estonia); Academy of Finland, MEC, and HIP (Finland); CEA and CNRS/IN2P3 (France); SRNSF (Georgia); BMBF, DFG, and HGF (Germany); GSRI (Greece); NKFIH (Hungary); DAE and DST (India); IPM (Iran); SFI (Ireland); INFN (Italy); MSIP and NRF (Republic of Korea); MES (Latvia); LMTLT (Lithuania); MOE and UM (Malaysia); BUAP, CINVESTAV, CONACYT, LNS, SEP, and UASLP-FAI (Mexico); MOS (Montenegro); MBIE (New Zealand); PAEC (Pakistan); MES and NSC (Poland); FCT (Portugal); MESTD (Serbia); MCIN/AEI and PCTI (Spain); MOSTR (Sri Lanka); Swiss Funding Agencies (Switzerland); MST (Taipei); MHESI and NSTDA (Thailand); TUBITAK and TENMAK (Turkey); NASU (Ukraine); STFC (United Kingdom); DOE and NSF (USA).

Individuals have received support from the Marie-Curie program and the European Research Council and Horizon 2020 Grant, contract Nos. 675440, 724704, 752730, 758316, 765710, 824093, 101115353, and COST Action CA16108 (European Union); the Leventis Foundation; the Alfred P. Sloan Foundation; the Alexander von Humboldt Foundation; the Science Committee, project no. 22rl-037 (Armenia); the Belgian Federal Science Policy Office; the Fonds pour la Formation à la Recherche dans l'Industrie et dans l'Agriculture (FRIA-Belgium); the Agentschap voor Innovatie door Wetenschap en Technologie (IWT-Belgium); the F.R.S.-FNRS and FWO (Belgium) under the "Excellence of Science – EOS" – be.h project n. 30820817; the Beijing Municipal Science & Technology Commission, No. Z191100007219010 and Fundamental Research Funds for the Central Universities (China); the Ministry of Education, Youth and Sports (MEYS) of the Czech Republic; the Shota Rustaveli National Science Foundation, grant FR-22-985 (Georgia); the Deutsche Forschungsgemeinschaft (DFG), under Germany's Excellence Strategy – EXC 2121 "Quantum Universe" – 390833306, and under project number 400140256 - GRK2497; the Hellenic Foundation for Research and Innovation (HFRI), Project Number 2288 (Greece); the Hungarian Academy of Sciences, the New National Excellence Program - ÚNKP, the NKFIH research grants K 124845, K 124850, K 128713, K 128786, K 129058, K 131991, K 133046, K 138136, K 143460, K 143477, 2020-2.2.1-ED-2021-00181, and TKP2021-NKTA-64 (Hungary); the Council of Science and Industrial Research, India; ICSC – National Research Center for High Performance Computing, Big Data and Quantum Computing, funded by the NextGenerationEU program (Italy); the Latvian Council of Science; the Ministry of Education and Science, project no. 2022/WK/14, and the National Science Center, contracts Opus 2021/41/B/ST2/01369 and 2021/43/B/ST2/01552 (Poland); the Fundação para a Ciência e a Tecnologia, grant CEECIND/01334/2018 (Portugal); the National Priorities Research Program by Qatar National Research Fund; MCIN/AEI/10.13039/501100011033, ERDF "a way of making Europe", and the Programa Estatal de Fomento de la Investigación Científica y Técnica de Excelencia María de Maeztu, grant MDM-2017-0765 and Programa Severo Ochoa del Principado de Asturias (Spain); the Chulalongkorn Academic into Its 2nd Century Project Advancement Project, and the National Science, Research and Innovation Fund via the Program Management Unit for Human Resources & Institutional Development, Research and Innovation, grant B37G660013 (Thailand); the Kavli Foundation; the Nvidia Corporation; the SuperMicro Corporation; the Welch Foundation, contract C-1845; and the Weston Havens Foundation (USA).

## References

[1] ATLAS Collaboration, "Observation of a new particle in the search for the standard model Higgs boson with the ATLAS detector at the LHC", *Phys. Lett. B* **716** (2012) 1,

doi:10.1016/j.physletb.2012.08.020, arXiv:1207.7214.

[2] CMS Collaboration, "Observation of a new boson at a mass of 125 GeV with the CMS experiment at the LHC", *Phys. Lett. B* **716** (2012) 30, doi:10.1016/j.physletb.2012.08.021, arXiv:1207.7235.

[3] CMS Collaboration, "Observation of a new boson with mass near 125 GeV in pp collisions at $\sqrt{s} = 7$ and 8 TeV", *JHEP* **06** (2013) 081, doi:10.1007/JHEP06(2013)081, arXiv:1303.4571.

[4] CMS Collaboration, "On the mass and spin-parity of the Higgs boson candidate via its decays to Z boson pairs", *Phys. Rev. Lett.* **110** (2013) 081803, doi:10.1103/PhysRevLett.110.081803, arXiv:1212.6639.

[5] CMS Collaboration, "Measurement of the properties of a Higgs boson in the four-lepton final state", *Phys. Rev. D* **89** (2014) 092007, doi:10.1103/PhysRevD.89.092007, arXiv:1312.5353.

[6] CMS Collaboration, "Constraints on the spin-parity and anomalous HVV couplings of the Higgs boson in proton collisions at 7 and 8 TeV", *Phys. Rev. D* **92** (2015) 012004, doi:10.1103/PhysRevD.92.012004, arXiv:1411.3441.

[7] CMS Collaboration, "Limits on the Higgs boson lifetime and width from its decay to four charged leptons", *Phys. Rev. D* **92** (2015) 072010, doi:10.1103/PhysRevD.92.072010, arXiv:1507.06656.

[8] CMS Collaboration, "Combined search for anomalous pseudoscalar HVV couplings in VH production and $H \to VV$ decay", *Phys. Lett. B* **759** (2016) 672, doi:10.1016/j.physletb.2016.06.004, arXiv:1602.04305.

[9] CMS Collaboration, "Constraints on anomalous Higgs boson couplings using production and decay information in the four-lepton final state", *Phys. Lett. B* **775** (2017) 1, doi:10.1016/j.physletb.2017.10.021, arXiv:1707.00541.

[10] CMS Collaboration, "Measurements of the Higgs boson width and anomalous HVV couplings from on-shell and off-shell production in the four-lepton final state", *Phys. Rev. D* **99** (2019) 112003, doi:10.1103/PhysRevD.99.112003, arXiv:1901.00174.

[11] CMS Collaboration, "Constraints on anomalous HVV couplings from the production of Higgs bosons decaying to $\tau$ lepton pairs", *Phys. Rev. D* **100** (2019) 112002, doi:10.1103/PhysRevD.100.112002, arXiv:1903.06973.

[12] ATLAS Collaboration, "Evidence for the spin-0 nature of the Higgs boson using ATLAS data", *Phys. Lett. B* **726** (2013) 120, doi:10.1016/j.physletb.2013.08.026, arXiv:1307.1432.

[13] ATLAS Collaboration, "Study of the spin and parity of the Higgs boson in diboson decays with the ATLAS detector", *Eur. Phys. J. C* **75** (2015) 476, doi:10.1140/epjc/s10052-015-3685-1, arXiv:1506.05669.

[14] ATLAS Collaboration, "Test of $CP$ invariance in vector-boson fusion production of the Higgs boson using the Optimal Observable method in the ditau decay channel with the ATLAS detector", *Eur. Phys. J. C* **76** (2016) 658, doi:10.1140/epjc/s10052-016-4499-5, arXiv:1602.04516.

[15] ATLAS Collaboration, "Measurement of inclusive and differential cross sections in the $H \to ZZ^* \to 4\ell$ decay channel in pp collisions at $\sqrt{s} = 13$ TeV with the ATLAS detector", *JHEP* **10** (2017) 132, doi:10.1007/JHEP10(2017)132, arXiv:1708.02810.

[16] ATLAS Collaboration, "Measurement of the Higgs boson coupling properties in the $H \to ZZ^* \to 4\ell$ decay channel at $\sqrt{s}$ = 13 TeV with the ATLAS detector", *JHEP* **03** (2018) 095, doi:10.1007/JHEP03(2018)095, arXiv:1712.02304.

[17] ATLAS Collaboration, "Measurements of Higgs boson properties in the diphoton decay channel with 36 $fb^{-1}$ of pp collision data at $\sqrt{s} = 13$ TeV with the ATLAS detector", *Phys. Rev. D* **98** (2018) 052005, doi:10.1103/PhysRevD.98.052005, arXiv:1802.04146.

[18] ATLAS Collaboration, "Test of $CP$ invariance in vector-boson fusion production of the Higgs boson in the $H \to \tau\tau$ channel in proton−proton collisions at $\sqrt{s}$ = 13 TeV with the ATLAS detector", *Phys. Lett. B* **805** (2020) 135426, doi:10.1016/j.physletb.2020.135426, arXiv:2002.05315.

[19] LHC Higgs Cross Section Working Group, "Handbook of LHC Higgs cross sections: 4. Deciphering the nature of the Higgs sector", CERN Report CERN-2017-002-M, 2016. doi:10.23731/CYRM-2017-002, arXiv:1610.07922.

[20] Y. Gao et al., "Spin determination of single-produced resonances at hadron colliders", *Phys. Rev. D* **81** (2010) 075022, doi:10.1103/PhysRevD.81.075022, arXiv:1001.3396.

[21] S. Bolognesi et al., "On the spin and parity of a single-produced resonance at the LHC", *Phys. Rev. D* **86** (2012) 095031, doi:10.1103/PhysRevD.86.095031, arXiv:1208.4018.

[22] I. Anderson et al., "Constraining anomalous HVV interactions at proton and lepton colliders", *Phys. Rev. D* **89** (2014) 035007, doi:10.1103/PhysRevD.89.035007, arXiv:1309.4819.

[23] A. V. Gritsan, R. Röntsch, M. Schulze, and M. Xiao, "Constraining anomalous Higgs boson couplings to the heavy flavor fermions using matrix element techniques", *Phys. Rev. D* **94** (2016) 055023, doi:10.1103/PhysRevD.94.055023, arXiv:1606.03107.

[24] A. V. Gritsan et al., "New features in the JHU generator framework: constraining Higgs boson properties from on-shell and off-shell production", *Phys. Rev. D* **102** (2020) 056022, doi:10.1103/PhysRevD.102.056022, arXiv:2002.09888.

[25] CMS Collaboration, "Measurements of the Higgs boson production cross section and couplings in the W boson pair decay channel in proton-proton collisions at $\sqrt{s}$ = 13 TeV", *Eur. Phys. J. C* **83** (2023) 667, doi:10.1140/epjc/s10052-023-11632-6, arXiv:2206.09466.

[26] LHC Higgs Cross Section Working Group, "Handbook of LHC Higgs cross sections: 3. Higgs Properties: Report of the LHC Higgs Cross Section Working Group", CERN Report CERN-2013-004, 2013. doi:10.5170/CERN-2013-004, arXiv:1307.1347.

[27] CMS Collaboration, "Measurements of $t\bar{t}H$ production and the *CP* structure of the Yukawa interaction between the Higgs boson and top quark in the diphoton decay channel", *Phys. Rev. Lett.* **125** (2020) 061801, doi:10.1103/PhysRevLett.125.061801, arXiv:2003.10866.

[28] CMS Collaboration, "Constraints on anomalous Higgs boson couplings to vector bosons and fermions in its production and decay using the four-lepton final state", *Phys. Rev. D* **104** (2021) 052004, doi:10.1103/physrevd.104.052004, arXiv:2104.12152.

[29] HEPData record for this analysis, 2024. doi:10.17182/hepdata.146013.

[30] B. Grzadkowski, M. Iskrzyński, M. Misiak, and J. Rosiek, "Dimension-six terms in the standard model lagrangian", *JHEP* **10** (2010) 085, doi:10.1007/jhep10(2010)085, arXiv:1008.4884.

[31] J. Davis et al., "Constraining anomalous Higgs boson couplings to virtual photons", *Phys. Rev. D* **105** (2022) 096027, doi:10.1103/PhysRevD.105.096027, arXiv:2109.13363.

[32] A. V. Gritsan et al., "New features in the JHU generator framework: Constraining Higgs boson properties from on-shell and off-shell production", *Phys. Rev. D* **102** (2020) doi:10.1103/physrevd.102.056022.

[33] CMS Collaboration, "The CMS experiment at the CERN LHC", *JINST* **3** (2008) S08004, doi:10.1088/1748-0221/3/08/S08004.

[34] CMS Collaboration, "Performance of electron reconstruction and selection with the CMS detector in proton-proton collisions at $\sqrt{s} = 8$ TeV", *JINST* **10** (2015) P06005, doi:10.1088/1748-0221/10/06/P06005, arXiv:1502.02701.

[35] CMS Collaboration, "Performance of the CMS muon detector and muon reconstruction with proton-proton collisions at $\sqrt{s} = 13$ TeV", *JINST* **13** (2018) P06015, doi:10.1088/1748-0221/13/06/P06015, arXiv:1804.04528.

[36] CMS Collaboration, "Performance of photon reconstruction and identification with the CMS detector in proton-proton collisions at sqrt(s) = 8 TeV", *JINST* **10** (2015) P08010, doi:10.1088/1748-0221/10/08/P08010, arXiv:1502.02702.

[37] CMS Collaboration, "Description and performance of track and primary-vertex reconstruction with the CMS tracker", *JINST* **9** (2014) P10009, doi:10.1088/1748-0221/9/10/P10009, arXiv:1405.6569.

[38] CMS Collaboration, "Particle-flow reconstruction and global event description with the CMS detector", *JINST* **12** (2017) P10003, doi:10.1088/1748-0221/12/10/P10003, arXiv:1706.04965.

[39] CMS Collaboration, "Performance of reconstruction and identification of $\tau$ leptons decaying to hadrons and $\nu_\tau$ in pp collisions at $\sqrt{s} = 13$ TeV", *JINST* **13** (2018) P10005, doi:10.1088/1748-0221/13/10/P10005, arXiv:1809.02816.

[40] CMS Collaboration, "Jet energy scale and resolution in the CMS experiment in pp collisions at 8 TeV", *JINST* **12** (2017) P02014, doi:10.1088/1748-0221/12/02/P02014, arXiv:1607.03663.

[41] CMS Collaboration, "Performance of missing transverse momentum reconstruction in proton-proton collisions at $\sqrt{s} = 13$ TeV using the CMS detector", *JINST* **14** (2019) P07004, doi:10.1088/1748-0221/14/07/P07004, arXiv:1903.06078.

[42] CMS Collaboration, "Performance of the CMS Level-1 trigger in proton-proton collisions at $\sqrt{s} = 13$ TeV", *JINST* **15** (2020) P10017, doi:10.1088/1748-0221/15/10/P10017, arXiv:2006.10165.

[43] CMS Collaboration, "The CMS trigger system", *JINST* **12** (2017) P01020, doi:10.1088/1748-0221/12/01/P01020, arXiv:1609.02366.

[44] CMS Collaboration, "Precision luminosity measurement in proton-proton collisions at $\sqrt{s} = 13$ TeV in 2015 and 2016 at CMS", *Eur. Phys. J. C* **800** (2021) 81, doi:10.1140/epjc/s10052-021-09538-2, arXiv:2104.01927.

[45] CMS Collaboration, "CMS luminosity measurement for the 2017 data-taking period at $\sqrt{s} = 13$ TeV", CMS Physics Analysis Summary CMS-PAS-LUM-17-004, 2017.

[46] CMS Collaboration, "CMS luminosity measurement for the 2018 data-taking period at $\sqrt{s} = 13$ TeV", CMS Physics Analysis Summary CMS-PAS-LUM-18-002, 2019.

[47] NNPDF Collaboration, "Parton distributions with QED corrections", *Nucl. Phys. B* **877** (2013) 290, doi:10.1016/j.nuclphysb.2013.10.010, arXiv:1308.0598.

[48] NNPDF Collaboration, "Unbiased global determination of parton distributions and their uncertainties at NNLO and at LO", *Nucl. Phys. B* **855** (2012) 153, doi:10.1016/j.nuclphysb.2011.09.024, arXiv:1107.2652.

[49] NNPDF Collaboration, "Parton distributions from high-precision collider data", *Eur. Phys. J. C* **77** (2017) 663, doi:10.1140/epjc/s10052-017-5199-5, arXiv:1706.00428.

[50] CMS Collaboration, "Event generator tunes obtained from underlying event and multiparton scattering measurements", *Eur. Phys. J. C* **76** (2016) 155, doi:10.1140/epjc/s10052-016-3988-x, arXiv:1512.00815.

[51] CMS Collaboration, "Extraction and validation of a new set of CMS PYTHIA8 tunes from underlying-event measurements", *Eur. Phys. J. C* **80** (2020) 4, doi:10.1140/epjc/s10052-019-7499-4, arXiv:1903.12179.

[52] T. Sjöstrand et al., "An introduction to PYTHIA 8.2", *Comput. Phys. Commun.* **191** (2015) 159, doi:10.1016/j.cpc.2015.01.024, arXiv:1410.3012.

[53] P. Nason, "A new method for combining NLO QCD with shower Monte Carlo algorithms", *JHEP* **11** (2004) 040, doi:10.1088/1126-6708/2004/11/040, arXiv:hep-ph/0409146.

[54] S. Frixione, P. Nason, and C. Oleari, "Matching NLO QCD computations with parton shower simulations: the POWHEG method", *JHEP* **11** (2007) 070, doi:10.1088/1126-6708/2007/11/070, arXiv:0709.2092.

[55] S. Alioli, P. Nason, C. Oleari, and E. Re, "A general framework for implementing NLO calculations in shower Monte Carlo programs: the POWHEG BOX", *JHEP* **06** (2010) 043, doi:10.1007/JHEP06(2010)043, arXiv:1002.2581.

[56] E. Bagnaschi, G. Degrassi, P. Slavich, and A. Vicini, "Higgs production via gluon fusion in the POWHEG approach in the SM and in the MSSM", *JHEP* **02** (2012) 088, doi:10.1007/JHEP02(2012)088, arXiv:1111.2854.

[57] P. Nason and C. Oleari, "NLO Higgs boson production via vector-boson fusion matched with shower in POWHEG", *JHEP* **02** (2010) 037, doi:10.1007/JHEP02(2010)037, arXiv:0911.5299.

[58] G. Luisoni, P. Nason, C. Oleari, and F. Tramontano, "$HW^{\pm}/HZ$ + 0 and 1 jet at NLO with the POWHEG BOX interfaced to GoSam and their merging within MiNLO", *JHEP* **10** (2013) 083, doi:10.1007/JHEP10(2013)083, arXiv:1306.2542.

[59] H. B. Hartanto, B. Jager, L. Reina, and D. Wackeroth, "Higgs boson production in association with top quarks in the POWHEG BOX", *Phys. Rev. D* **91** (2015) 094003, doi:10.1103/PhysRevD.91.094003, arXiv:1501.04498.

[60] K. Hamilton, P. Nason, E. Re, and G. Zanderighi, "NNLOPS simulation of Higgs boson production", *JHEP* **10** (2013) 222, doi:10.1007/JHEP10(2013)222, arXiv:1309.0017.

[61] K. Hamilton, P. Nason, and G. Zanderighi, "Finite quark-mass effects in the NNLOPS POWHEG+MiNLO Higgs generator", *JHEP* **05** (2015) 140, doi:10.1007/JHEP05(2015)140, arXiv:1501.04637.

[62] N. Berger et al., "Simplified template cross sections — stage 1.1", 2019. arXiv:1906.02754.

[63] R. Frederix and K. Hamilton, "Extending the MINLO method", *JHEP* **05** (2016) 042, doi:10.1007/JHEP05(2016)042, arXiv:1512.02663.

[64] J. Alwall et al., "The automated computation of tree-level and next-to-leading order differential cross sections, and their matching to parton shower simulations", *JHEP* **07** (2014) 079, doi:10.1007/JHEP07(2014)079, arXiv:1405.0301.

[65] CMS Collaboration, "A measurement of the Higgs boson mass in the diphoton decay channel", *Phys. Lett. B* **805** (2020) 135425, doi:10.1016/j.physletb.2020.135425, arXiv:2002.06398.

[66] P. Nason, C. Oleari, M. Rocco, and M. Zaro, "An interface between the POWHEG BOX and MadGraph5_aMC@NLO", *Eur. Phys. J. C* **80** (2020) 10, doi:10.1140/epjc/s10052-020-08559-7, arXiv:2008.06364.

[67] P. Nason and G. Zanderighi, "$W^+W^-$, $WZ$ and $ZZ$ production in the POWHEG-BOX-V2", *Eur. Phys. J. C* **74** (2014) 2702, doi:10.1140/epjc/s10052-013-2702-5, arXiv:1311.1365.

[68] P. Meade, H. Ramani, and M. Zeng, "Transverse momentum resummation effects in $W^+W^-$ measurements", *Phys. Rev. D* **90** (2014) 114006, doi:10.1103/PhysRevD.90.114006, arXiv:1407.4481.

[69] P. Jaiswal and T. Okui, "Explanation of the WW excess at the LHC by jet-veto resummation", *Phys. Rev. D* **90** (2014) 073009, doi:10.1103/PhysRevD.90.073009, arXiv:1407.4537.

[70] J. M. Campbell and R. K. Ellis, "An update on vector boson pair production at hadron colliders", *Phys. Rev. D* **60** (1999) 113006, doi:10.1103/PhysRevD.60.113006, arXiv:hep-ph/9905386.

[71] J. M. Campbell, R. K. Ellis, and C. Williams, "Vector boson pair production at the LHC", *JHEP* **07** (2011) 018, doi:10.1007/JHEP07(2011)018, arXiv:1105.0020.

[72] J. M. Campbell, R. K. Ellis, and W. T. Giele, "A multi-threaded version of MCFM", *Eur. Phys. J. C* **75** (2015) 246, doi:10.1140/epjc/s10052-015-3461-2, arXiv:1503.06182.

[73] F. Caola et al., "QCD corrections to vector boson pair production in gluon fusion including interference effects with off-shell Higgs at the LHC", *JHEP* **07** (2016) 087, doi:10.1007/JHEP07(2016)087, arXiv:1605.04610.

[74] Alwall, J. and others, "Comparative study of various algorithms for the merging of parton showers and matrix elements in hadronic collisions", *Eur. Phys. J. C* **53** (2008) 473, doi:10.1140/epjc/s10052-007-0490-5, arXiv:0706.2569.

[75] S. Frixione, P. Nason, and G. Ridolfi, "A positive-weight next-to-leading-order Monte Carlo for heavy flavour hadroproduction", *JHEP* **09** (2007) 126, doi:10.1088/1126-6708/2007/09/126, arXiv:0707.3088.

[76] S. Alioli, P. Nason, C. Oleari, and E. Re, "NLO single-top production matched with shower in POWHEG: $s$- and $t$-channel contributions", *JHEP* **09** (2009) 111, doi:10.1088/1126-6708/2009/09/111, arXiv:0907.4076. [Erratum: doi:10.1007/JHEP02(2010)011].

[77] E. Re, "Single-top Wt-channel production matched with parton showers using the POWHEG method", *Eur. Phys. J. C* **71** (2011) 1547, doi:10.1140/epjc/s10052-011-1547-z, arXiv:1009.2450.

[78] M. Czakon et al., "Top-pair production at the LHC through NNLO QCD and NLO EW", *JHEP* **10** (2017) 186, doi:10.1007/JHEP10(2017)186, arXiv:1705.04105.

[79] R. Frederix and S. Frixione, "Merging meets matching in MC@NLO", *JHEP* **12** (2012) 061, doi:10.1007/JHEP12(2012)061, arXiv:1209.6215.

[80] GEANT4 Collaboration, "GEANT4 — a simulation toolkit", *Nucl. Instrum. Meth. A* **506** (2003) 250, doi:10.1016/S0168-9002(03)01368-8.

[81] CMS Collaboration, "Muon identification using multivariate techniques in the CMS experiment in proton-proton collisions at $\sqrt{s}$ = 13 TeV", 2023. arXiv:2310.03844. Submitted to *JINST*.

[82] W. Waltenberger, R. Frühwirth, and P. Vanlaer, "Adaptive vertex fitting", *J. Phys. G* **34** (2007) N343, doi:10.1088/0954-3899/34/12/N01.

[83] CMS Collaboration, "Technical proposal for the Phase-II upgrade of the Compact Muon Solenoid", CMS Technical Proposal CERN-LHCC-2015-010, CMS-TDR-15-02, 2015.

[84] CMS Collaboration, "Pileup mitigation at CMS in 13 TeV data", *JINST* **15** (2020) P09018, doi:10.1088/1748-0221/15/09/p09018, arXiv:2003.00503.

[85] D. Bertolini, P. Harris, M. Low, and N. Tran, "Pileup per particle identification", *JHEP* **10** (2014) 059, doi:10.1007/JHEP10(2014)059, arXiv:1407.6013.

[86] J. Thaler and K. Van Tilburg, "Identifying boosted objects with $N$-subjettiness", *JHEP* **03** (2011) 015, doi:10.1007/JHEP03(2011)015, arXiv:1011.2268.

[87] M. Dasgupta, A. Fregoso, S. Marzani, and G. P. Salam, "Towards an understanding of jet substructure", *JHEP* **09** (2013) 029, doi:10.1007/JHEP09(2013)029, arXiv:1307.0007.

[88] J. M. Butterworth, A. R. Davison, M. Rubin, and G. P. Salam, "Jet substructure as a new Higgs search channel at the LHC", *Phys. Rev. Lett.* **100** (2008) 242001, doi:10.1103/PhysRevLett.100.242001, arXiv:0802.2470.

[89] A. J. Larkoski, S. Marzani, G. Soyez, and J. Thaler, "Soft Drop", *JHEP* **05** (2014) 146, doi:10.1007/JHEP05(2014)146, arXiv:1402.2657.

[90] CMS Collaboration, "Identification of heavy-flavour jets with the CMS detector in pp collisions at 13 TeV", *JINST* **13** (2018) P05011, doi:10.1088/1748-0221/13/05/P05011, arXiv:1712.07158.

[91] CMS Collaboration, "CMS Phase 1 heavy flavour identification performance and developments", CMS Detector Performance Summary CMS-DP-2020-019, 2017.

[92] CMS Collaboration, "Measurements of properties of the Higgs boson decaying to a W boson pair in pp collisions at $\sqrt{s} = 13$ TeV", *Phys. Lett. B* **791** (2019) 96, doi:10.1016/j.physletb.2018.12.073, arXiv:1806.05246.

[93] CMS Collaboration, "Measurements of inclusive W and Z cross sections in pp collisions at $\sqrt{s} = 7$ TeV", *JHEP* **01** (2011) 080, doi:10.1007/JHEP01(2011)080, arXiv:1012.2466.

[94] CMS Collaboration, "An embedding technique to determine $\tau\tau$ backgrounds in proton-proton collision data", *JINST* **14** (2019) P06032, doi:10.1088/1748-0221/14/06/P06032, arXiv:1903.01216.

[95] CMS Collaboration, "Identification techniques for highly boosted W bosons that decay into hadrons", *JHEP* **12** (2014) 017, doi:10.1007/JHEP12(2014)017, arXiv:1410.4227.

[96] R. Barlow and C. Beeston, "Fitting using finite Monte Carlo samples", *Comput. Phys. Commun.* **77** (1993) 219, doi:10.1016/0010-4655(93)90005-W.

[97] ATLAS Collaboration, "Measurement of the inelastic proton-proton cross section at $\sqrt{s} = 13$ TeV with the ATLAS detector at the LHC", *Phys. Rev. Lett.* **117** (2016) 182002, doi:10.1103/PhysRevLett.117.182002, arXiv:1606.02625.

[98] CMS Collaboration, "Measurement of the inelastic proton-proton cross section at $\sqrt{s} = 13$ TeV", *JHEP* **07** (2018) 161, doi:10.1007/JHEP07(2018)161, arXiv:1802.02613.

[99] G. Passarino, "Higgs CAT", *Eur. Phys. J. C* **74** (2014) 2866, doi:10.1140/epjc/s10052-014-2866-7, arXiv:1312.2397.

[100] CMS Collaboration, "Measurement of Higgs boson production and properties in the WW decay channel with leptonic final states", *JHEP* **01** (2014) 096, doi:10.1007/JHEP01(2014)096, arXiv:1312.1129.

[101] The ATLAS Collaboration, The CMS Collaboration, The LHC Higgs Combination Group, "Procedure for the LHC Higgs boson search combination in Summer 2011", Technical Report ATL-PHYS-PUB 2011-11, CMS NOTE 2011/005, 2011.

[102] CMS Collaboration, "Combined measurements of Higgs boson couplings in proton-proton collisions at $\sqrt{s} = 13$ TeV", *Eur. Phys. J. C* **79** (2019) 421, doi:10.1140/epjc/s10052-019-6909-y, arXiv:1809.10733.

[103] S. S. Wilks, "The large-sample distribution of the likelihood ratio for testing composite hypotheses", *Annals Math. Statist.* **9** (1938) 60, doi:10.1214/aoms/1177732360.

[104] G. Cowan, K. Cranmer, E. Gross, and O. Vitells, "Asymptotic formulae for likelihood-based tests of new physics", *Eur. Phys. J. C* **71** (2011) 1554, doi:10.1140/epjc/s10052-011-1554-0, arXiv:1007.1727.

# A The CMS Collaboration

**Yerevan Physics Institute, Yerevan, Armenia**
A. Hayrapetyan, A. Tumasyan[1]

**Institut für Hochenergiephysik, Vienna, Austria**
W. Adam, J.W. Andrejkovic, T. Bergauer, S. Chatterjee, K. Damanakis, M. Dragicevic, P.S. Hussain, M. Jeitler[2], N. Krammer, A. Li, D. Liko, I. Mikulec, J. Schieck[2], R. Schöfbeck, D. Schwarz, M. Sonawane, S. Templ, W. Waltenberger, C.-E. Wulz[2]

**Universiteit Antwerpen, Antwerpen, Belgium**
M.R. Darwish[3], T. Janssen, P. Van Mechelen

**Vrije Universiteit Brussel, Brussel, Belgium**
E.S. Bols, J. D'Hondt, S. Dansana, A. De Moor, M. Delcourt, H. El Faham, S. Lowette, I. Makarenko, D. Müller, A.R. Sahasransu, S. Tavernier, M. Tytgat[4], G.P. Van Onsem, S. Van Putte, D. Vannerom

**Université Libre de Bruxelles, Bruxelles, Belgium**
B. Clerbaux, A.K. Das, G. De Lentdecker, L. Favart, P. Gianneios, D. Hohov, J. Jaramillo, A. Khalilzadeh, K. Lee, M. Mahdavikhorrami, A. Malara, S. Paredes, L. Pétré, N. Postiau, L. Thomas, M. Vanden Bemden, C. Vander Velde, P. Vanlaer

**Ghent University, Ghent, Belgium**
M. De Coen, D. Dobur, Y. Hong, J. Knolle, L. Lambrecht, G. Mestdach, K. Mota Amarilo, C. Rendón, A. Samalan, K. Skovpen, N. Van Den Bossche, J. van der Linden, L. Wezenbeek

**Université Catholique de Louvain, Louvain-la-Neuve, Belgium**
A. Benecke, A. Bethani, G. Bruno, C. Caputo, C. Delaere, I.S. Donertas, A. Giammanco, K. Jaffel, Sa. Jain, V. Lemaitre, J. Lidrych, P. Mastrapasqua, K. Mondal, T.T. Tran, S. Wertz

**Centro Brasileiro de Pesquisas Fisicas, Rio de Janeiro, Brazil**
G.A. Alves, E. Coelho, C. Hensel, T. Menezes De Oliveira, A. Moraes, P. Rebello Teles, M. Soeiro

**Universidade do Estado do Rio de Janeiro, Rio de Janeiro, Brazil**
W.L. Aldá Júnior, M. Alves Gallo Pereira, M. Barroso Ferreira Filho, H. Brandao Malbouisson, W. Carvalho, J. Chinellato[5], E.M. Da Costa, G.G. Da Silveira[6], D. De Jesus Damiao, S. Fonseca De Souza, R. Gomes De Souza, J. Martins[7], C. Mora Herrera, L. Mundim, H. Nogima, J.P. Pinheiro, A. Santoro, A. Sznajder, M. Thiel, A. Vilela Pereira

**Universidade Estadual Paulista, Universidade Federal do ABC, São Paulo, Brazil**
C.A. Bernardes[6], L. Calligaris, T.R. Fernandez Perez Tomei, E.M. Gregores, P.G. Mercadante, S.F. Novaes, B. Orzari, Sandra S. Padula

**Institute for Nuclear Research and Nuclear Energy, Bulgarian Academy of Sciences, Sofia, Bulgaria**
A. Aleksandrov, G. Antchev, R. Hadjiiska, P. Iaydjiev, M. Misheva, M. Shopova, G. Sultanov

**University of Sofia, Sofia, Bulgaria**

A. Dimitrov, L. Litov, B. Pavlov, P. Petkov, A. Petrov, E. Shumka

**Instituto De Alta Investigación, Universidad de Tarapacá, Casilla 7 D, Arica, Chile**
S. Keshri, S. Thakur

**Beihang University, Beijing, China**
T. Cheng, T. Javaid, L. Yuan

**Department of Physics, Tsinghua University, Beijing, China**
Z. Hu, J. Liu, K. Yi[8,9]

**Institute of High Energy Physics, Beijing, China**
G.M. Chen[10], H.S. Chen[10], M. Chen[10], F. Iemmi, C.H. Jiang, A. Kapoor[11], H. Liao, Z.-A. Liu[12], R. Sharma[13], J.N. Song[12], J. Tao, C. Wang[10], J. Wang, Z. Wang[10], H. Zhang

**State Key Laboratory of Nuclear Physics and Technology, Peking University, Beijing, China**
A. Agapitos, Y. Ban, A. Levin, C. Li, Q. Li, Y. Mao, S.J. Qian, X. Sun, D. Wang, H. Yang, L. Zhang, C. Zhou

**Sun Yat-Sen University, Guangzhou, China**
Z. You

**University of Science and Technology of China, Hefei, China**
N. Lu

**Nanjing Normal University, Nanjing, China**
G. Bauer[14]

**Institute of Modern Physics and Key Laboratory of Nuclear Physics and Ion-beam Application (MOE) - Fudan University, Shanghai, China**
X. Gao[15], D. Leggat, H. Okawa

**Zhejiang University, Hangzhou, Zhejiang, China**
Z. Lin, C. Lu, M. Xiao

**Universidad de Los Andes, Bogota, Colombia**
C. Avila, D.A. Barbosa Trujillo, A. Cabrera, C. Florez, J. Fraga, J.A. Reyes Vega

**Universidad de Antioquia, Medellin, Colombia**
J. Mejia Guisao, F. Ramirez, M. Rodriguez, J.D. Ruiz Alvarez

**University of Split, Faculty of Electrical Engineering, Mechanical Engineering and Naval Architecture, Split, Croatia**
D. Giljanovic, N. Godinovic, D. Lelas, A. Sculac

**University of Split, Faculty of Science, Split, Croatia**
M. Kovac, T. Sculac

**Institute Rudjer Boskovic, Zagreb, Croatia**
P. Bargassa, V. Brigljevic, B.K. Chitroda, D. Ferencek, S. Mishra, A. Starodumov[16], T. Susa

**University of Cyprus, Nicosia, Cyprus**
A. Attikis, K. Christoforou, S. Konstantinou, J. Mousa, C. Nicolaou, F. Ptochos, P.A. Razis, H. Rykaczewski, H. Saka, A. Stepennov

**Charles University, Prague, Czech Republic**

M. Finger, M. Finger Jr., A. Kveton

**Escuela Politecnica Nacional, Quito, Ecuador**
E. Ayala

**Universidad San Francisco de Quito, Quito, Ecuador**
E. Carrera Jarrin

**Academy of Scientific Research and Technology of the Arab Republic of Egypt, Egyptian Network of High Energy Physics, Cairo, Egypt**
S. Elgammal[17], A. Ellithi Kamel[18]

**Center for High Energy Physics (CHEP-FU), Fayoum University, El-Fayoum, Egypt**
M.A. Mahmoud, Y. Mohammed

**National Institute of Chemical Physics and Biophysics, Tallinn, Estonia**
K. Ehataht, M. Kadastik, T. Lange, S. Nandan, C. Nielsen, J. Pata, M. Raidal, L. Tani, C. Veelken

**Department of Physics, University of Helsinki, Helsinki, Finland**
H. Kirschenmann, K. Osterberg, M. Voutilainen

**Helsinki Institute of Physics, Helsinki, Finland**
S. Bharthuar, E. Brücken, F. Garcia, K.T.S. Kallonen, R. Kinnunen, T. Lampén, K. Lassila-Perini, S. Lehti, T. Lindén, L. Martikainen, M. Myllymäki, M.m. Rantanen, H. Siikonen, E. Tuominen, J. Tuominiemi

**Lappeenranta-Lahti University of Technology, Lappeenranta, Finland**
P. Luukka, H. Petrow

**IRFU, CEA, Université Paris-Saclay, Gif-sur-Yvette, France**
M. Besancon, F. Couderc, M. Dejardin, D. Denegri, J.L. Faure, F. Ferri, S. Ganjour, P. Gras, G. Hamel de Monchenault, V. Lohezic, J. Malcles, J. Rander, A. Rosowsky, M.Ö. Sahin, A. Savoy-Navarro[19], P. Simkina, M. Titov, M. Tornago

**Laboratoire Leprince-Ringuet, CNRS/IN2P3, Ecole Polytechnique, Institut Polytechnique de Paris, Palaiseau, France**
C. Baldenegro Barrera, F. Beaudette, A. Buchot Perraguin, P. Busson, A. Cappati, C. Charlot, M. Chiusi, F. Damas, O. Davignon, A. De Wit, B.A. Fontana Santos Alves, S. Ghosh, A. Gilbert, R. Granier de Cassagnac, A. Hakimi, B. Harikrishnan, L. Kalipoliti, G. Liu, J. Motta, M. Nguyen, C. Ochando, L. Portales, R. Salerno, J.B. Sauvan, Y. Sirois, A. Tarabini, E. Vernazza, A. Zabi, A. Zghiche

**Université de Strasbourg, CNRS, IPHC UMR 7178, Strasbourg, France**
J.-L. Agram[20], J. Andrea, D. Apparu, D. Bloch, J.-M. Brom, E.C. Chabert, C. Collard, S. Falke, U. Goerlach, C. Grimault, R. Haeberle, A.-C. Le Bihan, M. Meena, G. Saha, M.A. Sessini, P. Van Hove

**Institut de Physique des 2 Infinis de Lyon (IP2I ), Villeurbanne, France**
S. Beauceron, B. Blancon, G. Boudoul, N. Chanon, J. Choi, D. Contardo, P. Depasse, C. Dozen[21], H. El Mamouni, J. Fay, S. Gascon, M. Gouzevitch, C. Greenberg, G. Grenier, B. Ille, I.B. Laktineh, M. Lethuillier, L. Mirabito, S. Perries, A. Purohit, M. Vander Donckt, P. Verdier, J. Xiao

**Georgian Technical University, Tbilisi, Georgia**

G. Adamov, I. Lomidze, Z. Tsamalaidze[16]

**RWTH Aachen University, I. Physikalisches Institut, Aachen, Germany**
V. Botta, L. Feld, K. Klein, M. Lipinski, D. Meuser, A. Pauls, N. Röwert, M. Teroerde

**RWTH Aachen University, III. Physikalisches Institut A, Aachen, Germany**
S. Diekmann, A. Dodonova, N. Eich, D. Eliseev, F. Engelke, J. Erdmann, M. Erdmann, P. Fackeldey, B. Fischer, T. Hebbeker, K. Hoepfner, F. Ivone, A. Jung, M.y. Lee, L. Mastrolorenzo, F. Mausolf, M. Merschmeyer, A. Meyer, S. Mukherjee, D. Noll, F. Nowotny, A. Pozdnyakov, Y. Rath, W. Redjeb, F. Rehm, H. Reithler, U. Sarkar, V. Sarkisovi, A. Schmidt, A. Sharma, J.L. Spah, A. Stein, F. Torres Da Silva De Araujo[22], L. Vigilante, S. Wiedenbeck, S. Zaleski

**RWTH Aachen University, III. Physikalisches Institut B, Aachen, Germany**
C. Dziwok, G. Flügge, W. Haj Ahmad[23], T. Kress, A. Nowack, O. Pooth, A. Stahl, T. Ziemons, A. Zotz

**Deutsches Elektronen-Synchrotron, Hamburg, Germany**
H. Aarup Petersen, M. Aldaya Martin, J. Alimena, S. Amoroso, Y. An, S. Baxter, M. Bayatmakou, H. Becerril Gonzalez, O. Behnke, A. Belvedere, S. Bhattacharya, F. Blekman[24], K. Borras[25], A. Campbell, A. Cardini, C. Cheng, F. Colombina, S. Consuegra Rodríguez, G. Correia Silva, M. De Silva, G. Eckerlin, D. Eckstein, L.I. Estevez Banos, O. Filatov, E. Gallo[24], A. Geiser, A. Giraldi, G. Greau, V. Guglielmi, M. Guthoff, A. Hinzmann, A. Jafari[26], L. Jeppe, N.Z. Jomhari, B. Kaech, M. Kasemann, C. Kleinwort, R. Kogler, M. Komm, D. Krücker, W. Lange, D. Leyva Pernia, K. Lipka[27], W. Lohmann[28], R. Mankel, I.-A. Melzer-Pellmann, M. Mendizabal Morentin, A.B. Meyer, G. Milella, A. Mussgiller, L.P. Nair, A. Nürnberg, Y. Otarid, J. Park, D. Pérez Adán, E. Ranken, A. Raspereza, B. Ribeiro Lopes, J. Rübenach, A. Saggio, M. Scham[29,25], S. Schnake[25], P. Schütze, C. Schwanenberger[24], D. Selivanova, K. Sharko, M. Shchedrolosiev, R.E. Sosa Ricardo, D. Stafford, F. Vazzoler, A. Ventura Barroso, R. Walsh, Q. Wang, Y. Wen, K. Wichmann, L. Wiens[25], C. Wissing, Y. Yang, A. Zimermmane Castro Santos

**University of Hamburg, Hamburg, Germany**
A. Albrecht, S. Albrecht, M. Antonello, S. Bein, L. Benato, S. Bollweg, M. Bonanomi, P. Connor, M. Eich, K. El Morabit, Y. Fischer, A. Fröhlich, C. Garbers, E. Garutti, A. Grohsjean, M. Hajheidari, J. Haller, H.R. Jabusch, G. Kasieczka, P. Keicher, R. Klanner, W. Korcari, T. Kramer, V. Kutzner, F. Labe, J. Lange, A. Lobanov, C. Matthies, A. Mehta, L. Moureaux, M. Mrowietz, A. Nigamova, Y. Nissan, A. Paasch, K.J. Pena Rodriguez, T. Quadfasel, B. Raciti, M. Rieger, D. Savoiu, J. Schindler, P. Schleper, M. Schröder, J. Schwandt, M. Sommerhalder, H. Stadie, G. Steinbrück, A. Tews, M. Wolf

**Karlsruher Institut fuer Technologie, Karlsruhe, Germany**
S. Brommer, M. Burkart, E. Butz, T. Chwalek, A. Dierlamm, A. Droll, N. Faltermann, M. Giffels, A. Gottmann, F. Hartmann[30], R. Hofsaess, M. Horzela, U. Husemann, J. Kieseler, M. Klute, R. Koppenhöfer, J.M. Lawhorn, M. Link, A. Lintuluoto, S. Maier, S. Mitra, M. Mormile, Th. Müller, M. Neukum, M. Oh, M. Presilla, G. Quast, K. Rabbertz, B. Regnery, N. Shadskiy, I. Shvetsov, H.J. Simonis, M. Toms, N. Trevisani, R. Ulrich, R.F. Von Cube, M. Wassmer,

S. Wieland, F. Wittig, R. Wolf, X. Zuo

**Institute of Nuclear and Particle Physics (INPP), NCSR Demokritos, Aghia Paraskevi, Greece**
G. Anagnostou, G. Daskalakis, A. Kyriakis, A. Papadopoulos[30], A. Stakia

**National and Kapodistrian University of Athens, Athens, Greece**
P. Kontaxakis, G. Melachroinos, A. Panagiotou, I. Papavergou, I. Paraskevas, N. Saoulidou, K. Theofilatos, E. Tziaferi, K. Vellidis, I. Zisopoulos

**National Technical University of Athens, Athens, Greece**
G. Bakas, T. Chatzistavrou, G. Karapostoli, K. Kousouris, I. Papakrivopoulos, E. Siamarkou, G. Tsipolitis, A. Zacharopoulou

**University of Ioánnina, Ioánnina, Greece**
K. Adamidis, I. Bestintzanos, I. Evangelou, C. Foudas, C. Kamtsikis, P. Katsoulis, P. Kokkas, P.G. Kosmoglou Kioseoglou, N. Manthos, I. Papadopoulos, J. Strologas

**HUN-REN Wigner Research Centre for Physics, Budapest, Hungary**
M. Bartók[31], C. Hajdu, D. Horvath[32,33], K. Márton, F. Sikler, V. Veszpremi

**MTA-ELTE Lendület CMS Particle and Nuclear Physics Group, Eötvös Loránd University, Budapest, Hungary**
M. Csanád, K. Farkas, M.M.A. Gadallah[34], Á. Kadlecsik, P. Major, K. Mandal, G. Pásztor, A.J. Rádl[35], G.I. Veres

**Faculty of Informatics, University of Debrecen, Debrecen, Hungary**
P. Raics, B. Ujvari, G. Zilizi

**Institute of Nuclear Research ATOMKI, Debrecen, Hungary**
G. Bencze, S. Czellar, J. Molnar, Z. Szillasi

**Karoly Robert Campus, MATE Institute of Technology, Gyongyos, Hungary**
T. Csorgo[35], F. Nemes[35], T. Novak

**Panjab University, Chandigarh, India**
J. Babbar, S. Bansal, S.B. Beri, V. Bhatnagar, G. Chaudhary, S. Chauhan, N. Dhingra[36], A. Kaur, A. Kaur, H. Kaur, M. Kaur, S. Kumar, K. Sandeep, T. Sheokand, J.B. Singh, A. Singla

**University of Delhi, Delhi, India**
A. Ahmed, A. Bhardwaj, A. Chhetri, B.C. Choudhary, A. Kumar, A. Kumar, M. Naimuddin, K. Ranjan, S. Saumya

**Saha Institute of Nuclear Physics, HBNI, Kolkata, India**
S. Baradia, S. Barman[37], S. Bhattacharya, S. Dutta, S. Dutta, S. Sarkar

**Indian Institute of Technology Madras, Madras, India**
M.M. Ameen, P.K. Behera, S.C. Behera, S. Chatterjee, P. Jana, P. Kalbhor, J.R. Komaragiri[38], D. Kumar[38], L. Panwar[38], P.R. Pujahari, N.R. Saha, A. Sharma, A.K. Sikdar, S. Verma

**Tata Institute of Fundamental Research-A, Mumbai, India**
S. Dugad, M. Kumar, G.B. Mohanty, P. Suryadevara

**Tata Institute of Fundamental Research-B, Mumbai, India**
A. Bala, S. Banerjee, R.M. Chatterjee, R.K. Dewanjee[39], M. Guchait, Sh. Jain,

A. Jaiswal, S. Karmakar, S. Kumar, G. Majumder, K. Mazumdar, S. Parolia, A. Thachayath

**National Institute of Science Education and Research, An OCC of Homi Bhabha National Institute, Bhubaneswar, Odisha, India**
S. Bahinipati[40], C. Kar, D. Maity[41], P. Mal, T. Mishra, V.K. Muraleedharan Nair Bindhu[41], K. Naskar[41], A. Nayak[41], P. Sadangi, P. Saha, S.K. Swain, S. Varghese[41], D. Vats[41]

**Indian Institute of Science Education and Research (IISER), Pune, India**
S. Acharya[42], A. Alpana, S. Dube, B. Gomber[42], B. Kansal, A. Laha, B. Sahu[42], S. Sharma, K.Y. Vaish

**Isfahan University of Technology, Isfahan, Iran**
H. Bakhshiansohi[43], E. Khazaie[44], M. Zeinali[45]

**Institute for Research in Fundamental Sciences (IPM), Tehran, Iran**
S. Chenarani[46], S.M. Etesami, M. Khakzad, M. Mohammadi Najafabadi

**University College Dublin, Dublin, Ireland**
M. Grunewald

**INFN Sezione di Bari[a], Università di Bari[b], Politecnico di Bari[c], Bari, Italy**
M. Abbrescia[a,b], R. Aly[a,c,47], A. Colaleo[a,b], D. Creanza[a,c], B. D'Anzi[a,b], N. De Filippis[a,c], M. De Palma[a,b], A. Di Florio[a,c], W. Elmetenawee[a,b,47], L. Fiore[a], G. Iaselli[a,c], M. Louka[a,b], G. Maggi[a,c], M. Maggi[a], I. Margjeka[a,b], V. Mastrapasqua[a,b], S. My[a,b], S. Nuzzo[a,b], A. Pellecchia[a,b], A. Pompili[a,b], G. Pugliese[a,c], R. Radogna[a], G. Ramirez-Sanchez[a,c], D. Ramos[a], A. Ranieri[a], L. Silvestris[a], F.M. Simone[a,b], Ü. Sözbilir[a], A. Stamerra[a], R. Venditti[a], P. Verwilligen[a], A. Zaza[a,b]

**INFN Sezione di Bologna[a], Università di Bologna[b], Bologna, Italy**
G. Abbiendi[a], C. Battilana[a,b], D. Bonacorsi[a,b], L. Borgonovi[a], R. Campanini[a,b], P. Capiluppi[a,b], A. Castro[a,b], F.R. Cavallo[a], M. Cuffiani[a,b], G.M. Dallavalle[a], T. Diotalevi[a,b], F. Fabbri[a], A. Fanfani[a,b], D. Fasanella[a,b], P. Giacomelli[a], L. Giommi[a,b], C. Grandi[a], L. Guiducci[a,b], S. Lo Meo[a,48], L. Lunerti[a,b], G. Masetti[a], F.L. Navarria[a,b], A. Perrotta[a], F. Primavera[a,b], A.M. Rossi[a,b], T. Rovelli[a,b], G.P. Siroli[a,b]

**INFN Sezione di Catania[a], Università di Catania[b], Catania, Italy**
S. Costa[a,b,49], A. Di Mattia[a], R. Potenza[a,b], A. Tricomi[a,b,49], C. Tuve[a,b]

**INFN Sezione di Firenze[a], Università di Firenze[b], Firenze, Italy**
P. Assiouras[a], G. Barbagli[a], G. Bardelli[a,b], B. Camaiani[a,b], A. Cassese[a], R. Ceccarelli[a], V. Ciulli[a,b], C. Civinini[a], R. D'Alessandro[a,b], E. Focardi[a,b], T. Kello[a], G. Latino[a,b], P. Lenzi[a,b], M. Lizzo[a], M. Meschini[a], S. Paoletti[a], A. Papanastassiou[a,b], G. Sguazzoni[a], L. Viliani[a]

**INFN Laboratori Nazionali di Frascati, Frascati, Italy**
L. Benussi, S. Bianco, S. Meola[50], D. Piccolo

**INFN Sezione di Genova[a], Università di Genova[b], Genova, Italy**
P. Chatagnon[a], F. Ferro[a], E. Robutti[a], S. Tosi[a,b]

**INFN Sezione di Milano-Bicocca[a], Università di Milano-Bicocca[b], Milano, Italy**

A. Benaglia[a], G. Boldrini[a,b], F. Brivio[a], F. Cetorelli[a], F. De Guio[a,b], M.E. Dinardo[a,b], P. Dini[a], S. Gennai[a], R. Gerosa[a,b], A. Ghezzi[a,b], P. Govoni[a,b], L. Guzzi[a], M.T. Lucchini[a,b], M. Malberti[a], S. Malvezzi[a], A. Massironi[a], D. Menasce[a], L. Moroni[a], M. Paganoni[a,b], D. Pedrini[a], B.S. Pinolini[a], S. Ragazzi[a,b], T. Tabarelli de Fatis[a,b], D. Zuolo[a]

**INFN Sezione di Napoli[a], Università di Napoli 'Federico II'[b], Napoli, Italy; Università della Basilicata[c], Potenza, Italy; Scuola Superiore Meridionale (SSM)[d], Napoli, Italy**
S. Buontempo[a], A. Cagnotta[a,b], F. Carnevali[a,b], N. Cavallo[a,c], F. Fabozzi[a,c], A.O.M. Iorio[a,b], L. Lista[a,b,51], P. Paolucci[a,30], B. Rossi[a], C. Sciacca[a,b]

**INFN Sezione di Padova[a], Università di Padova[b], Padova, Italy; Università di Trento[c], Trento, Italy**
R. Ardino[a], P. Azzi[a], N. Bacchetta[a,52], D. Bisello[a,b], P. Bortignon[a], A. Bragagnolo[a,b], R. Carlin[a,b], P. Checchia[a], T. Dorigo[a], F. Gasparini[a,b], U. Gasparini[a,b], F. Gonella[a], E. Lusiani[a], M. Margoni[a,b], F. Marini[a], M. Migliorini[a,b], J. Pazzini[a,b], P. Ronchese[a,b], R. Rossin[a,b], F. Simonetto[a,b], G. Strong[a], M. Tosi[a,b], A. Triossi[a,b], S. Ventura[a], H. Yarar[a,b], M. Zanetti[a,b], P. Zotto[a,b], A. Zucchetta[a,b], G. Zumerle[a,b]

**INFN Sezione di Pavia[a], Università di Pavia[b], Pavia, Italy**
S. Abu Zeid[a,53], C. Aimè[a,b], A. Braghieri[a], S. Calzaferri[a], D. Fiorina[a], P. Montagna[a,b], V. Re[a], C. Riccardi[a,b], P. Salvini[a], I. Vai[a,b], P. Vitulo[a,b]

**INFN Sezione di Perugia[a], Università di Perugia[b], Perugia, Italy**
S. Ajmal[a,b], G.M. Bilei[a], D. Ciangottini[a,b], L. Fanò[a,b], M. Magherini[a,b], G. Mantovani[a,b], V. Mariani[a,b], M. Menichelli[a], F. Moscatelli[a,54], A. Rossi[a,b], A. Santocchia[a,b], D. Spiga[a], T. Tedeschi[a,b]

**INFN Sezione di Pisa[a], Università di Pisa[b], Scuola Normale Superiore di Pisa[c], Pisa, Italy; Università di Siena[d], Siena, Italy**
P. Asenov[a,b], P. Azzurri[a], G. Bagliesi[a], R. Bhattacharya[a], L. Bianchini[a,b], T. Boccali[a], E. Bossini[a], D. Bruschini[a,c], R. Castaldi[a], M.A. Ciocci[a,b], M. Cipriani[a,b], V. D'Amante[a,d], R. Dell'Orso[a], S. Donato[a], A. Giassi[a], F. Ligabue[a,c], D. Matos Figueiredo[a], A. Messineo[a,b], M. Musich[a,b], F. Palla[a], A. Rizzi[a,b], G. Rolandi[a,c], S. Roy Chowdhury[a], T. Sarkar[a], A. Scribano[a], P. Spagnolo[a], R. Tenchini[a], G. Tonelli[a,b], N. Turini[a,d], A. Venturi[a], P.G. Verdini[a]

**INFN Sezione di Roma[a], Sapienza Università di Roma[b], Roma, Italy**
P. Barria[a], M. Campana[a,b], F. Cavallari[a], L. Cunqueiro Mendez[a,b], D. Del Re[a,b], E. Di Marco[a], M. Diemoz[a], F. Errico[a,b], E. Longo[a,b], P. Meridiani[a], J. Mijuskovic[a,b], G. Organtini[a,b], F. Pandolfi[a], R. Paramatti[a,b], C. Quaranta[a,b], S. Rahatlou[a,b], C. Rovelli[a], F. Santanastasio[a,b], L. Soffi[a]

**INFN Sezione di Torino[a], Università di Torino[b], Torino, Italy; Università del Piemonte Orientale[c], Novara, Italy**
N. Amapane[a,b], R. Arcidiacono[a,c], S. Argiro[a,b], M. Arneodo[a,c], N. Bartosik[a], R. Bellan[a,b], A. Bellora[a,b], C. Biino[a], C. Borca[a,b], N. Cartiglia[a], M. Costa[a,b], R. Covarelli[a,b], N. Demaria[a], L. Finco[a], M. Grippo[a,b], B. Kiani[a,b], F. Legger[a], F. Luongo[a,b], C. Mariotti[a], L. Markovic[a,b], S. Maselli[a], A. Mecca[a,b], E. Migliore[a,b], M. Monteno[a], R. Mulargia[a], M.M. Obertino[a,b], G. Ortona[a], L. Pacher[a,b], N. Pastrone[a], M. Pelliccioni[a], M. Ruspa[a,c], F. Siviero[a,b], V. Sola[a,b], A. Solano[a,b], A. Staiano[a], C. Tarricone[a,b], D. Trocino[a], G. Umoret[a,b],

E. Vlasov[a,b]

**INFN Sezione di Trieste[a], Università di Trieste[b], Trieste, Italy**
S. Belforte[a], V. Candelise[a,b], M. Casarsa[a], F. Cossutti[a], K. De Leo[a,b], G. Della Ricca[a,b]

**Kyungpook National University, Daegu, Korea**
S. Dogra, J. Hong, C. Huh, B. Kim, D.H. Kim, J. Kim, H. Lee, S.W. Lee, C.S. Moon, Y.D. Oh, M.S. Ryu, S. Sekmen, Y.C. Yang

**Department of Mathematics and Physics - GWNU, Gangneung, Korea**
M.S. Kim

**Chonnam National University, Institute for Universe and Elementary Particles, Kwangju, Korea**
G. Bak, P. Gwak, H. Kim, D.H. Moon

**Hanyang University, Seoul, Korea**
E. Asilar, D. Kim, T.J. Kim, J.A. Merlin

**Korea University, Seoul, Korea**
S. Choi, S. Han, B. Hong, K. Lee, K.S. Lee, S. Lee, J. Park, S.K. Park, J. Yoo

**Kyung Hee University, Department of Physics, Seoul, Korea**
J. Goh, S. Yang

**Sejong University, Seoul, Korea**
H. S. Kim, Y. Kim, S. Lee

**Seoul National University, Seoul, Korea**
J. Almond, J.H. Bhyun, J. Choi, W. Jun, J. Kim, S. Ko, H. Kwon, H. Lee, J. Lee, J. Lee, B.H. Oh, S.B. Oh, H. Seo, U.K. Yang, I. Yoon

**University of Seoul, Seoul, Korea**
W. Jang, D.Y. Kang, Y. Kang, S. Kim, B. Ko, J.S.H. Lee, Y. Lee, I.C. Park, Y. Roh, I.J. Watson

**Yonsei University, Department of Physics, Seoul, Korea**
S. Ha, H.D. Yoo

**Sungkyunkwan University, Suwon, Korea**
M. Choi, M.R. Kim, H. Lee, Y. Lee, I. Yu

**College of Engineering and Technology, American University of the Middle East (AUM), Dasman, Kuwait**
T. Beyrouthy, Y. Maghrbi

**Riga Technical University, Riga, Latvia**
K. Dreimanis, A. Gaile, G. Pikurs, A. Potrebko, M. Seidel, V. Veckalns[55]

**University of Latvia (LU), Riga, Latvia**
N.R. Strautnieks

**Vilnius University, Vilnius, Lithuania**
M. Ambrozas, A. Juodagalvis, A. Rinkevicius, G. Tamulaitis

**National Centre for Particle Physics, Universiti Malaya, Kuala Lumpur, Malaysia**
N. Bin Norjoharuddeen, I. Yusuff[56], Z. Zolkapli

**Universidad de Sonora (UNISON), Hermosillo, Mexico**
J.F. Benitez, A. Castaneda Hernandez, H.A. Encinas Acosta, L.G. Gallegos Maríñez, M. León Coello, J.A. Murillo Quijada, A. Sehrawat, L. Valencia Palomo

**Centro de Investigacion y de Estudios Avanzados del IPN, Mexico City, Mexico**
G. Ayala, H. Castilla-Valdez, H. Crotte Ledesma, E. De La Cruz-Burelo, I. Heredia-De La Cruz[57], R. Lopez-Fernandez, C.A. Mondragon Herrera, A. Sánchez Hernández

**Universidad Iberoamericana, Mexico City, Mexico**
C. Oropeza Barrera, M. Ramírez García

**Benemerita Universidad Autonoma de Puebla, Puebla, Mexico**
I. Bautista, I. Pedraza, H.A. Salazar Ibarguen, C. Uribe Estrada

**University of Montenegro, Podgorica, Montenegro**
I. Bubanja, N. Raicevic

**University of Canterbury, Christchurch, New Zealand**
P.H. Butler

**National Centre for Physics, Quaid-I-Azam University, Islamabad, Pakistan**
A. Ahmad, M.I. Asghar, A. Awais, M.I.M. Awan, H.R. Hoorani, W.A. Khan

**AGH University of Krakow, Faculty of Computer Science, Electronics and Telecommunications, Krakow, Poland**
V. Avati, L. Grzanka, M. Malawski

**National Centre for Nuclear Research, Swierk, Poland**
H. Bialkowska, M. Bluj, B. Boimska, M. Górski, M. Kazana, M. Szleper, P. Zalewski

**Institute of Experimental Physics, Faculty of Physics, University of Warsaw, Warsaw, Poland**
K. Bunkowski, K. Doroba, A. Kalinowski, M. Konecki, J. Krolikowski, A. Muhammad

**Warsaw University of Technology, Warsaw, Poland**
K. Pozniak, W. Zabolotny

**Laboratório de Instrumentação e Física Experimental de Partículas, Lisboa, Portugal**
M. Araujo, D. Bastos, C. Beirão Da Cruz E Silva, A. Boletti, M. Bozzo, T. Camporesi, G. Da Molin, P. Faccioli, M. Gallinaro, J. Hollar, N. Leonardo, T. Niknejad, A. Petrilli, M. Pisano, J. Seixas, J. Varela, J.W. Wulff

**Faculty of Physics, University of Belgrade, Belgrade, Serbia**
P. Adzic, P. Milenovic

**VINCA Institute of Nuclear Sciences, University of Belgrade, Belgrade, Serbia**
M. Dordevic, J. Milosevic, V. Rekovic

**Centro de Investigaciones Energéticas Medioambientales y Tecnológicas (CIEMAT), Madrid, Spain**
M. Aguilar-Benitez, J. Alcaraz Maestre, Cristina F. Bedoya, M. Cepeda, M. Cerrada, N. Colino, B. De La Cruz, A. Delgado Peris, A. Escalante Del Valle, D. Fernández Del Val, J.P. Fernández Ramos, J. Flix, M.C. Fouz, O. Gonzalez Lopez, S. Goy Lopez, J.M. Hernandez, M.I. Josa, D. Moran, C. M. Morcillo Perez, Á. Navarro Tobar, C. Perez Dengra, A. Pérez-Calero Yzquierdo, J. Puerta Pelayo,

I. Redondo, D.D. Redondo Ferrero, L. Romero, S. Sánchez Navas, L. Urda Gómez, J. Vazquez Escobar, C. Willmott

**Universidad Autónoma de Madrid, Madrid, Spain**
J.F. de Trocóniz

**Universidad de Oviedo, Instituto Universitario de Ciencias y Tecnologías Espaciales de Asturias (ICTEA), Oviedo, Spain**
B. Alvarez Gonzalez, J. Cuevas, J. Fernandez Menendez, S. Folgueras, I. Gonzalez Caballero, J.R. González Fernández, E. Palencia Cortezon, C. Ramón Álvarez, V. Rodríguez Bouza, A. Soto Rodríguez, A. Trapote, C. Vico Villalba, P. Vischia

**Instituto de Física de Cantabria (IFCA), CSIC-Universidad de Cantabria, Santander, Spain**
S. Bhowmik, S. Blanco Fernández, J.A. Brochero Cifuentes, I.J. Cabrillo, A. Calderon, J. Duarte Campderros, M. Fernandez, G. Gomez, C. Lasaosa García, C. Martinez Rivero, P. Martinez Ruiz del Arbol, F. Matorras, P. Matorras Cuevas, E. Navarrete Ramos, J. Piedra Gomez, L. Scodellaro, I. Vila, J.M. Vizan Garcia

**University of Colombo, Colombo, Sri Lanka**
M.K. Jayananda, B. Kailasapathy[58], D.U.J. Sonnadara, D.D.C. Wickramarathna

**University of Ruhuna, Department of Physics, Matara, Sri Lanka**
W.G.D. Dharmaratna[59], K. Liyanage, N. Perera, N. Wickramage

**CERN, European Organization for Nuclear Research, Geneva, Switzerland**
D. Abbaneo, C. Amendola, E. Auffray, G. Auzinger, J. Baechler, D. Barney, A. Bermúdez Martínez, M. Bianco, B. Bilin, A.A. Bin Anuar, A. Bocci, C. Botta, E. Brondolin, C. Caillol, G. Cerminara, N. Chernyavskaya, D. d'Enterria, A. Dabrowski, A. David, A. De Roeck, M.M. Defranchis, M. Deile, M. Dobson, L. Forthomme, G. Franzoni, W. Funk, S. Giani, D. Gigi, K. Gill, F. Glege, L. Gouskos, M. Haranko, J. Hegeman, B. Huber, V. Innocente, T. James, P. Janot, S. Laurila, P. Lecoq, E. Leutgeb, C. Lourenço, B. Maier, L. Malgeri, M. Mannelli, A.C. Marini, M. Matthewman, F. Meijers, S. Mersi, E. Meschi, V. Milosevic, F. Monti, F. Moortgat, M. Mulders, I. Neutelings, S. Orfanelli, F. Pantaleo, G. Petrucciani, A. Pfeiffer, M. Pierini, D. Piparo, H. Qu, D. Rabady, G. Reales Gutiérrez, M. Rovere, H. Sakulin, S. Scarfi, C. Schwick, M. Selvaggi, A. Sharma, K. Shchelina, P. Silva, P. Sphicas[60], A.G. Stahl Leiton, A. Steen, S. Summers, D. Treille, P. Tropea, A. Tsirou, D. Walter, J. Wanczyk[61], J. Wang, S. Wuchterl, P. Zehetner, P. Zejdl, W.D. Zeuner

**Paul Scherrer Institut, Villigen, Switzerland**
T. Bevilacqua[62], L. Caminada[62], A. Ebrahimi, W. Erdmann, R. Horisberger, Q. Ingram, H.C. Kaestli, D. Kotlinski, C. Lange, M. Missiroli[62], L. Noehte[62], T. Rohe

**ETH Zurich - Institute for Particle Physics and Astrophysics (IPA), Zurich, Switzerland**
T.K. Aarrestad, K. Androsov[61], M. Backhaus, A. Calandri, C. Cazzaniga, K. Datta, A. De Cosa, G. Dissertori, M. Dittmar, M. Donegà, F. Eble, M. Galli, K. Gedia, F. Glessgen, C. Grab, D. Hits, W. Lustermann, A.-M. Lyon, R.A. Manzoni, M. Marchegiani, L. Marchese, C. Martin Perez, A. Mascellani[61], F. Nessi-Tedaldi, F. Pauss, V. Perovic, S. Pigazzini, C. Reissel, T. Reitenspiess, B. Ristic, F. Riti, D. Ruini, R. Seidita, J. Steggemann[61], D. Valsecchi, R. Wallny

**Universität Zürich, Zurich, Switzerland**

C. Amsler[63], P. Bärtschi, D. Brzhechko, M.F. Canelli, K. Cormier, J.K. Heikkilä, M. Huwiler, W. Jin, A. Jofrehei, B. Kilminster, S. Leontsinis, S.P. Liechti, A. Macchiolo, P. Meiring, U. Molinatti, A. Reimers, P. Robmann, S. Sanchez Cruz, M. Senger, Y. Takahashi, R. Tramontano

**National Central University, Chung-Li, Taiwan**
C. Adloff[64], D. Bhowmik, C.M. Kuo, W. Lin, P.K. Rout, P.C. Tiwari[38], S.S. Yu

**National Taiwan University (NTU), Taipei, Taiwan**
L. Ceard, Y. Chao, K.F. Chen, P.s. Chen, Z.g. Chen, A. De Iorio, W.-S. Hou, T.h. Hsu, Y.w. Kao, R. Khurana, G. Kole, Y.y. Li, R.-S. Lu, E. Paganis, X.f. Su, J. Thomas-Wilsker, L.s. Tsai, H.y. Wu, E. Yazgan

**High Energy Physics Research Unit, Department of Physics, Faculty of Science, Chulalongkorn University, Bangkok, Thailand**
C. Asawatangtrakuldee, N. Srimanobhas, V. Wachirapusitanand

**Çukurova University, Physics Department, Science and Art Faculty, Adana, Turkey**
D. Agyel, F. Boran, Z.S. Demiroglu, F. Dolek, I. Dumanoglu[65], E. Eskut, Y. Guler[66], E. Gurpinar Guler[66], C. Isik, O. Kara, A. Kayis Topaksu, U. Kiminsu, G. Onengut, K. Ozdemir[67], A. Polatoz, B. Tali[68], U.G. Tok, S. Turkcapar, E. Uslan, I.S. Zorbakir

**Middle East Technical University, Physics Department, Ankara, Turkey**
M. Yalvac[69]

**Bogazici University, Istanbul, Turkey**
B. Akgun, I.O. Atakisi, E. Gülmez, M. Kaya[70], O. Kaya[71], S. Tekten[72]

**Istanbul Technical University, Istanbul, Turkey**
A. Cakir, K. Cankocak[65,73], Y. Komurcu, S. Sen[74]

**Istanbul University, Istanbul, Turkey**
O. Aydilek, S. Cerci[68], V. Epshteyn, B. Hacisahinoglu, I. Hos[75], B. Kaynak, S. Ozkorucuklu, O. Potok, H. Sert, C. Simsek, C. Zorbilmez

**Yildiz Technical University, Istanbul, Turkey**
B. Isildak[76], D. Sunar Cerci[68]

**Institute for Scintillation Materials of National Academy of Science of Ukraine, Kharkiv, Ukraine**
A. Boyaryntsev, B. Grynyov

**National Science Centre, Kharkiv Institute of Physics and Technology, Kharkiv, Ukraine**
L. Levchuk

**University of Bristol, Bristol, United Kingdom**
D. Anthony, J.J. Brooke, A. Bundock, F. Bury, E. Clement, D. Cussans, H. Flacher, M. Glowacki, J. Goldstein, H.F. Heath, L. Kreczko, S. Paramesvaran, S. Seif El Nasr-Storey, V.J. Smith, N. Stylianou[77], K. Walkingshaw Pass, R. White

**Rutherford Appleton Laboratory, Didcot, United Kingdom**
A.H. Ball, K.W. Bell, A. Belyaev[78], C. Brew, R.M. Brown, D.J.A. Cockerill, C. Cooke, K.V. Ellis, K. Harder, S. Harper, M.-L. Holmberg[79], J. Linacre, K. Manolopoulos, D.M. Newbold, E. Olaiya, D. Petyt, T. Reis, G. Salvi, T. Schuh, C.H. Shepherd-Themistocleous, I.R. Tomalin, T. Williams

**Imperial College, London, United Kingdom**
R. Bainbridge, P. Bloch, C.E. Brown, O. Buchmuller, V. Cacchio, C.A. Carrillo Montoya, G.S. Chahal[80], D. Colling, J.S. Dancu, I. Das, P. Dauncey, G. Davies, J. Davies, M. Della Negra, S. Fayer, G. Fedi, G. Hall, M.H. Hassanshahi, A. Howard, G. Iles, M. Knight, J. Langford, J. León Holgado, L. Lyons, A.-M. Magnan, S. Malik, M. Mieskolainen, J. Nash[81], M. Pesaresi, B.C. Radburn-Smith, A. Richards, A. Rose, K. Savva, C. Seez, R. Shukla, A. Tapper, K. Uchida, G.P. Uttley, L.H. Vage, T. Virdee[30], M. Vojinovic, N. Wardle, D. Winterbottom

**Brunel University, Uxbridge, United Kingdom**
K. Coldham, J.E. Cole, A. Khan, P. Kyberd, I.D. Reid

**Baylor University, Waco, Texas, USA**
S. Abdullin, A. Brinkerhoff, B. Caraway, J. Dittmann, K. Hatakeyama, J. Hiltbrand, B. McMaster, M. Saunders, S. Sawant, C. Sutantawibul, J. Wilson

**Catholic University of America, Washington, DC, USA**
R. Bartek, A. Dominguez, C. Huerta Escamilla, A.E. Simsek, R. Uniyal, A.M. Vargas Hernandez

**The University of Alabama, Tuscaloosa, Alabama, USA**
B. Bam, R. Chudasama, S.I. Cooper, S.V. Gleyzer, C.U. Perez, P. Rumerio[82], E. Usai, R. Yi

**Boston University, Boston, Massachusetts, USA**
A. Akpinar, D. Arcaro, C. Cosby, Z. Demiragli, C. Erice, C. Fangmeier, C. Fernandez Madrazo, E. Fontanesi, D. Gastler, F. Golf, S. Jeon, I. Reed, J. Rohlf, K. Salyer, D. Sperka, D. Spitzbart, I. Suarez, A. Tsatsos, S. Yuan, A.G. Zecchinelli

**Brown University, Providence, Rhode Island, USA**
G. Benelli, X. Coubez[25], D. Cutts, M. Hadley, U. Heintz, J.M. Hogan[83], T. Kwon, G. Landsberg, K.T. Lau, D. Li, J. Luo, S. Mondal, M. Narain[†], N. Pervan, S. Sagir[84], F. Simpson, M. Stamenkovic, W.Y. Wong, X. Yan, W. Zhang

**University of California, Davis, Davis, California, USA**
S. Abbott, J. Bonilla, C. Brainerd, R. Breedon, M. Calderon De La Barca Sanchez, M. Chertok, M. Citron, J. Conway, P.T. Cox, R. Erbacher, F. Jensen, O. Kukral, G. Mocellin, M. Mulhearn, D. Pellett, W. Wei, Y. Yao, F. Zhang

**University of California, Los Angeles, California, USA**
M. Bachtis, R. Cousins, A. Datta, G. Flores Avila, J. Hauser, M. Ignatenko, M.A. Iqbal, T. Lam, E. Manca, A. Nunez Del Prado, D. Saltzberg, V. Valuev

**University of California, Riverside, Riverside, California, USA**
R. Clare, J.W. Gary, M. Gordon, G. Hanson, W. Si, S. Wimpenny[†]

**University of California, San Diego, La Jolla, California, USA**
J.G. Branson, S. Cittolin, S. Cooperstein, D. Diaz, J. Duarte, L. Giannini, J. Guiang, R. Kansal, V. Krutelyov, R. Lee, J. Letts, M. Masciovecchio, F. Mokhtar, S. Mukherjee, M. Pieri, M. Quinnan, B.V. Sathia Narayanan, V. Sharma, M. Tadel, E. Vourliotis, F. Würthwein, Y. Xiang, A. Yagil

**University of California, Santa Barbara - Department of Physics, Santa Barbara, California, USA**

A. Barzdukas, L. Brennan, C. Campagnari, A. Dorsett, J. Incandela, J. Kim, A.J. Li, P. Masterson, H. Mei, J. Richman, U. Sarica, R. Schmitz, F. Setti, J. Sheplock, D. Stuart, T.Á. Vámi, S. Wang

**California Institute of Technology, Pasadena, California, USA**
A. Bornheim, O. Cerri, A. Latorre, J. Mao, H.B. Newman, M. Spiropulu, J.R. Vlimant, C. Wang, S. Xie, R.Y. Zhu

**Carnegie Mellon University, Pittsburgh, Pennsylvania, USA**
J. Alison, S. An, M.B. Andrews, P. Bryant, M. Cremonesi, V. Dutta, T. Ferguson, A. Harilal, C. Liu, T. Mudholkar, S. Murthy, P. Palit, M. Paulini, A. Roberts, A. Sanchez, W. Terrill

**University of Colorado Boulder, Boulder, Colorado, USA**
J.P. Cumalat, W.T. Ford, A. Hart, A. Hassani, G. Karathanasis, E. MacDonald, N. Manganelli, A. Perloff, C. Savard, N. Schonbeck, K. Stenson, K.A. Ulmer, S.R. Wagner, N. Zipper

**Cornell University, Ithaca, New York, USA**
J. Alexander, S. Bright-Thonney, X. Chen, D.J. Cranshaw, J. Fan, X. Fan, D. Gadkari, S. Hogan, P. Kotamnives, J. Monroy, M. Oshiro, J.R. Patterson, J. Reichert, M. Reid, A. Ryd, J. Thom, P. Wittich, R. Zou

**Fermi National Accelerator Laboratory, Batavia, Illinois, USA**
M. Albrow, M. Alyari, O. Amram, G. Apollinari, A. Apresyan, L.A.T. Bauerdick, D. Berry, J. Berryhill, P.C. Bhat, K. Burkett, J.N. Butler, A. Canepa, G.B. Cerati, H.W.K. Cheung, F. Chlebana, G. Cummings, J. Dickinson, I. Dutta, V.D. Elvira, Y. Feng, J. Freeman, A. Gandrakota, Z. Gecse, L. Gray, D. Green, A. Grummer, S. Grünendahl, D. Guerrero, O. Gutsche, R.M. Harris, R. Heller, T.C. Herwig, J. Hirschauer, L. Horyn, B. Jayatilaka, S. Jindariani, M. Johnson, U. Joshi, T. Klijnsma, B. Klima, K.H.M. Kwok, S. Lammel, D. Lincoln, R. Lipton, T. Liu, C. Madrid, K. Maeshima, C. Mantilla, D. Mason, P. McBride, P. Merkel, S. Mrenna, S. Nahn, J. Ngadiuba, D. Noonan, V. Papadimitriou, N. Pastika, K. Pedro, C. Pena[85], F. Ravera, A. Reinsvold Hall[86], L. Ristori, E. Sexton-Kennedy, N. Smith, A. Soha, L. Spiegel, S. Stoynev, J. Strait, L. Taylor, S. Tkaczyk, N.V. Tran, L. Uplegger, E.W. Vaandering, I. Zoi

**University of Florida, Gainesville, Florida, USA**
C. Aruta, P. Avery, D. Bourilkov, L. Cadamuro, P. Chang, V. Cherepanov, R.D. Field, E. Koenig, M. Kolosova, J. Konigsberg, A. Korytov, K.H. Lo, K. Matchev, N. Menendez, G. Mitselmakher, K. Mohrman, A. Muthirakalayil Madhu, N. Rawal, D. Rosenzweig, S. Rosenzweig, K. Shi, J. Wang

**Florida State University, Tallahassee, Florida, USA**
T. Adams, A. Al Kadhim, A. Askew, S. Bower, R. Habibullah, V. Hagopian, R. Hashmi, R.S. Kim, S. Kim, T. Kolberg, G. Martinez, H. Prosper, P.R. Prova, M. Wulansatiti, R. Yohay, J. Zhang

**Florida Institute of Technology, Melbourne, Florida, USA**
B. Alsufyani, M.M. Baarmand, S. Butalla, T. Elkafrawy[53], M. Hohlmann, R. Kumar Verma, M. Rahmani, E. Yanes

**University of Illinois Chicago, Chicago, USA, Chicago, USA**

M.R. Adams, A. Baty, C. Bennett, R. Cavanaugh, R. Escobar Franco, O. Evdokimov, C.E. Gerber, D.J. Hofman, J.h. Lee, D. S. Lemos, A.H. Merrit, C. Mills, S. Nanda, G. Oh, B. Ozek, D. Pilipovic, R. Pradhan, T. Roy, S. Rudrabhatla, M.B. Tonjes, N. Varelas, Z. Ye, J. Yoo

**The University of Iowa, Iowa City, Iowa, USA**
M. Alhusseini, D. Blend, K. Dilsiz[87], L. Emediato, G. Karaman, O.K. Köseyan, J.-P. Merlo, A. Mestvirishvili[88], J. Nachtman, O. Neogi, H. Ogul[89], Y. Onel, A. Penzo, C. Snyder, E. Tiras[90]

**Johns Hopkins University, Baltimore, Maryland, USA**
B. Blumenfeld, L. Corcodilos, J. Davis, A.V. Gritsan, L. Kang, S. Kyriacou, P. Maksimovic, M. Roguljic, J. Roskes, S. Sekhar, M. Swartz

**The University of Kansas, Lawrence, Kansas, USA**
A. Abreu, L.F. Alcerro Alcerro, J. Anguiano, P. Baringer, A. Bean, Z. Flowers, D. Grove, J. King, G. Krintiras, M. Lazarovits, C. Le Mahieu, C. Lindsey, J. Marquez, N. Minafra, M. Murray, M. Nickel, M. Pitt, S. Popescu[91], C. Rogan, C. Royon, R. Salvatico, S. Sanders, C. Smith, Q. Wang, G. Wilson

**Kansas State University, Manhattan, Kansas, USA**
B. Allmond, A. Ivanov, K. Kaadze, A. Kalogeropoulos, D. Kim, Y. Maravin, K. Nam, J. Natoli, D. Roy, G. Sorrentino

**Lawrence Livermore National Laboratory, Livermore, California, USA**
F. Rebassoo, D. Wright

**University of Maryland, College Park, Maryland, USA**
A. Baden, A. Belloni, Y.M. Chen, S.C. Eno, N.J. Hadley, S. Jabeen, R.G. Kellogg, T. Koeth, Y. Lai, S. Lascio, A.C. Mignerey, S. Nabili, C. Palmer, C. Papageorgakis, M.M. Paranjpe, L. Wang

**Massachusetts Institute of Technology, Cambridge, Massachusetts, USA**
J. Bendavid, I.A. Cali, M. D'Alfonso, J. Eysermans, C. Freer, G. Gomez-Ceballos, M. Goncharov, G. Grosso, P. Harris, D. Hoang, D. Kovalskyi, J. Krupa, L. Lavezzo, Y.-J. Lee, K. Long, C. Mironov, A. Novak, C. Paus, D. Rankin, C. Roland, G. Roland, S. Rothman, G.S.F. Stephans, Z. Wang, B. Wyslouch, T. J. Yang

**University of Minnesota, Minneapolis, Minnesota, USA**
B. Crossman, B.M. Joshi, C. Kapsiak, M. Krohn, D. Mahon, J. Mans, B. Marzocchi, S. Pandey, M. Revering, R. Rusack, R. Saradhy, N. Schroeder, N. Strobbe, M.A. Wadud

**University of Mississippi, Oxford, Mississippi, USA**
L.M. Cremaldi

**University of Nebraska-Lincoln, Lincoln, Nebraska, USA**
K. Bloom, D.R. Claes, G. Haza, J. Hossain, C. Joo, I. Kravchenko, J.E. Siado, W. Tabb, A. Vagnerini, A. Wightman, F. Yan, D. Yu

**State University of New York at Buffalo, Buffalo, New York, USA**
H. Bandyopadhyay, L. Hay, I. Iashvili, A. Kharchilava, M. Morris, D. Nguyen, S. Rappoccio, H. Rejeb Sfar, A. Williams

**Northeastern University, Boston, Massachusetts, USA**

G. Alverson, E. Barberis, J. Dervan, Y. Haddad, Y. Han, A. Krishna, J. Li, M. Lu, G. Madigan, R. Mccarthy, D.M. Morse, V. Nguyen, T. Orimoto, A. Parker, L. Skinnari, A. Tishelman-Charny, B. Wang, D. Wood

**Northwestern University, Evanston, Illinois, USA**
S. Bhattacharya, J. Bueghly, Z. Chen, S. Dittmer, K.A. Hahn, Y. Liu, Y. Miao, D.G. Monk, M.H. Schmitt, A. Taliercio, M. Velasco

**University of Notre Dame, Notre Dame, Indiana, USA**
G. Agarwal, R. Band, R. Bucci, S. Castells, A. Das, R. Goldouzian, M. Hildreth, K.W. Ho, K. Hurtado Anampa, T. Ivanov, C. Jessop, K. Lannon, J. Lawrence, N. Loukas, L. Lutton, J. Mariano, N. Marinelli, I. Mcalister, T. McCauley, C. Mcgrady, C. Moore, Y. Musienko[16], H. Nelson, M. Osherson, A. Piccinelli, R. Ruchti, A. Townsend, Y. Wan, M. Wayne, H. Yockey, M. Zarucki, L. Zygala

**The Ohio State University, Columbus, Ohio, USA**
A. Basnet, B. Bylsma, M. Carrigan, L.S. Durkin, C. Hill, M. Joyce, M. Nunez Ornelas, K. Wei, B.L. Winer, B. R. Yates

**Princeton University, Princeton, New Jersey, USA**
F.M. Addesa, H. Bouchamaoui, P. Das, G. Dezoort, P. Elmer, A. Frankenthal, B. Greenberg, N. Haubrich, G. Kopp, S. Kwan, D. Lange, A. Loeliger, D. Marlow, I. Ojalvo, J. Olsen, A. Shevelev, D. Stickland, C. Tully

**University of Puerto Rico, Mayaguez, Puerto Rico, USA**
S. Malik

**Purdue University, West Lafayette, Indiana, USA**
A.S. Bakshi, V.E. Barnes, S. Chandra, R. Chawla, S. Das, A. Gu, L. Gutay, M. Jones, A.W. Jung, D. Kondratyev, A.M. Koshy, M. Liu, G. Negro, N. Neumeister, G. Paspalaki, S. Piperov, V. Scheurer, J.F. Schulte, M. Stojanovic, J. Thieman, A. K. Virdi, F. Wang, W. Xie

**Purdue University Northwest, Hammond, Indiana, USA**
J. Dolen, N. Parashar, A. Pathak

**Rice University, Houston, Texas, USA**
D. Acosta, T. Carnahan, K.M. Ecklund, P.J. Fernández Manteca, S. Freed, P. Gardner, F.J.M. Geurts, W. Li, O. Miguel Colin, B.P. Padley, R. Redjimi, J. Rotter, E. Yigitbasi, Y. Zhang

**University of Rochester, Rochester, New York, USA**
A. Bodek, P. de Barbaro, R. Demina, J.L. Dulemba, A. Garcia-Bellido, O. Hindrichs, A. Khukhunaishvili, N. Parmar, P. Parygin[92], E. Popova[92], R. Taus

**The Rockefeller University, New York, New York, USA**
K. Goulianos

**Rutgers, The State University of New Jersey, Piscataway, New Jersey, USA**
B. Chiarito, J.P. Chou, Y. Gershtein, E. Halkiadakis, M. Heindl, D. Jaroslawski, O. Karacheban[28], I. Laflotte, A. Lath, R. Montalvo, K. Nash, H. Routray, S. Salur, S. Schnetzer, S. Somalwar, R. Stone, S.A. Thayil, S. Thomas, J. Vora, H. Wang

**University of Tennessee, Knoxville, Tennessee, USA**
H. Acharya, D. Ally, A.G. Delannoy, S. Fiorendi, S. Higginbotham, T. Holmes,

A.R. Kanuganti, N. Karunarathna, L. Lee, E. Nibigira, S. Spanier

**Texas A&M University, College Station, Texas, USA**
D. Aebi, M. Ahmad, O. Bouhali[93], R. Eusebi, J. Gilmore, T. Huang, T. Kamon[94], H. Kim, S. Luo, R. Mueller, D. Overton, D. Rathjens, A. Safonov

**Texas Tech University, Lubbock, Texas, USA**
N. Akchurin, J. Damgov, V. Hegde, A. Hussain, Y. Kazhykarim, K. Lamichhane, S.W. Lee, A. Mankel, T. Peltola, I. Volobouev, A. Whitbeck

**Vanderbilt University, Nashville, Tennessee, USA**
E. Appelt, Y. Chen, S. Greene, A. Gurrola, W. Johns, R. Kunnawalkam Elayavalli, A. Melo, F. Romeo, P. Sheldon, S. Tuo, J. Velkovska, J. Viinikainen

**University of Virginia, Charlottesville, Virginia, USA**
B. Cardwell, B. Cox, J. Hakala, R. Hirosky, A. Ledovskoy, C. Neu, C.E. Perez Lara

**Wayne State University, Detroit, Michigan, USA**
P.E. Karchin

**University of Wisconsin - Madison, Madison, Wisconsin, USA**
A. Aravind, S. Banerjee, K. Black, T. Bose, S. Dasu, I. De Bruyn, P. Everaerts, C. Galloni, H. He, M. Herndon, A. Herve, C.K. Koraka, A. Lanaro, R. Loveless, J. Madhusudanan Sreekala, A. Mallampalli, A. Mohammadi, S. Mondal, G. Parida, D. Pinna, A. Savin, V. Shang, V. Sharma, W.H. Smith, D. Teague, H.F. Tsoi, W. Vetens, A. Warden

**Authors affiliated with an institute or an international laboratory covered by a cooperation agreement with CERN**
S. Afanasiev, V. Andreev, Yu. Andreev, T. Aushev, M. Azarkin, A. Babaev, A. Belyaev, V. Blinov[95], E. Boos, V. Borshch, D. Budkouski, V. Chekhovsky, R. Chistov[95], M. Danilov[95], A. Dermenev, T. Dimova[95], D. Druzhkin[96], M. Dubinin[85], L. Dudko, A. Ershov, G. Gavrilov, V. Gavrilov, S. Gninenko, V. Golovtcov, N. Golubev, I. Golutvin, I. Gorbunov, A. Gribushin, Y. Ivanov, V. Kachanov, V. Karjavine, A. Karneyeu, V. Kim[95], M. Kirakosyan, D. Kirpichnikov, M. Kirsanov, V. Klyukhin, O. Kodolova[97], V. Korenkov, A. Kozyrev[95], N. Krasnikov, A. Lanev, P. Levchenko[98], N. Lychkovskaya, V. Makarenko, A. Malakhov, V. Matveev[95], V. Murzin, A. Nikitenko[99,97], S. Obraztsov, V. Oreshkin, V. Palichik, V. Perelygin, S. Petrushanko, S. Polikarpov[95], V. Popov, O. Radchenko[95], M. Savina, V. Savrin, V. Shalaev, S. Shmatov, S. Shulha, Y. Skovpen[95], S. Slabospitskii, V. Smirnov, A. Snigirev, D. Sosnov, V. Sulimov, E. Tcherniaev, A. Terkulov, O. Teryaev, I. Tlisova, A. Toropin, L. Uvarov, A. Uzunian, A. Vorobyev†, N. Voytishin, B.S. Yuldashev[100], A. Zarubin, I. Zhizhin, A. Zhokin

†: Deceased
[1]Also at Yerevan State University, Yerevan, Armenia
[2]Also at TU Wien, Vienna, Austria
[3]Also at Institute of Basic and Applied Sciences, Faculty of Engineering, Arab Academy for Science, Technology and Maritime Transport, Alexandria, Egypt
[4]Also at Ghent University, Ghent, Belgium
[5]Also at Universidade Estadual de Campinas, Campinas, Brazil

[6]Also at Federal University of Rio Grande do Sul, Porto Alegre, Brazil
[7]Also at UFMS, Nova Andradina, Brazil
[8]Also at Nanjing Normal University, Nanjing, China
[9]Now at The University of Iowa, Iowa City, Iowa, USA
[10]Also at University of Chinese Academy of Sciences, Beijing, China
[11]Also at China Center of Advanced Science and Technology, Beijing, China
[12]Also at University of Chinese Academy of Sciences, Beijing, China
[13]Also at China Spallation Neutron Source, Guangdong, China
[14]Now at Henan Normal University, Xinxiang, China
[15]Also at Université Libre de Bruxelles, Bruxelles, Belgium
[16]Also at an institute or an international laboratory covered by a cooperation agreement with CERN
[17]Now at British University in Egypt, Cairo, Egypt
[18]Now at Cairo University, Cairo, Egypt
[19]Also at Purdue University, West Lafayette, Indiana, USA
[20]Also at Université de Haute Alsace, Mulhouse, France
[21]Also at Department of Physics, Tsinghua University, Beijing, China
[22]Also at The University of the State of Amazonas, Manaus, Brazil
[23]Also at Erzincan Binali Yildirim University, Erzincan, Turkey
[24]Also at University of Hamburg, Hamburg, Germany
[25]Also at RWTH Aachen University, III. Physikalisches Institut A, Aachen, Germany
[26]Also at Isfahan University of Technology, Isfahan, Iran
[27]Also at Bergische University Wuppertal (BUW), Wuppertal, Germany
[28]Also at Brandenburg University of Technology, Cottbus, Germany
[29]Also at Forschungszentrum Jülich, Juelich, Germany
[30]Also at CERN, European Organization for Nuclear Research, Geneva, Switzerland
[31]Also at Institute of Physics, University of Debrecen, Debrecen, Hungary
[32]Also at Institute of Nuclear Research ATOMKI, Debrecen, Hungary
[33]Now at Universitatea Babes-Bolyai - Facultatea de Fizica, Cluj-Napoca, Romania
[34]Also at Physics Department, Faculty of Science, Assiut University, Assiut, Egypt
[35]Also at HUN-REN Wigner Research Centre for Physics, Budapest, Hungary
[36]Also at Punjab Agricultural University, Ludhiana, India
[37]Also at University of Visva-Bharati, Santiniketan, India
[38]Also at Indian Institute of Science (IISc), Bangalore, India
[39]Also at Birla Institute of Technology, Mesra, Mesra, India
[40]Also at IIT Bhubaneswar, Bhubaneswar, India
[41]Also at Institute of Physics, Bhubaneswar, India
[42]Also at University of Hyderabad, Hyderabad, India
[43]Also at Deutsches Elektronen-Synchrotron, Hamburg, Germany
[44]Also at Department of Physics, Isfahan University of Technology, Isfahan, Iran
[45]Also at Sharif University of Technology, Tehran, Iran
[46]Also at Department of Physics, University of Science and Technology of Mazandaran, Behshahr, Iran
[47]Also at Helwan University, Cairo, Egypt
[48]Also at Italian National Agency for New Technologies, Energy and Sustainable Economic Development, Bologna, Italy
[49]Also at Centro Siciliano di Fisica Nucleare e di Struttura Della Materia, Catania, Italy
[50]Also at Università degli Studi Guglielmo Marconi, Roma, Italy
[51]Also at Scuola Superiore Meridionale, Università di Napoli 'Federico II', Napoli, Italy

[52]Also at Fermi National Accelerator Laboratory, Batavia, Illinois, USA
[53]Also at Ain Shams University, Cairo, Egypt
[54]Also at Consiglio Nazionale delle Ricerche - Istituto Officina dei Materiali, Perugia, Italy
[55]Also at Riga Technical University, Riga, Latvia
[56]Also at Department of Applied Physics, Faculty of Science and Technology, Universiti Kebangsaan Malaysia, Bangi, Malaysia
[57]Also at Consejo Nacional de Ciencia y Tecnología, Mexico City, Mexico
[58]Also at Trincomalee Campus, Eastern University, Sri Lanka, Nilaveli, Sri Lanka
[59]Also at Saegis Campus, Nugegoda, Sri Lanka
[60]Also at National and Kapodistrian University of Athens, Athens, Greece
[61]Also at Ecole Polytechnique Fédérale Lausanne, Lausanne, Switzerland
[62]Also at Universität Zürich, Zurich, Switzerland
[63]Also at Stefan Meyer Institute for Subatomic Physics, Vienna, Austria
[64]Also at Laboratoire d'Annecy-le-Vieux de Physique des Particules, IN2P3-CNRS, Annecy-le-Vieux, France
[65]Also at Near East University, Research Center of Experimental Health Science, Mersin, Turkey
[66]Also at Konya Technical University, Konya, Turkey
[67]Also at Izmir Bakircay University, Izmir, Turkey
[68]Also at Adiyaman University, Adiyaman, Turkey
[69]Also at Bozok Universitetesi Rektörlügü, Yozgat, Turkey
[70]Also at Marmara University, Istanbul, Turkey
[71]Also at Milli Savunma University, Istanbul, Turkey
[72]Also at Kafkas University, Kars, Turkey
[73]Now at stanbul Okan University, Istanbul, Turkey
[74]Also at Hacettepe University, Ankara, Turkey
[75]Also at Istanbul University - Cerrahpasa, Faculty of Engineering, Istanbul, Turkey
[76]Also at Yildiz Technical University, Istanbul, Turkey
[77]Also at Vrije Universiteit Brussel, Brussel, Belgium
[78]Also at School of Physics and Astronomy, University of Southampton, Southampton, United Kingdom
[79]Also at University of Bristol, Bristol, United Kingdom
[80]Also at IPPP Durham University, Durham, United Kingdom
[81]Also at Monash University, Faculty of Science, Clayton, Australia
[82]Also at Università di Torino, Torino, Italy
[83]Also at Bethel University, St. Paul, Minnesota, USA
[84]Also at Karamanoğlu Mehmetbey University, Karaman, Turkey
[85]Also at California Institute of Technology, Pasadena, California, USA
[86]Also at United States Naval Academy, Annapolis, Maryland, USA
[87]Also at Bingol University, Bingol, Turkey
[88]Also at Georgian Technical University, Tbilisi, Georgia
[89]Also at Sinop University, Sinop, Turkey
[90]Also at Erciyes University, Kayseri, Turkey
[91]Also at Horia Hulubei National Institute of Physics and Nuclear Engineering (IFIN-HH), Bucharest, Romania
[92]Now at an institute or an international laboratory covered by a cooperation agreement with CERN
[93]Also at Texas A&M University at Qatar, Doha, Qatar
[94]Also at Kyungpook National University, Daegu, Korea

[95]Also at another institute or international laboratory covered by a cooperation agreement with CERN
[96]Also at Universiteit Antwerpen, Antwerpen, Belgium
[97]Also at Yerevan Physics Institute, Yerevan, Armenia
[98]Also at Northeastern University, Boston, Massachusetts, USA
[99]Also at Imperial College, London, United Kingdom
[100]Also at Institute of Nuclear Physics of the Uzbekistan Academy of Sciences, Tashkent, Uzbekistan